50272-101

REPORT DOCUMENTATION PAGE

1. REPORT NO. NCEER-95-0002

2.

3. PB95-220042

4. Title and Subtitle
Experimental and Analytical Study of Low-Cycle Fatigue Behavior of Semi-Rigid Top-And-Seat Angle Connections

5. Report Date
January 5, 1995

6.

7. Author(s)
G. Pekcan, J.B. Mander and S.S. Chen

8. Performing Organization Rept. No.

9. Performing Organization Name and Address
State University of New York at Buffalo
Department of Civil Engineering
Buffalo, New York 14260

10. Project/Task/Work Unit No.

11. Contract(C) or Grant(G) No.
(C) BCS 90-25010
(G) NEC-91029

12. Sponsoring Organization Name and Address
National Center for Earthquake Engineering Research
State University of New York at Buffalo
Red Jacket Quadrangle
Buffalo, New York 14261

13. Type of Report & Period Covered
Technical report

14.

15. Supplementary Notes
This research was conducted at the State University of New York at Buffalo and was partially supported by the National Science Foundation under Grant No. BCS 90-25010 and the New York State Science and Technology Foundation under Grant No. NEC-91029.

16. Abstract (Limit: 200 words)

One common type of existing structure is the steel frame with semi-rigid connections. In previous studies, analytical models have been developed, the effects of floor slabs and masonry infills have been studied, and parametric response analyses have been performed. This report summarizes work on the low-cycle fatigue behavior of a common type of semi-rigid connection, those made of top and seat angles. Nineteen tests were performed using various load histories and they showed that the hysteretic energy-life and rotation-life models are applicable for this type of connection. The analysis showed that if the plastic hinge rotations are kept below 2%, the connections can sustain at least fifty cycles of complete load reversals. The report contains a valuable database on the cyclic behavior of one type of semi-rigid connection.

17. Document Analysis a. Descriptors

b. Identifiers/Open-Ended Terms

Earthquake engineering. Steel frames. Semi-rigid connections. Top angles. Seat angles. Low cycle fatigue. Cyclic energy dissipation. Drift reversal. Damage accumulation. Plastic connection rotation.

c. COSATI Field/Group

18. Availability Statement
Release Unlimited

19. Security Class (This Report)
Unclassified

20. Security Class (This Page)
Unclassified

21. No. of Pages
136

22. Price

(See ANSI-Z39.18) See Instructions on Reverse OPTIONAL FORM 272 (4-77) (Formerly NTIS-35)

NATIONAL CENTER FOR EARTHQUAKE ENGINEERING RESEARCH

State University of New York at Buffalo

Experimental and Analytical Study of Low-Cycle Fatigue Behavior of Semi-Rigid Top-And-Seat Angle Connections

by

G. Pekcan, J.B. Mander and S.S. Chen
State University of New York at Buffalo
Department of Civil Engineering
Buffalo, New York 14260

Technical Report NCEER-95-0002

January 5, 1995

This research was conducted at the State University of New York at Buffalo and was partially supported by the National Science Foundation under Grant No. BCS 90-25010 and the New York State Science and Technology Foundation under Grant No. NEC-91029.

NOTICE

PB95-220042

Experimental and Analytical Study of Low-Cycle Fatigue Behavior of Semi-Rigid Top-And-Seat Angle Connections

by

G. Pekcan[1], J.B. Mander[2] and S.S. Chen[2]

January 5, 1995

Technical Report NCEER-95-0002

NCEER Task Numbers 91-3122A and 92-3108

NSF Master Contract Number BCS 90-25010
and
NYSSTF Grant Number NEC-91029

1 Research Assistant, Department of Civil Engineering, State University of New York at Buffalo
2 Assistant Professor, Department of Civil Engineering, State University of New York at Buffalo

NATIONAL CENTER FOR EARTHQUAKE ENGINEERING RESEARCH
State University of New York at Buffalo
Red Jacket Quadrangle, Buffalo, NY 14261

PREFACE

The National Center for Earthquake Engineering Research (NCEER) was established to expand and disseminate knowledge about earthquakes, improve earthquake-resistant design, and implement seismic hazard mitigation procedures to minimize loss of lives and property. The emphasis is on structures in the eastern and central United States and lifelines throughout the country that are found in zones of low, moderate, and high seismicity.

NCEER's research and implementation plan in years six through ten (1991-1996) comprises four interlocked elements, as shown in the figure below. Element I, Basic Research, is carried out to support projects in the Applied Research area. Element II, Applied Research, is the major focus of work for years six through ten. Element III, Demonstration Projects, have been planned to support Applied Research projects, and will be either case studies or regional studies. Element IV, Implementation, will result from activity in the four Applied Research projects, and from Demonstration Projects.

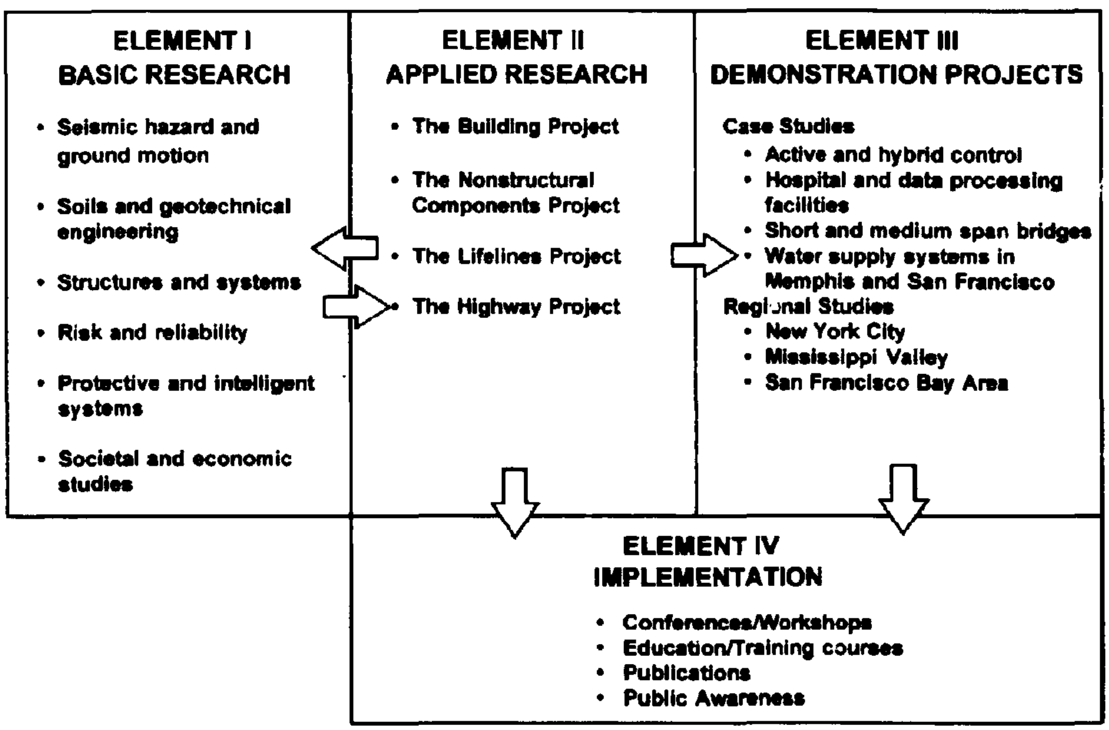

Research in the **Building Project** focuses on the evaluation and retrofit of buildings in regions of moderate seismicity. Emphasis is on lightly reinforced concrete buildings, steel semi-rigid frames, and masonry walls or infills. The research involves small- and medium-scale shake table tests and full-scale component tests at several institutions. In a parallel effort, analytical models and computer programs are being developed to aid in the prediction of the response of these buildings to various types of ground motion.

Two of the short-term products of the **Building Project** will be a monograph on the evaluation of lightly reinforced concrete buildings and a state-of-the-art report on unreinforced masonry.

The **structures and systems program** constitutes one of the important areas of research in the **Building Project**. Current tasks include the following:

1. Continued testing of lightly reinforced concrete external joints.
2. Continued development of analytical tools, such as system identification, idealization, and computer programs.
3. Perform parametric studies of building response.
4. Retrofit of lightly reinforced concrete frames, flat plates and unreinforced masonry.
5. Enhancement of the IDARC (inelastic damage analysis of reinforced concrete) computer program.
6. Research infilled frames, including the development of an experimental program, development of analytical models and response simulation.
7. Investigate the torsional response of symmetrical buildings.

One common type of existing structure investigated to a limited extent in the buildings area is steel frames with semi-rigid connections. In previous studies, analytical models have been developed, the effects of floor slabs and masonry infills have been studied, and parametric response analyses have been performed. This report summarizes work on the low-cycle fatigue behavior of a common type of semi-rigid connection, those made of top and seat angles. Nineteen tests were performed using various load histories and they showed that the hysteretic energy-life and rotation-life models are applicable for this type of connection. The analysis showed that if the plastic hinge rotations are kept below 2%, the connections can sustain at least fifty cycles of complete load reversals. The report contains a valuable database on the cyclic behavior of one type of semi-rigid connection.

ABSTRACT

A specific type of semi-rigid top-and-seat angle connection was experimentally evaluated for its low-cycle fatigue behavior under drift controlled cyclic tests. The experimental program consisted of static, constant amplitude and variable amplitude tests. Constant amplitude tests consisted of equi-amplitude fully reversed (R=-1) and one-sided (R=0) tests. Variable amplitude tests included incremental-decremental and step tests to investigate the effects of different displacement squences.

Strength and stiffness were found to be very sensitive to the nut and bolt orientation, which do not appear to affect the fatigue life.

Fatigue life relationships were derived based on the constant amplitude test results. To use these in variable amplitude investigations, the concept of an effective equi-amplitude rotation is introduced as the characteristic measure of rotation history. It is shown that effective rotation is independent of load path when compared to constant amplitude test results. Hence, an energy based cumulative damage model is developed and expressed in terms of energy-life and energy-rotation relationships. The proposed damage model is employed in the fatigue damage prediction analysis and compared with the classical Miner's linear damage accumulation model coupled with the rainflow cycle counting method. The proposed energy based damage model implicitly incorporates the memory effects of the previous loading history and precludes the necessity of performing explicit cycle counting. This model is easily implemented into non linear time-history analyses for seismic design and evaluation purposes.

ACKNOWLEDGEMENTS

Specimens were donated by Mr. T. Latona of Buffalo Structural Steel Corporation. Partial financial support for this project was provided by the National Center for Earthquake Engineering Research (NCEER) headquartered at SUNY at Buffalo. Assistance in testing some of the specimens was provided by several graduate students in the Metal Structures course in the Department of Civil Engineering at SUNY at Buffalo. NCEER technicians Mark Pitman and Dan Walch assisted in the setup and testing. Their help is gratefully acknowledged.

TABLE OF CONTENTS

TABLE OF CONTENTS (CONT'D.)

LIST OF ILLUSTRATIONS

LIST OF ILLUSTRATIONS (CONT'D.)

LIST OF TABLES

SECTION 1

INTRODUCTION

1.1 Background

Although the influence of semi-rigid connection behavior on the overall response of steel frames has long been recognized, the beam-to-column connections are traditionally considered to be either pinned or rigid. Pin-ended connections are assumed to have no resistance to moment and are consequently designed to transmit only shear and axial forces. This assumption leads to: (i) large positive moment and deflections at the center of beams under gravity loads, and (ii) columns having no rotational restraint at their ends, being subjected to only axial forces. Conversely, rigid connections are assumed to ensure full continuity between connected members and are consequently required to have an infinite rotational stiffness which in turn leads to small beam deflections and large column moments.

The appeal of semi-rigid connections is further evident due to the brittle fracture problems occuring in some fully-rigid connections in January 1994 Northridge earthquake. Although these idealizations present many simplifications in the analysis and design of frames, being the two extreme cases, they are far from reality for most cases. In any case, the actual behavior of the connection will have a significant effect on the overall dynamic as well as static behavior of the structure. The corresponding structural response may be nonlinear, with both material and geometric nonlinearities. The need for including the effects of connection flexibility in the analysis of building systems is particularly important for use in limit state design methods and in evaluating the seismic risk for new and existing structures.

Under normal service loads, AISC-ASD (1989) procedures assume elastic behavior of various components. However, in the seismic design of structures, it becomes uneconomical and hardly feasible to require that a structure remain elastic when subjected to an earthquake. Therefore, in AISC-LRFD Seismic Provisions (1992), it is required that the design forces resulting from earthquake motions be determined on the basis of energy dissipation in the nonlinear range of response of both members and connections.

Due to the lower yield strength of a semi-rigid connection, when subjected to a moderate earthquake, it will become inelastic more quickly than its fully rigid counterpart. Therefore, consideration of ductile behavior is important. It is also important that the study of cyclic energy dissipation be considered when repeated inelastic loads are of concern. Moreover, under seismic ground shaking, the ability of the connection to absorb cyclic energy will depend on its low-cycle fatigue capacity. Low-cycle fatigue capacity is mainly dependent on three variables: the number of cycles of loading, the amplitude of inelastic cycling and the connection geometry. This study constitutes an important step towards the assessment of the seismic vulnerability and damage potential of flexible frames for one commonly used class of semi-rigid connection: the top-and-seat angle.

1.2 Objectives

Recently, the effects of connection flexibility on the behavior of building frames, subjected to both static and dynamic loadings, have been studied experimentally (Azizinamini et.al. 1985, Harper et.al. 1990, Astaneh et.al. 1989, Chasten et.al. 1989, Dunai and Lu 1992, Huang and Morris 1992, Nader and Astaneh 1992). The need for such information arises from the fact that semi-rigid connection behavior is intrinsically nonlinear. Hence, analytical predictions of frame behavior based on *assumed* non-linear mathematical models can only be substantiated by experimentally obtained data. This nonlinear behavior can be better understood by distinguishing the sources of possible flexibility. Based on the available test data, these are:

1) Connection flexibility which consists of the deformation of its components (in the present case "top-and-seat angles") and its fastener deformation (bolt elongation due to prying)

2) Localized deformation of the column (panel zone deformation) and column flange bending

3) Localized deformation of the beam, which has less significance than the previous cases.

The basic objectives in this study were:

1) To determine the low-cycle fatigue characteristics of top-and-seat angle

connections by determining a Drift-Cyclic relationship (similar to S-N in metals). For this purpose, a fatigue-life model based on cyclic energy dissipation as well as on relative connection rotation is developed for this specific type of connection.

2) To examine the sequence effects or local history effects on low-cycle fatigue damage accumulation and accordingly model such behavior to enable prediction of fatigue failure under random (seismic) loading.

3) To characterize monotonic and cyclic loading behavior, and

4) To determine whether the type of drift reversal (i.e. R=0 or R=-1) affects the fatigue-life.

From cyclic tests of various types of connections and frames, it has been observed that the performance of such structures, under seismically induced load histories, may be limited by low-cycle fatigue of the connection elements. Consequently, the present study constitutes an investigation of the potential applicability of cumulative damage models based on energy dissipation as well as plastic connection rotation, for predicting the cyclic response of structural connections.

Section 2 describes the experimental procedures adopted in the study, and Section 3 presents the experimental Force-Drift and Moment-Rotation plots for each of the tests. Section 4 characterizes the monotonic behavior of the specimens, and Section 5 develops connection rotation and energy based low-cycle fatigue relationships for constant amplitude tests. In Section 6, a damage model is advanced for this semi-rigid connection and applied to the variable amplitude fatigue tests. Finally, conclusions are drawn in Section 7.

SECTION 2

THE EXPERIMENTAL SYSTEM AND PROCEDURES

2.1 Introduction

The experimental program consisted of testing nineteen sets of top-and-seat angle connections subjected to cyclic loading with different controlled amplitude displacements. Only one monotonic test was conducted to generate the static moment-rotation relationship and to determine maximum connection rotation that can be reached. This section describes the experimental setup and procedures adopted in this study.

The test setup which consisted of a reaction frame, a hydraulic actuator and part of a frame system which was tested, is firstly described. Next connection cleats (L6x4x3/8-6 1/2') are described, together with the entire geometry of the connection.

Determination of connection rotation is explained within the description of instrumentation and data acquisition system which had total of five channels. Each test was extended to complete fracture failure. After the termination of a test, another set of specimens was mounted in place and the system was zero-calibrated prior to the next test.

Several coupon tests were conducted to investigate the material characteristics of the test specimens. Finally, these test results are summarized.

2.2 Test Setup

Complete details of the test setup are given in Figures 2-1 and 2-2.

The test setup consisted of a reaction frame supporting an actuator with a ±12″ (610 mm), stroke and 55 kips (245 kN) force capacity. The reaction frame was fixed to the strong floor as shown in Figure 2-1a. The column section (W8x31) was seated on the strong floor at two points, 8 ft. apart (Figure 2-2). The beam section (W8x21) was mounted on the column flange at the center (i.e. 4 ft. apart from the support points), then connected to the actuator 51″ (1.295 m) above the column flange. In this experimental study, since only in-plane response of top-and-seat angle connections was of concern, the experiments were conducted not on the whole structure but on a structural subassamblage. This subassamblage represents a typical exterior beam column connection in a steel frame as shown in Figure 2-1b. This figure also shows the deflected shape of a simple frame system under lateral forces with the specimen substructure located between points of inflection.

A Unistrut reference frame bolted to the column ends was used for the drift measurement and also provided the external control for the hydraulic actuator (Figure 2-1a).

2.3 Test Specimen Assembly

The specimens consisted of W8x21 beam section, W8x31 column section and L6x4x3/8-6 1/2" connection cleats. All of the sections were of ASTM A36 steel. Details of the test specimens are given in Figure 2-3a.

Connections contained top-and-seat angles bolted to the beam and column flanges. The bolt holes in the angles were of standard 13/16" (20.64 cm) diameter which includes 1/16" (2 mm) erection tolerance for 3/4" (19 mm) diameter bolts. Those on beam and column sections were 15/16" (24 mm) diameter.

Each angle contained one row of bolts with 3 1/2" (89 mm) center-to-center bolt gage on the leg attached to the column flange and 1 1/2" (38.10 mm) edge distance. Two rows of bolts had 2 1/2" (64 mm) center-to-center bolt gage with 2 3/8" (60 mm) bolt spacing and 2" (51 mm) edge distance, on the leg attached to the beam flange.

A325-SC high strength bolts, 3/4" diameter were used together with A325 flat hardened washers under both the head and nut of the bolt, consistent with typical installation procedures involving calibrated wrenches. For the first two tests (2% and 4% drift) load indicator washers were also used under the nut along with flat hardened washers. It was observed in these tests that proper bolt tensioning required tightening torques of approximately 450 ft-lbs (610.0 Nm). Therefore, in the rest of the testing program, only A325 hardened flat washers were used with installation torques of 450 ft-lbs. This was considered to apply proper bolt tensioning, as no slip was observed to occur in any of the tests. Clean mill scale (surface class A) existed on all faying surfaces.

Excessive local bending of the top flange of the column was prevented by using two-1" thick steel plates under the column flange at the connection, as shown in Figure 2-3b.

2.4 Instrumentation and Data Acquisition

The layout of the instrumentation in the joint region is shown in Figure 2-4. A total of six

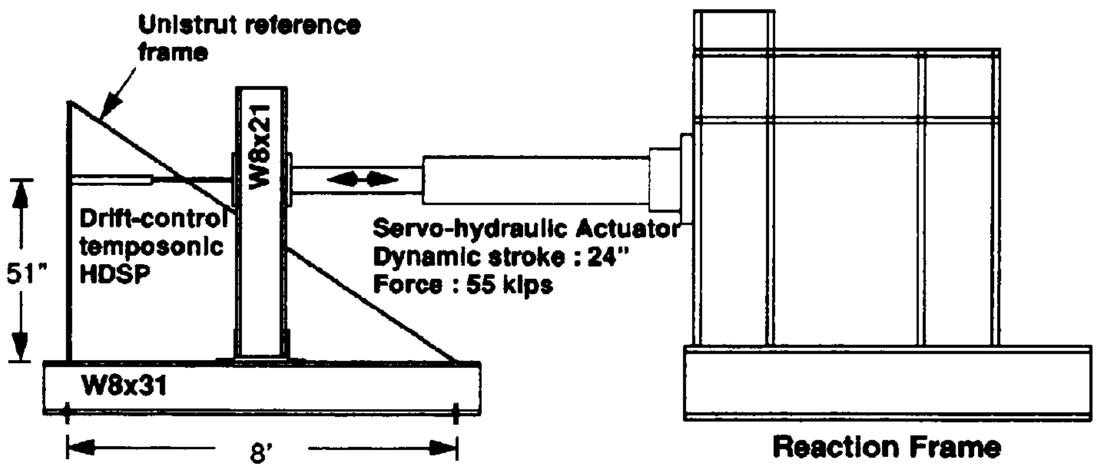

Figure 2-1a Test Setup

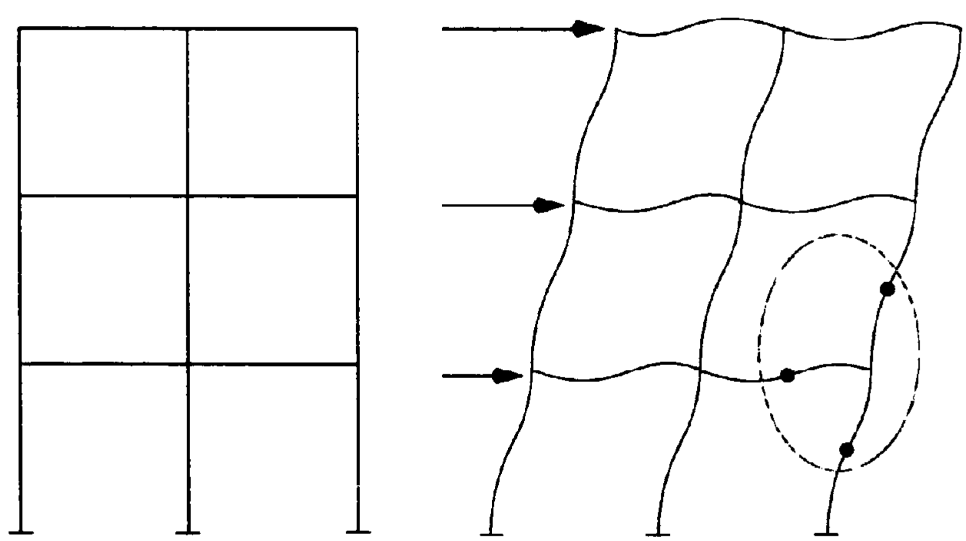

Figure 2-1b Structural Subassamblage

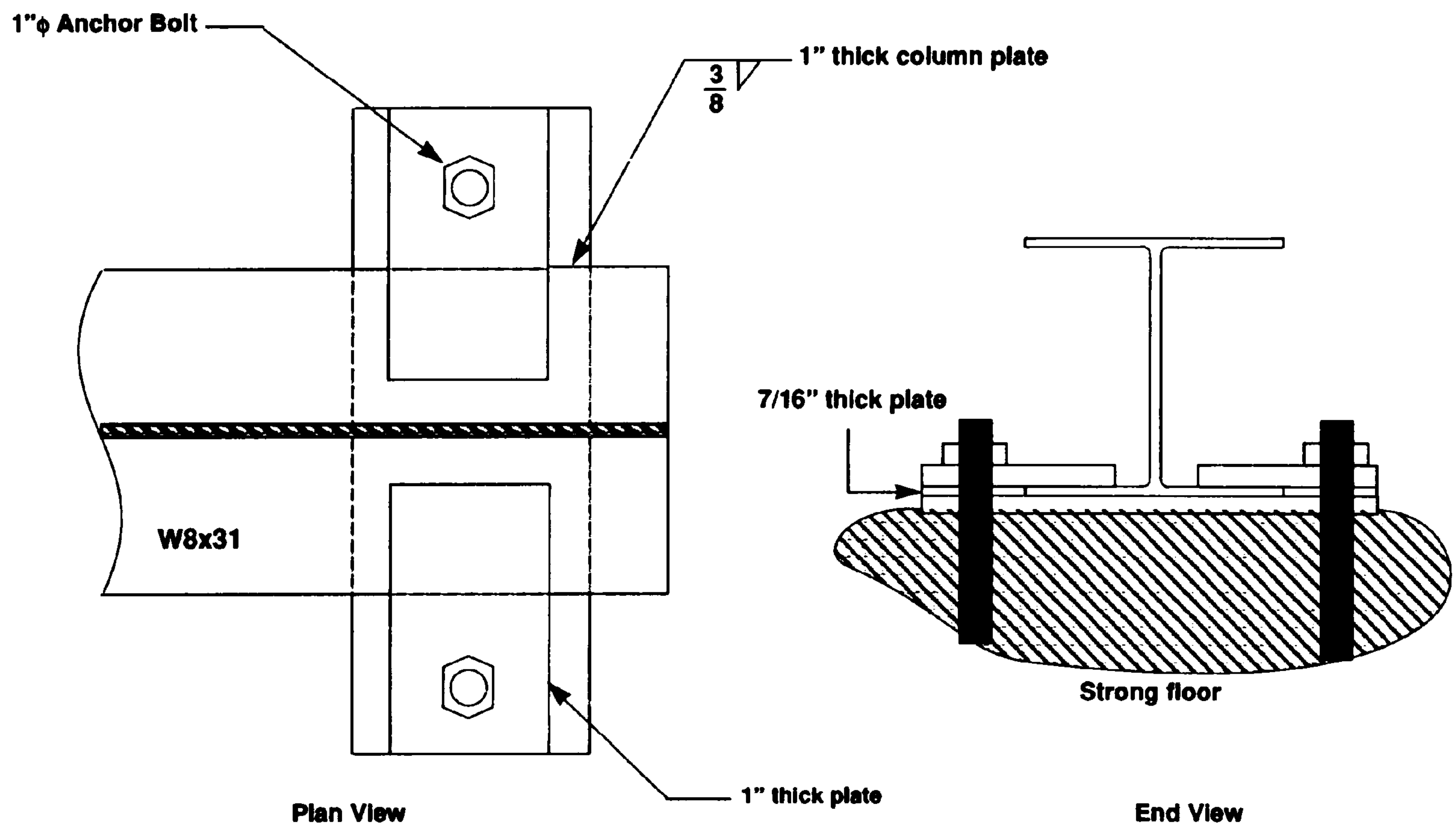

Figure 2-2 End support connection

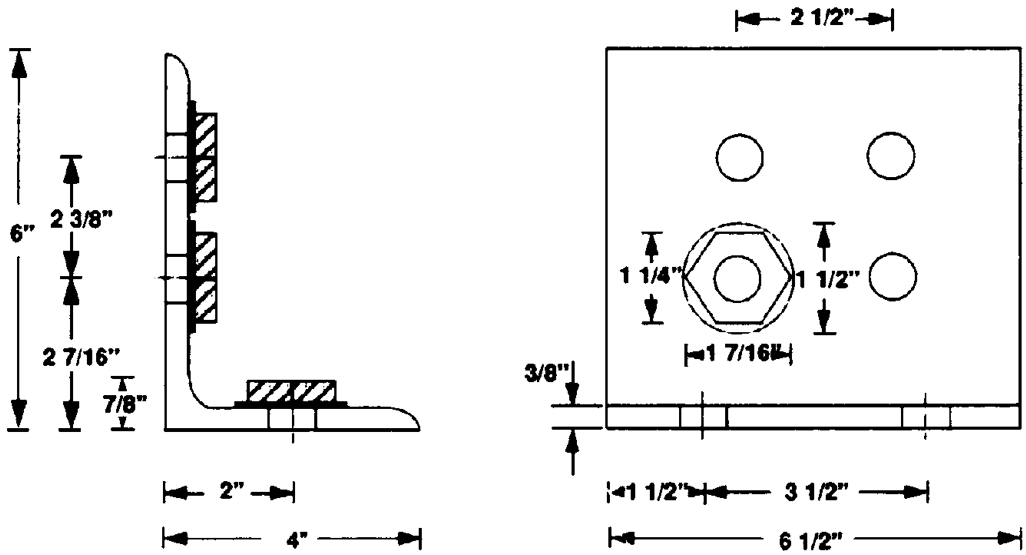

Figure 2-3a Angle used in Test (L6x4x3/8)

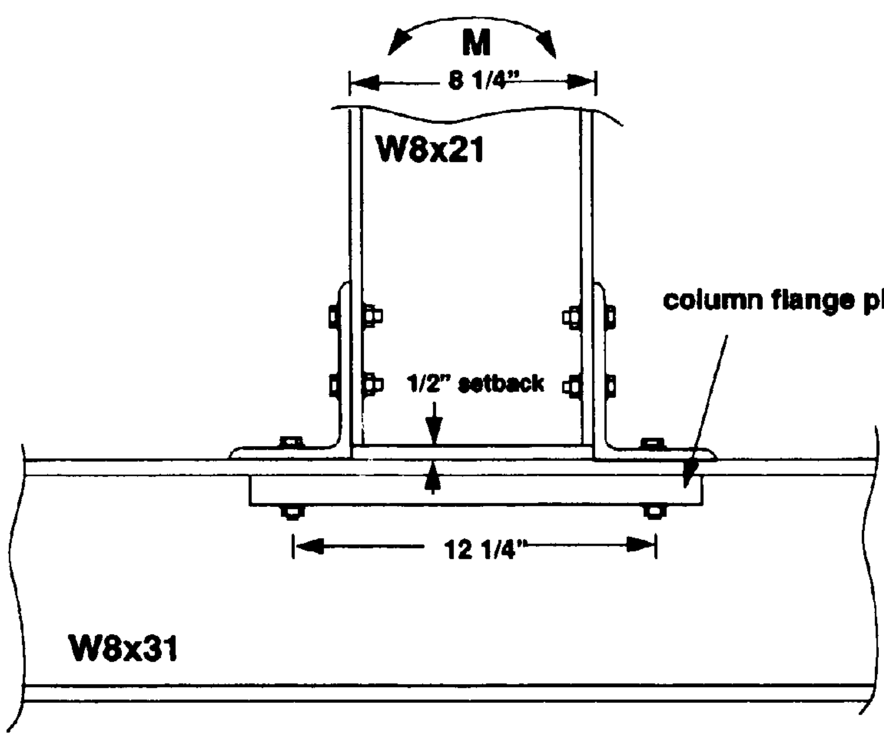

Figure 2-3b Joint Detail

channels of displacement data were taken; two longitudinally mounted potentiometers (P1VS, P2VN) were used at the connection to measure displacement related to the connection rotation. Two other potentiometers (P3HS, P4HN) were transverse to the beam at the connection for an alternate measurement of the connection rotation. Determination of relative connection rotation θ_j, using P1VS, P2VN and P3HS, P4HN is shown on Figure 2-5.

A sonic displacement transducer (HDSP) was used in order to provide drift control to the actuator. The sixth channel measured the displacement in the actuator. The applied force was measured by a load cell in the actuator. Thus, a total of seven channels were used for data recording purposes. Data produced by the transducers was recorded by an analog-digital (A/D) converter (Data Translation model DT2801A) mounted in a 486-33 MHz Personal Computer.

A back-up Force vs. Displacement graph was also plotted on an analog XY plotter for each test.

2.5 Test Specimens and Procedure

Nineteen identical pairs of $L6x4x3/8x6\frac{1}{2}''$ specimens, all of which were cut from the same stock piece of A36 steel, were tested under various conditions. A summary of test specimens and test parameters is given in Table 2-I. Thirteen specimens were tested under equi-amplitude displacement blocks varying the maximum drift each time. Two tests (R0_10, R0_11) were conducted at R=0 (one-sided test) for equi-amplitudes of 2% (0 to +4%) and 4% (0 to +8%) drift. Finally eleven specimens were tested at R=-1 for ±0.6, ±0.8, ±1.5, ±2, ±2.5, ±3, ±4, ±5, ±6, ±7, ±8 % drift (complete reversals). Two of the tests, R1_12 and R1_13, were conducted in order to clarify the transition from low-cycle fatigue to high-cycle fatigue on fatigue plots.

One of the specimens (V_16) was subjected to low-to-high equi-amplitude (±2 % and then ±4 % drift) displacement blocks. Two of the specimens were tested under high-to-low equi-amplitude displacement blocks, one of which was first subjected to ±4 % and then ±2 % drift (V_17), and the second 4%-3%-2% drift blocks (V_18). Two other variable amplitude tests (V_14, V_15) were conducted by cycling sinusoidally, starting with 4% drift (or 0%), and then decreasing (or increasing) the drift value at the beginning of each cycle. In each of the tests, an initial drift of 4% (or 0%) was decreased (or increased) to

Table 2-1 Specimen Testing Parameters

Specimen Id.	Cycling Type	R Ratio	Specimen Drift [a](%)	Cyc. Freq. (Hz.)
M_19	Monotonic	-	±12 [b]	0.01
R1_08	Constant	-1	±1.5	0.25
R1_01	"	-1	±2	0.05
R1_07	"	-1	±2.5	0.1
R1_04	"	-1	±3	0.1
R1_02	"	-1	±4	0.05
R1_03	"	-1	±5	0.1
R1_05	"	-1	±6	0.1
R1_09	"	-1	±7	0.1
R1_06	"	-1	±8	0.01
R0_10	"	0	+4[c]	0.1
R0_11	"	0	+8[d]	0.1
R1_12	"	-1	±0.6	1
R1_13	"	-1	±0.8	0.5
V_14	Variable	-	0 to 4	0.1
V_15	"	-	4 to 0	0.1
V_16	"	-	2 and 4	0.1
V_17	"	-	4 and 2	0.1
V_18	"	-	4 and 3 and 2	0.1

a. Nominal drift based on moment arm of 51".
b. Drift reached at the monotonic failure.
c. Total of 4% drift from the upright position.
d. Total of 8% drift from the upright position.

0% (or 4%) within 20 cycles with a cycling frequency of 0.1 Hz.

Typical displacement histories are shown in Figure 2-6. All of the cyclic tests were extended to the point of complete fracture of one of the angles.

The following steps were performed for each test after failure of the specimen:

1) From the end of the previous test the beam was brought back to the upright vertical position,

2) The previously failed set of angles was replaced with a new set,

3) Bolts were tightened as explained above (see Section 2.3),

4) Potentiometers used at the connection were zero-calibrated,

5) Parameters controlling drift, test speed, sampling rate etc. for a specific test were specified to the computer software which in turn controlled the actuator. However, for the $\pm 0.8\%$ and $\pm 0.6\%$ drift tests, due to the large amount of estimated number of cycles to the failure (~5,000 and 15,000 cycles respectively), not all cycles were recorded. Instead, two consecutive cycles were recorded at every 250, 200, 100 or 50th cycle, depending on the stage of the test.

6) The test was performed by applying a cyclic drift-control load until one of the angles was completely fractured.

7) During the test, significant events such as cycle at which the initial surface crack was observed, were noted, video-recorded and photographed.

2.6 Material Tests

A total of eight coupon tests were conducted to establish the material properties of the angles. The tests were conducted in accordance with the ASTM-E8, "Standard Methods of Tension Testing of Metallic Materials"(1992). The gage length for the autographic recording of the stress-strain curves and for the ultimate elongation measurement was 2" (51 mm) Coupons were taken from an unused portion of the same piece of steel from which the top and seat angle specimens were taken. Complete details for the coupon specimens are given in Figure 2-7.

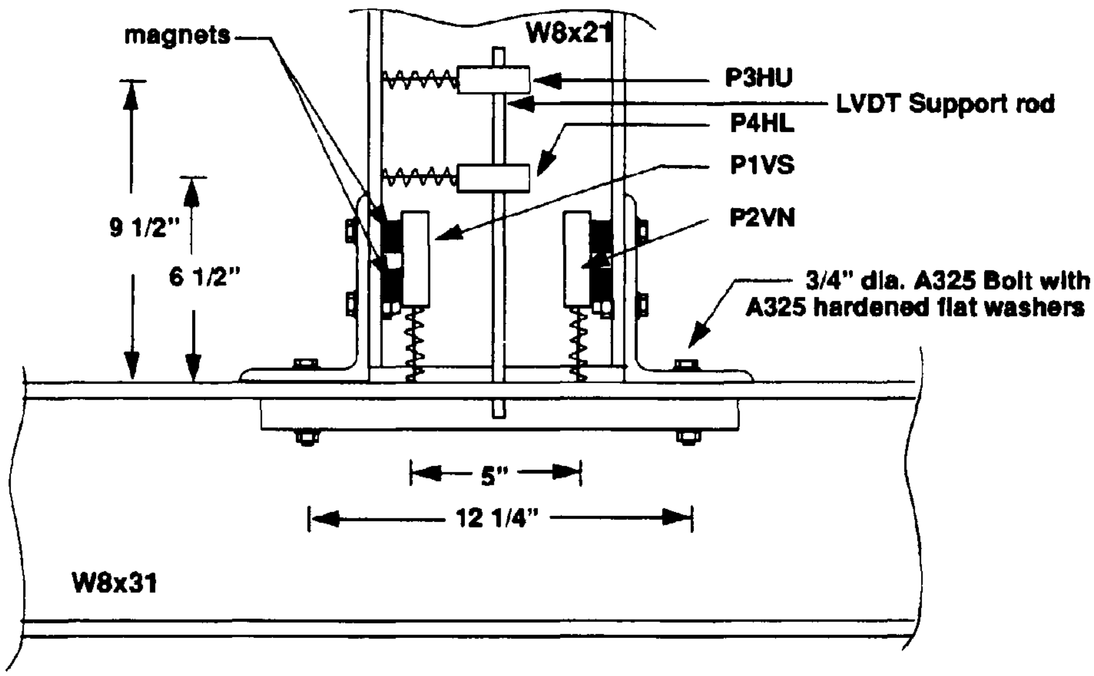

Figure 2-4 Joint Instrumentation

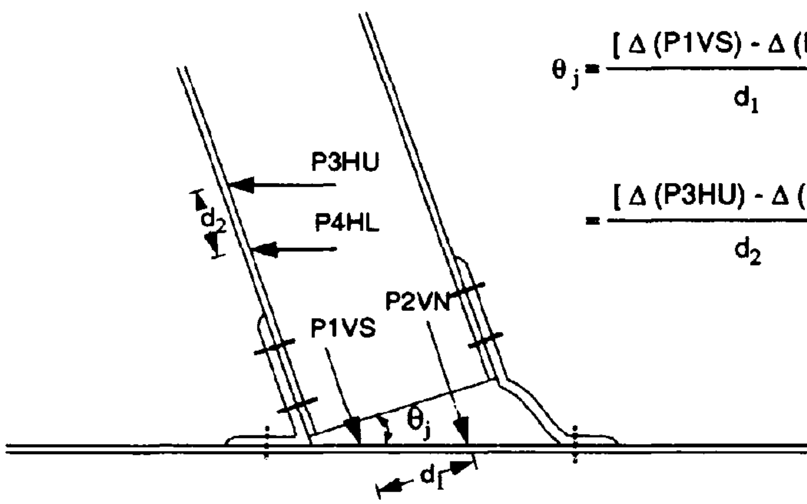

$$\theta_j = \frac{[\Delta(P1VS) - \Delta(P2VN)]}{d_1}$$

$$= \frac{[\Delta(P3HU) - \Delta(P4HL)]}{d_2}$$

Figure 2-5 Determination of Connection Rotation

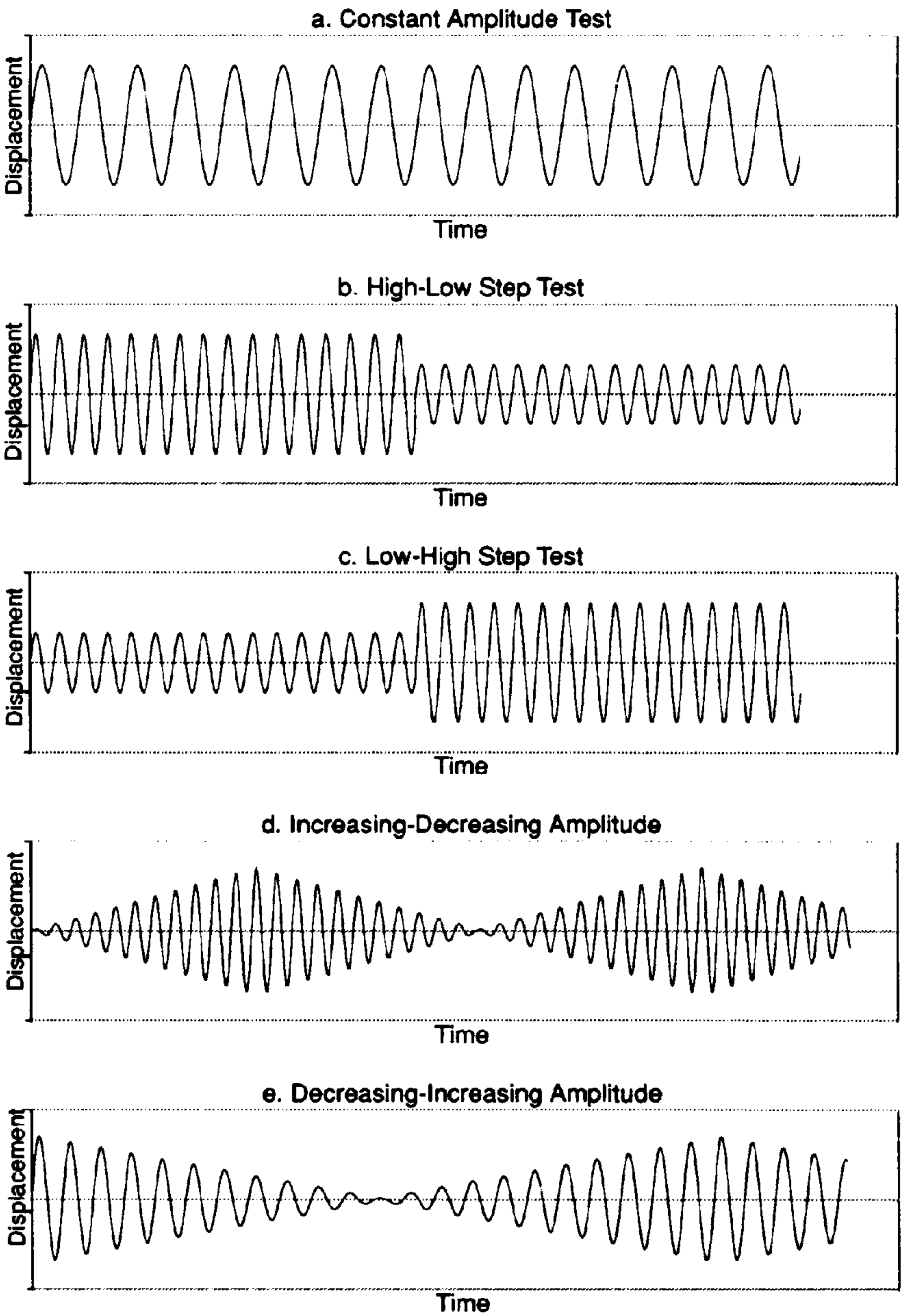

Figure 2-6. Typical Displacement Histories

Due to possible anisotropy of the rolled steel in the longitudinal and transverse directions, four of the eight specimens were taken perpendicular to the rolling direction, and the other four along the rolling direction. Specimens were tested under two different strain rates and each test was duplicated. A summary of the coupon tests is given in Table 2-II. The average stress-strain curve for the two direction is plotted in Figure 2-7.

According to these coupon tests, the yield strength varied between 38.5 ksi (265 MPa) and 48.0 ksi (331 MPa), while ultimate strength varied between 63.5 ksi (438 MPa) and 68.0 ksi (469 MPa). It can be observed from Figure 2-7 and Table 2-II that some directional dependence is apparent. Young's modulus as well as strain hardening modulus is larger for the longitudinal coupon specimens (i.e. specimens that were taken along the rolling direction.). However, as can be concluded from Table 2-II, strain rate did not have a significant effect on the stress-strain properties of the specimens. Specimen elongation at strain hardening is almost the same for each test. The yield strength came out to be larger for longitudinal specimens.

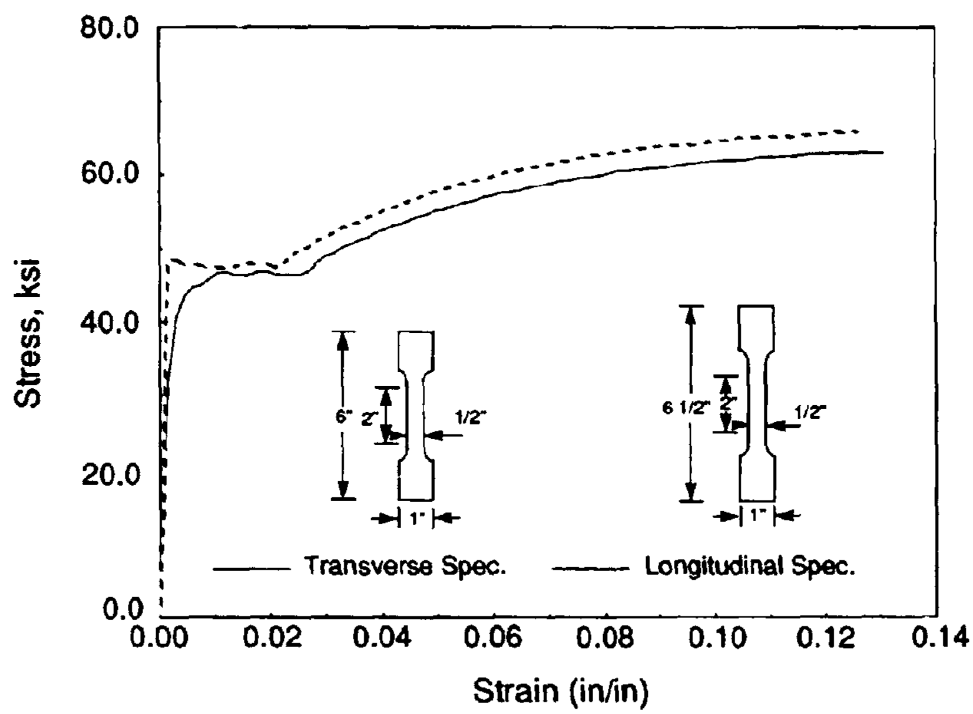

Figure 2-7 Coupon Test Results

Table 2-II Mechanical Properties of Test Specimens[a]

Coupon Id.	Loading Direction	Strain Rate[b] %	Yield Strength (ksi)	Ultimate Strength (ksi)	E_s (ksi)	E_{sh} (ksi)	ε_{sh} (in/in)	ε_{su} (in/ in)
CT1	Trans.[c]	20	41.65	64.16	29,200	420.7	0.0203	0.121
CT2	"	80	42.13	63.47	32,900	489.8	0.0226	0.129
CT3	"	20	38.45	65.07	30,100	432.4	0.0215	0.127
CT4	"	80	43.20	66.13	32,000	419.8	0.0190	0.143
CL5	Longit.[d]	20	45.39	65.60	44,500	549.9	0.0190	0.132
CL6	"	80	48.00	66.13	39,700	519.6	0.0203	0.125
CL7	"	20	45.76	68.00	43,800	503.2	0.0199	0.129
CL8	"	80	44.16	66.67	42,900	592.6	0.0225	0.132

a. To convert ksi to MPa multiply by 6.89495.
b. Defined as the % capacity of the tensile test machine.
c. Loading perpendicular to the rolling direction of the specimen.
d. Loading along the rolling direction.

SECTION 3

EXPERIMENTAL RESULTS

3.1 Introduction

In this section, experimental observations and results are presented in both graphical and tabular form. A summary of testing parameters is given in Section 2, Table 2-I.

One monotonic test was conducted. A total of thirteen specimens were tested under constant amplitude cyclic loading. Specimens R0_10 and R0_11 were subjected to half stress reversals (R=0). The rest of the specimens were cycled through complete stress reversals (R=-1). Five further specimens were tested under variable amplitude displacement histories.

Specific test results are summarized in Tables 3-I to 3-III. Moment-Rotation, Force-Drift hysteretic plots are given in the figures together with the following discussion.

3.2 General Observations

In all of the tests, the same kind of failure mode was observed. The first fine surface cracks occurred on the leg of one of the angles attached to the beam flange, near the toe of the fillet. A hinge line also formed at the same location on the leg attached to the column flange. Especially for the higher drift tests (>5%), another hinge line was observed passing through the bolt holes on the leg of the angle on the column flange, as shown on Figure 3-2. This is not a straight line through the angle width; it also forms half circles around the washers together with radial cracks under the washers. Plastic deformation was also observed in "dishing" of the washers seated on the leg on the column flange (Figure 3-2). Photographs of typical deformation and fatigue crack patterns and failure modes observed in the connection angles are shown in Figures 3-3 to 3-5.

Panel zone deformation in the joint region was observed to be significant, especially for the higher drift tests as discussed in the next section. No observable slip occured between the connection elements.

3.3 Monotonic Test Results

One monotonic test was conducted. Details of the specimen and connection properties are

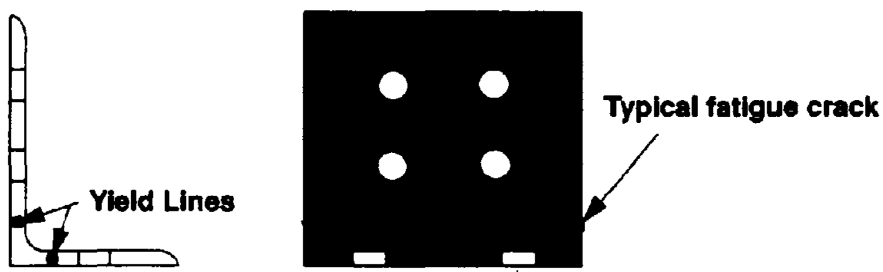

Figure 3-1 Failure Mode

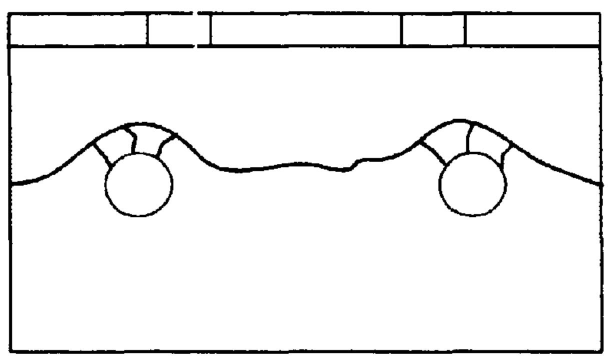

Figure 3-2 Yield Line (Cracks) at Failure

Figure 3-3 Initial Surface Cracks

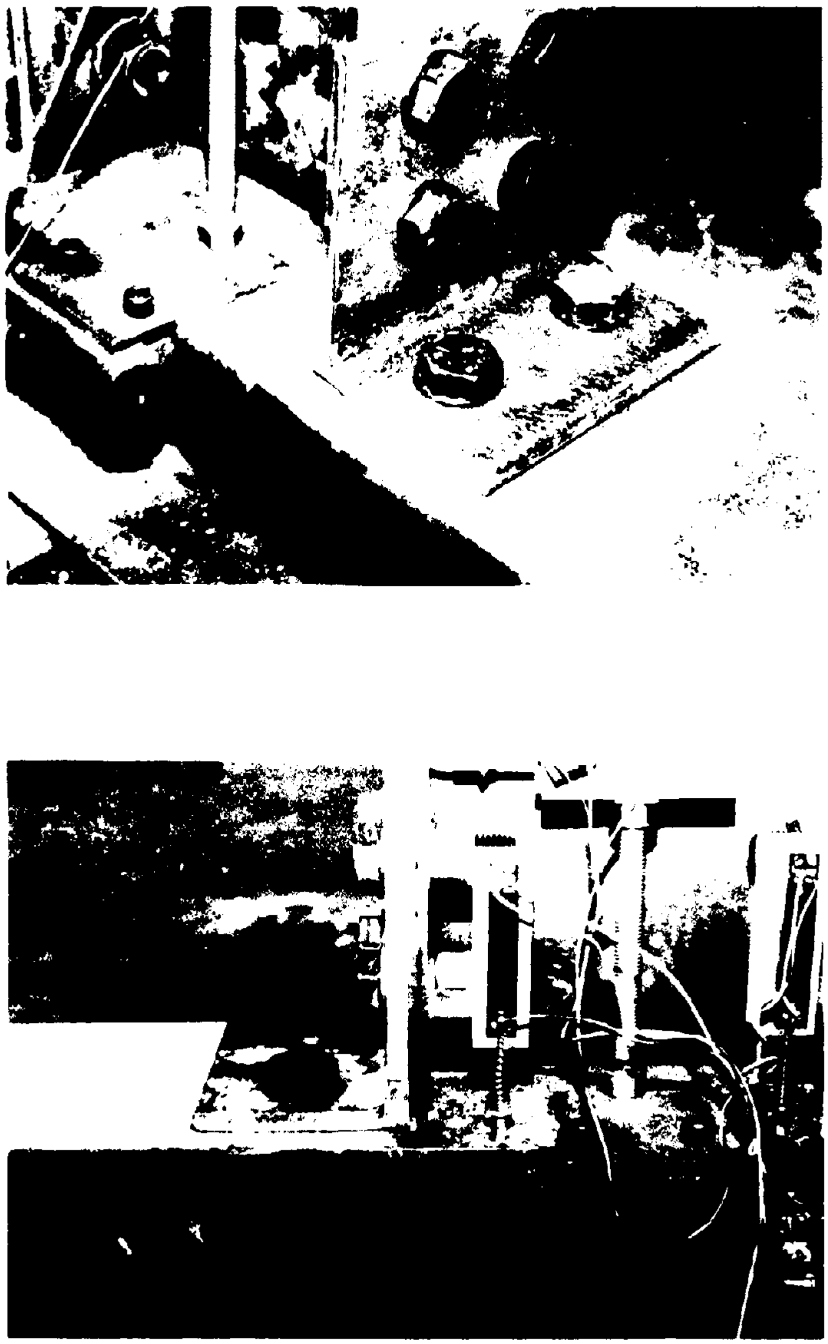

Figure 3-4 Fatigue Cracks Near the End of Cycling

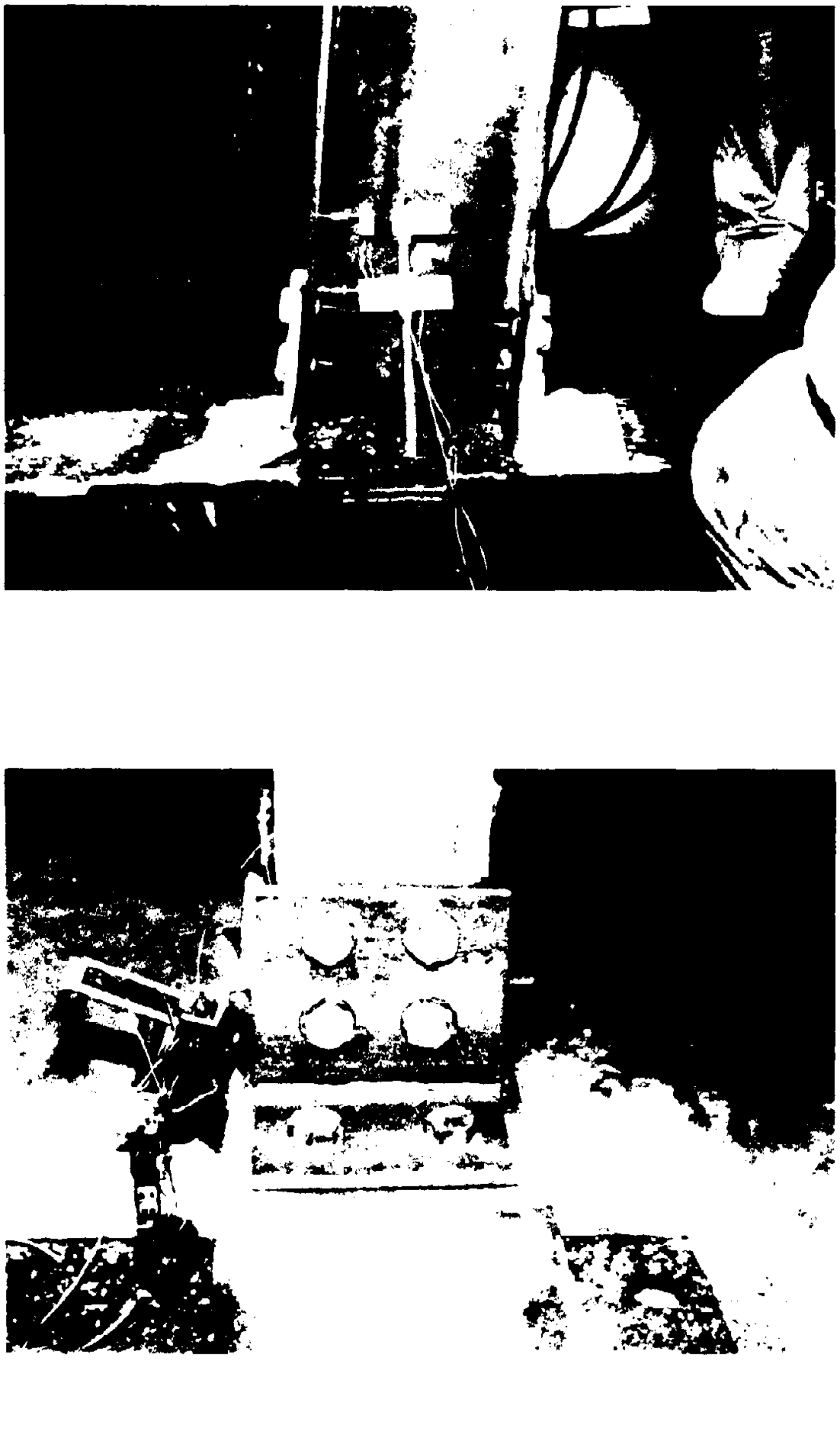

Figure 3-5 Final Fracture

as shown in Figure 2-3. The purposes of this test were to analyze the failure mode and to investigate the ultimate moment capacity of this specific type of top-and-seat angle connection. Force-Drift and M-θ_j graphs are plotted in Figure 3-6.

The ultimate load obtained from the monotonic test was 14.7 kips (65.0 kN) which corresponds to 750 kip-in (84.2 kN-m) connection moment. The connection rotation θ_j, corresponding to the ultimate moment was 0.1 rad. The initial connection stiffness which is determined from M-θ_j plot (Figure 3-6) is 122,500 kip-in/rad (13,750 kN-m/rad).

3.4 Constant, Equi-Amplitude (R=-1) Cyclic Test Results

A series of equi-amplitude cyclic tests were conducted in order to investigate the low-cycle fatigue behavior and to establish a relation between low-cycle fatigue life and energy dissipated as well as connection rotation for this specific type of connection. Eleven specimens were tested under constant amplitude cyclic loading with complete stress reversals (R=-1). Testing parameters for the specimens are reported in Table 2-I, and test specimens and procedures are described in Section 2. A summary of test results is given in Table 3-I. The table includes actuator displacement, testing frequency, percent fatigue life and corresponding moment and connection rotation ranges as well as single and cumulative hysteresis loop areas.

The displacement amplitudes were chosen such that enough data points can be plotted in the low-cycle range on both Rotation vs. Life and Energy vs. Life graphs, in order to establish accurate fatigue life relationships.

M-θ_j and Force-Drift graphs are plotted in Figures 3-7 to 3-13. Hysteretic energy vs. Cycle Number plots are also given for various specimens in Figure 3-14a. It can be observed from Table 3-I that hysteretic energy was almost constant after a few cycles, until the initial fatigue crack occurred. There also appears to be a general trend toward increasing total hysteretic energy accumulation at the longer fatigue lives corresponding to the smaller per-cycle loop areas. The cycle at which the incipient failure occurred (N_f) was defined in two ways; by visual inspection and as the point at which the "Hysteretic energy vs. Cycle Number" graph drops sharply as shown in Figure 3-14b.

Each specimen was tested to complete fracture failure (N_{ff} cycles) and had similar failure modes as described in Section 3.2. However, for lower drift tests (R1_12, R1_13), the

Table 3-I Constant Amplitude Test Results[a]

Spec. Id.	Actuator Displ. (in.)	% Nominal Drift	Freq. (Hz.)	Cyc. #	% Fatigue Life	Range of Moment (kip-in)	Range of Connection Rotation, θj (rad)	Area of Single Hysteresis Loop[b] (kip-in)	Cumulative Area of Hysteresis Loops[c] (kip-in)	Remarks
R1_06	±4.08	8	0.01	1	57	1616	0.1365	119.8	119.8	First crack
				1.75	100	1120	0.1453	86.1	206.0	
R1_09	±3.57	7	0.1	1	31	1508	0.1183	96.8	96.8	First crack Complete failure at 3.25 cycles.
				2	62	1334	0.1229	82.4	179.2	
				3	92	1267	0.1247	79.9	274.1	
R1_05	±3.06	6	0.1	1	24	1466	0.0987	81.2	81.2	First crack observed at 2nd cycle, complete failure at 4.25 cycles
				2	47	1360	0.1023	69.7	150.9	
				3	71	1289	0.1036	67.4	218.3	
				4	94	894.4	0.1101	65.0	295.5	
R1_03	±2.55	5	0.1	1	12	923.5	0.1000	38.2	38.2	First crack observed at 6th cycle, complete failure at 7.75 cycles
				2	26	823.5	0.1020	32.8	70.9	
				3	39	752.9	0.1030	30.3	101.2	
				4	52	741.2	0.1030	29.8	131.1	
				5	65	723.5	0.1030	29.1	160.1	
				6	77	682.4	0.1040	29.1	189.2	
				7	90	576.5	0.1060	27.0	233.6	

Table 3-I Cont'd

Spec. Id.	Actuator Displ. (in.)	% Nominal Drift	Freq. (Hz.)	Cyc. #	% Fatigue Life	Range of Moment (kip-in)	Range of Connection Rotation, θj (rad)	Area of Single Hysteresis Loop[b] (kip-in)	Cumulative Area of Hysteresis Loops[c] (kip-in)	Remarks
R1_02	± 2.04	4	0.05	1	7	805.2	0.0693	26.3[d]	26.3	First crack
				2	15	729.8	0.0686	23.0	49.4	observed at
				8	58	680.9	0.0710	21.1	177.7	9th cycle,
				9	65	672.3	0.0715	21.1	198.8	complete
				12	87	572.2	0.0786	19.1	260.1	failure at
				13	95	508.5	0.0784	15.7	279.3	13.75 cycles
R1_04	± 1.53	3	0.1	1	4	715.0	0.0453	15.1	15.1	First crack
				3	12	693.0	0.0452	13.0	41.3	observed at
				8	32	661.5	0.0458	13.4	107.2	22nd cycle,
				15	59	642.4	0.0463	14.1	204.2	complete
				23	91	523.2	0.0486	13.5	316.7	failure at
				25	99	445.1	0.0510	11.0	345.8	25.25 cycles
R1_01	± 1.02	2	0.05	1	1	577.9	0.0426	6.8	6.8	First crack
				11	11	557.4	0.0423	4.2	54.3	observed at
				25	26	539.6	0.0423	4.2	113.2	73th cycle,
				75	78	530.1	0.0423	4.2	328.5	complete
				95	99	380.8	0.0423	3.0	396.6	failure at
										95.75 cycle.
R1_08	± 0.77	1.5	0.25	1	0.2	543.7	0.0186	3.8	3.8	First crack
				100	22	488.5	0.0200	2.3	237.8	observed at
				250	56	453.1	0.0197	2.3	592.8	397th cycle,
				397	89	400.0	0.0199	2.3	944.1	complete
				445	100	311.5	0.0180	1.3	1043	failure at
										446 cycles

Table 3-I Cont'd

Spec. Id.	Actuator Displ. (in.)	% Nominal Drift	Freq. (Hz.)	Cyc. #	% Fatigue Life	Range of Moment (kip-in)	Range of Connection Rotation, θj (rad)	Area of Single Hysteresis Loop[b] (kip-in)	Cumulative Area of Hysteresis Loops[c] (kip-in)	Remarks
R1_13	±0.408	0.8	0.5	1	0.02	402.7	0.0170	0.528	0.53	First crack observed at 4379th cycle, complete failure at 5341st cycle.
				255	5	386.2	0.0167	0.631	150.4	
				1100	21	380.8	0.0167	0.703	751.5	
				1550	29	379.4	0.0166	0.641	1053	
				2250	42	375.3	0.0164	0.646	1440	
				3100	58	371.2	0.0165	0.629	1854	
				4300	81	361.6	0.0165	0.634	2612	
				5100	95	328.7	0.0164	0.653	3063	
				5320	99	220.5	0.0166	0.506	3245	
				5341	100	213.7	0.0167	0.465	3255	
R1_12	± 0.306	0.6	1	590	3	339.7	0.0112	0.381	224.4	First crack observed at 14461st cycle, complete failure at 17064th cycle.
				4226	25	343.8	0.0116	0.327	1065	
				5406	32	335.6	0.0109	0.756	1258	
				7727	45	327.4	0.0111	0.890	3459	
				9197	54	323.2	0.0109	0.868	4769	
				11292	66	317.8	0.0108	0.749	6589	
				14947	88	300.0	0.0108	0.780	9328	
				15837	93	282.2	0.0109	0.780	10024	
				16477	97	260.2	0.0109	0.773	10520	
				17064	100	257.8	0.0119	0.001	10874	

Table 3-I Cont'd

Spec. Id.	Actuator Displ. (in.)	% Nominal Drift	Freq. (Hz.)	Cyc. #	% Fatigue Life	Range of Moment (kip-in)	Range of Connection Rotation, θ_j (rad)	Area of Single Hysteresis Loop[b] (kip-in)	Cumulative Area of Hysteresis Loops[c] (kip-in)	Remarks
R0_11	+4.08	8	0.1	1	15	827.3	0.0590	33.7	33.7	First crack observed at 3.75 cycle, complete failure at 6.5 cycles
				2	31	755.4	0.0609	19.4	53.1	
				3	46	750.2	0.0619	18.1	71.2	
				4	62	730.5	0.0622	17.8	89.0	
				5	77	690.2	0.0624	17.8	106.7	
				6	92	665.2	0.0652	20.7	127.4	
R0_10	+2.04	4	0.1	1	1	604.4	0.0292	10.3	10.3	First crack observed at 62nd cycle, complete failure at 75.5 cycles
				28	37	543.5	0.0304	4.7	133.5	
				31	41	538.5	0.0305	4.6	147.4	
				62	82	508.7	0.0318	4.6	290.8	
				75	99	391.3	0.0354	7.5	352.4	

a. To convert in. to cm. multiply by 2.54, kip-in to kN.m multiply by 0.11225
b. Includes the area under fractional final cycles.
c. For specimens R1_12 and R1_13, these values are estimated.
d. Estimated value.

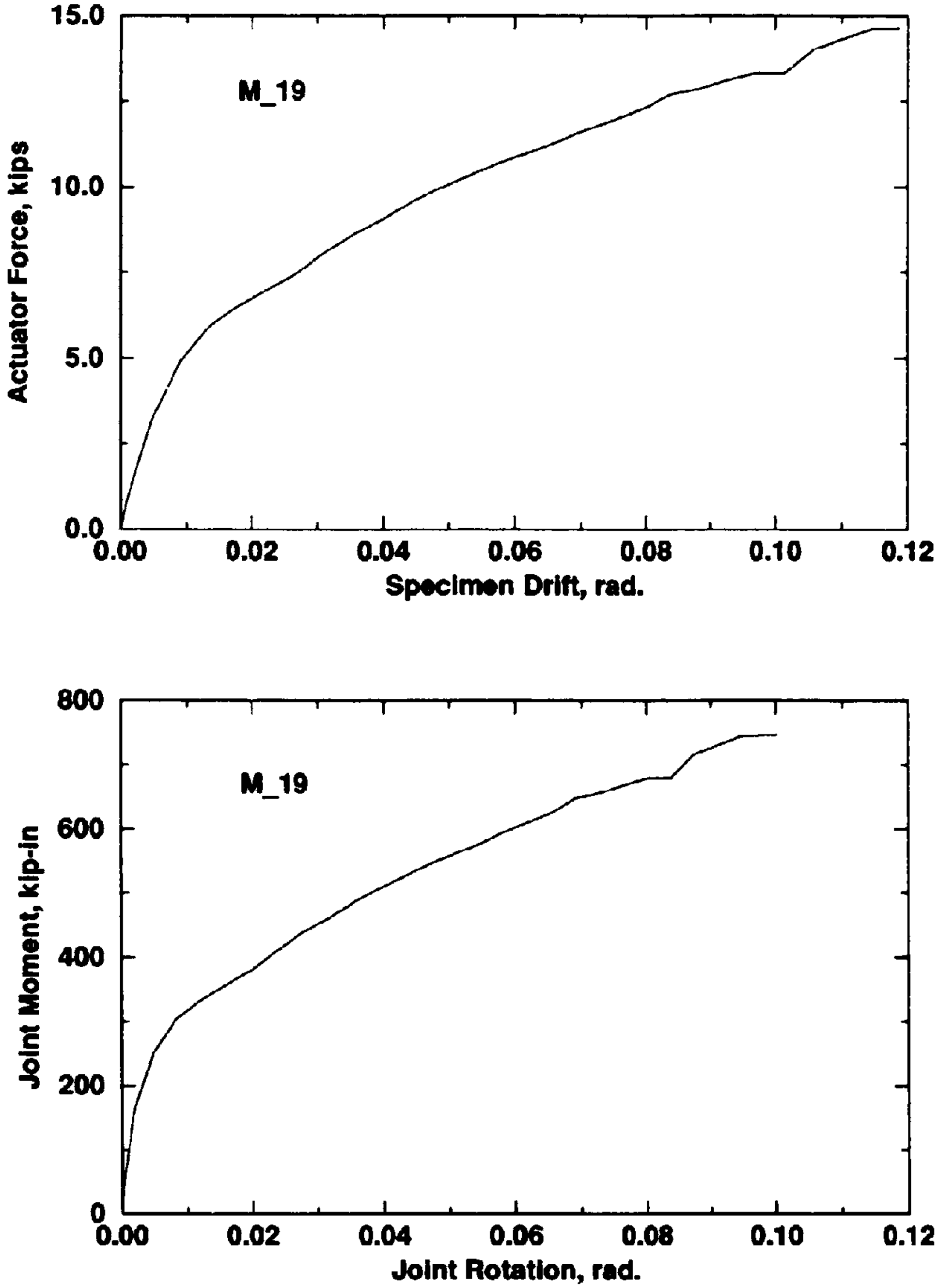

Figure 3-6 Experimental Results for the Monotonic Test Specimen M_19

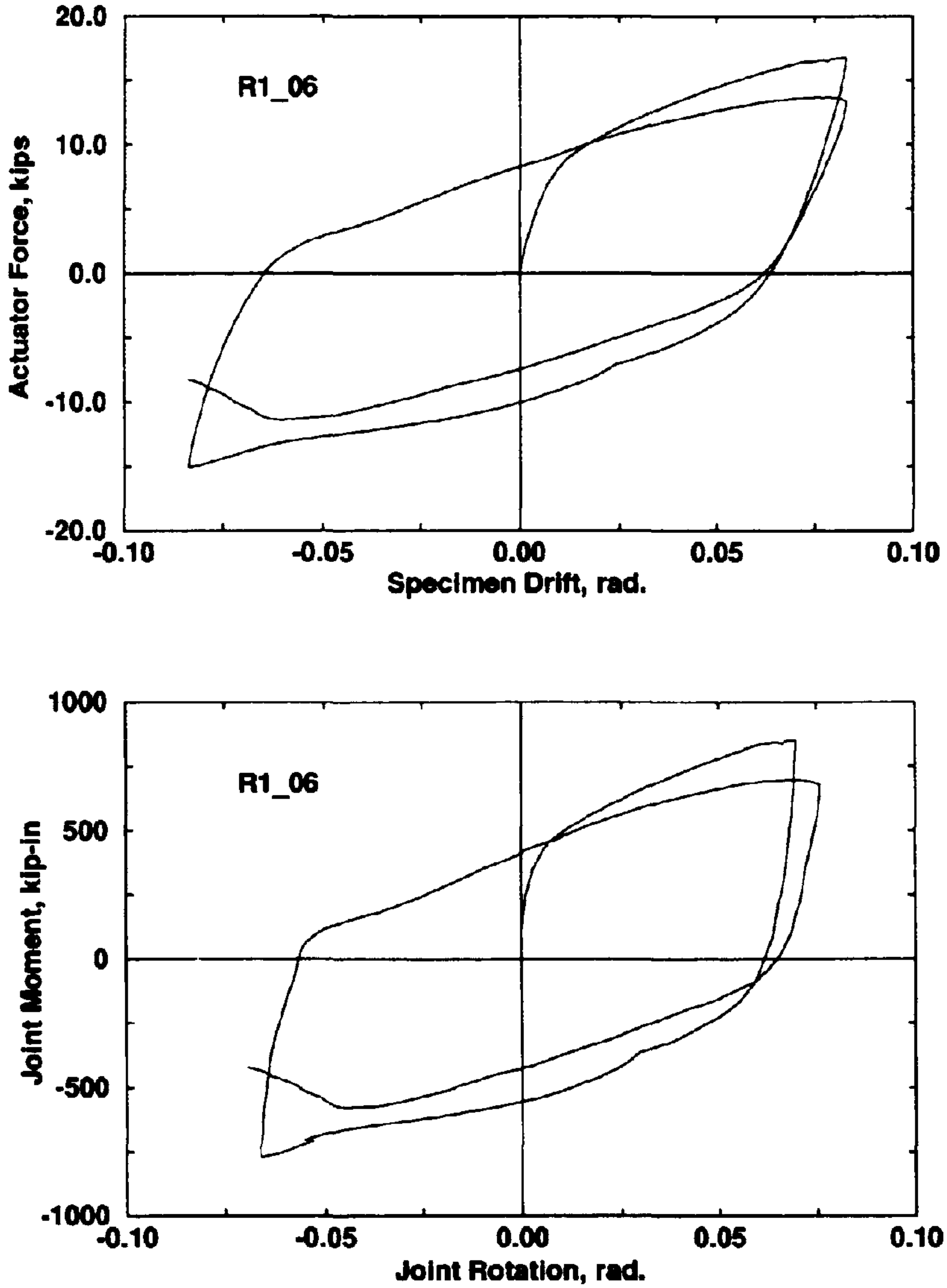

Figure 3-7 Experimental Results for ± 8% Drift Specimen R1_06

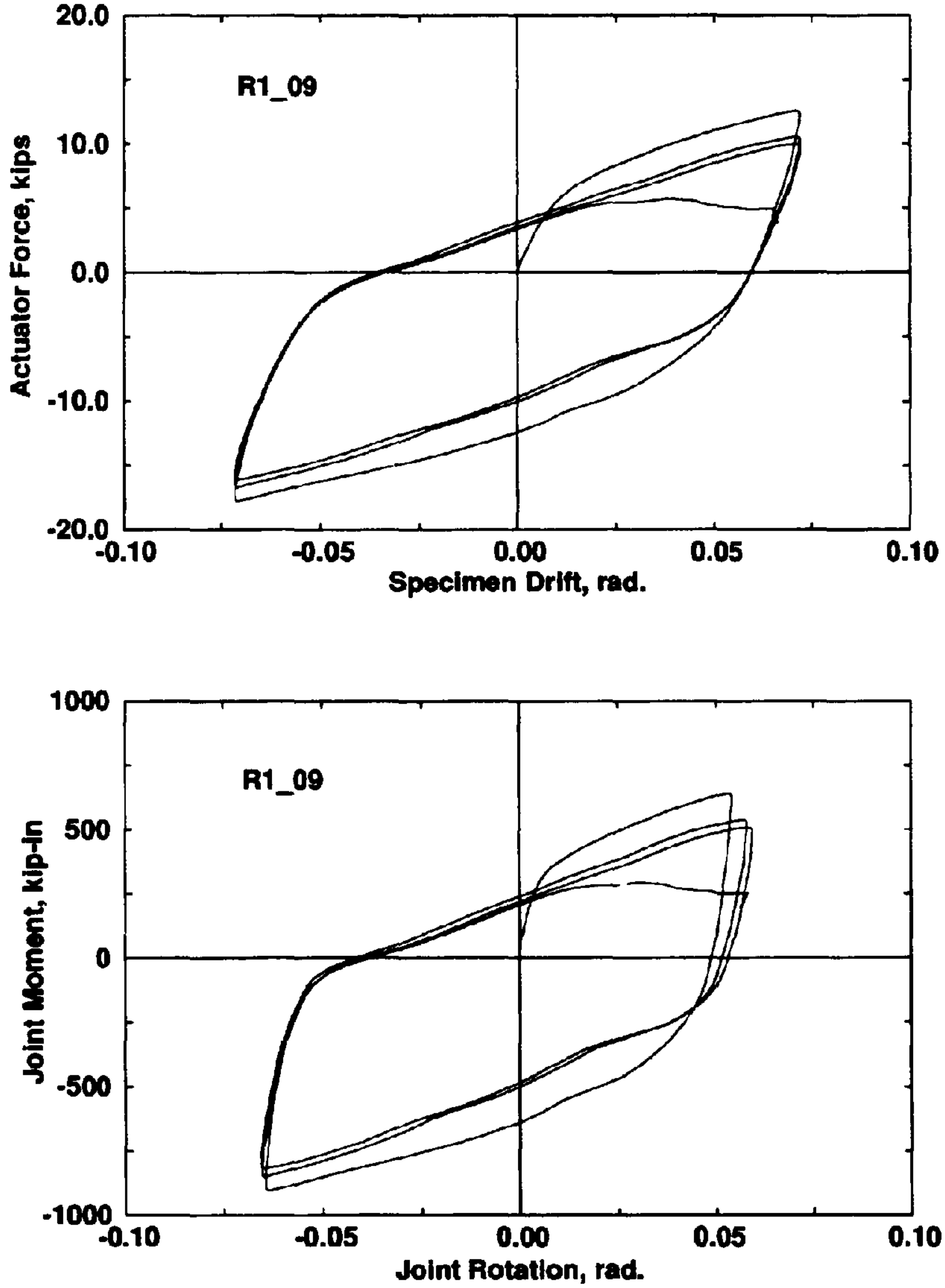

Figure 3-8 Experimental Results for ± 7% Drift Specimen R1_09

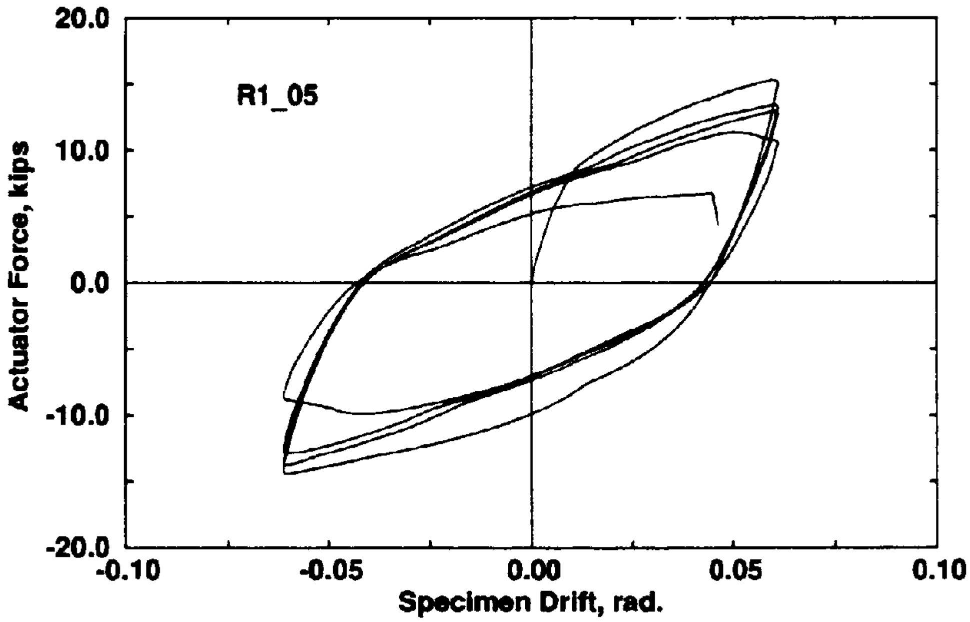

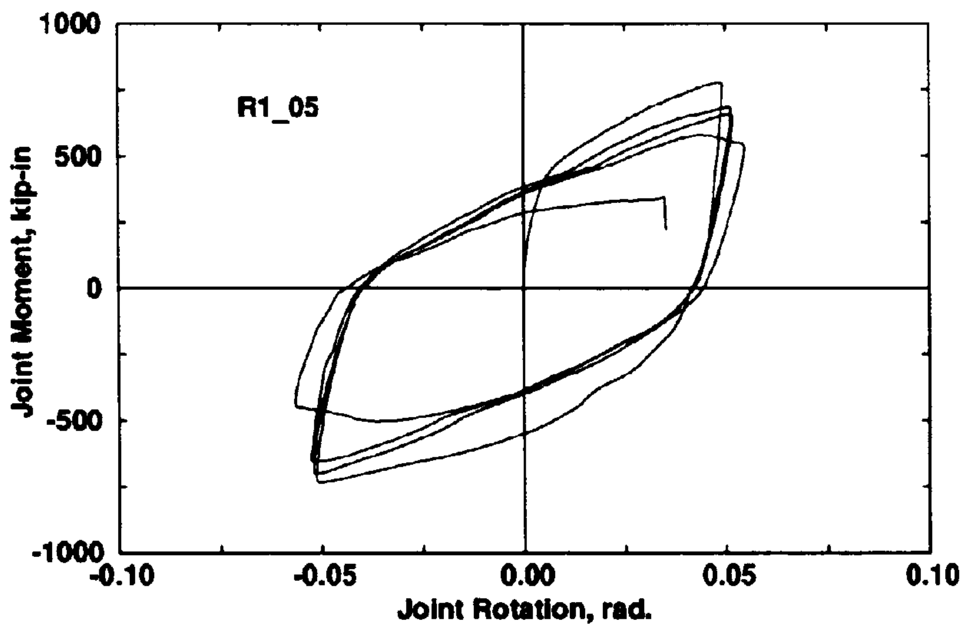

Figure 3-9 Experimental Results for ± 6% Drift Specimen R1_05

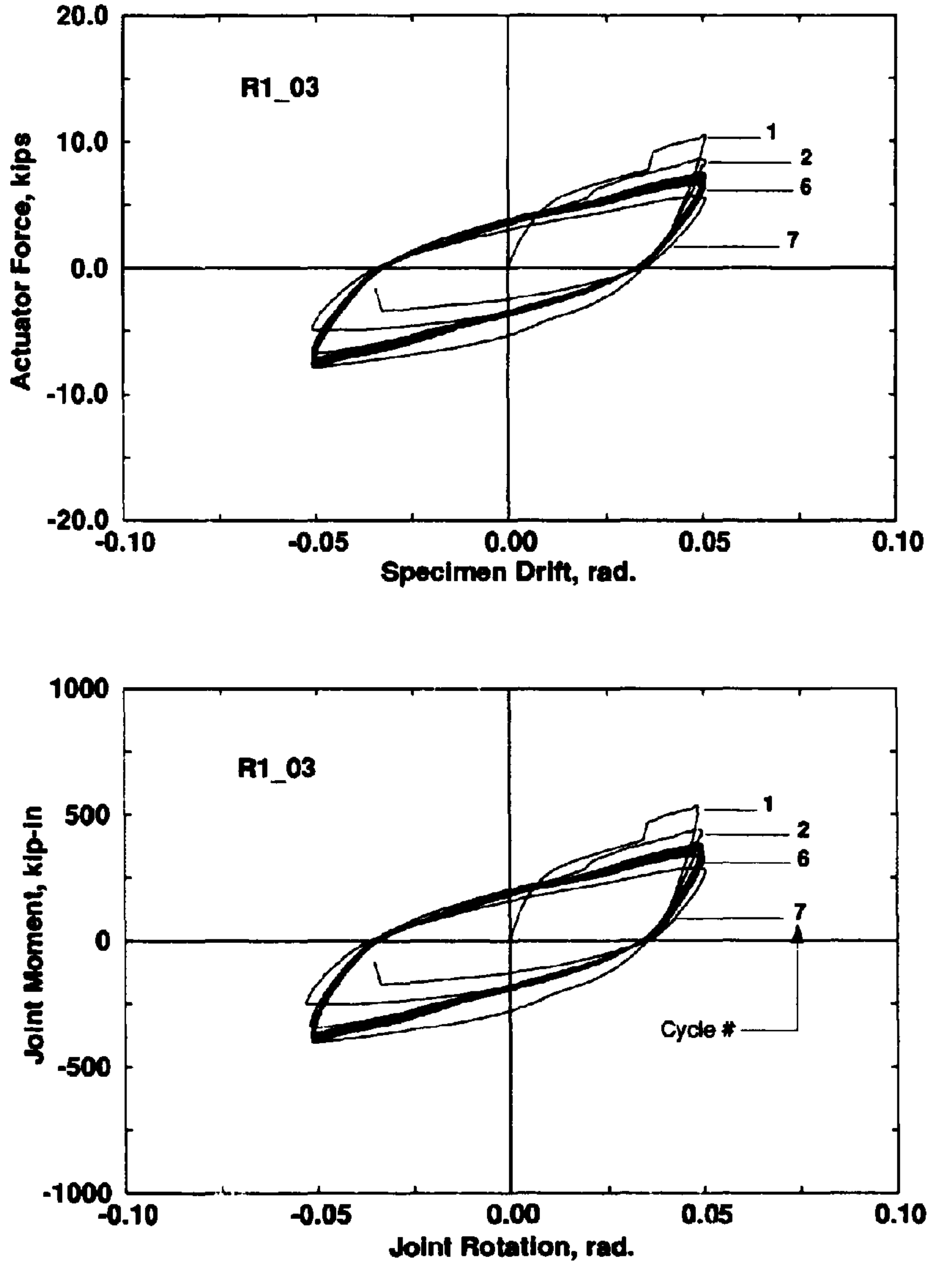

Figure 3-10 Experimental Results for ± 5% Drift Specimen R1_03

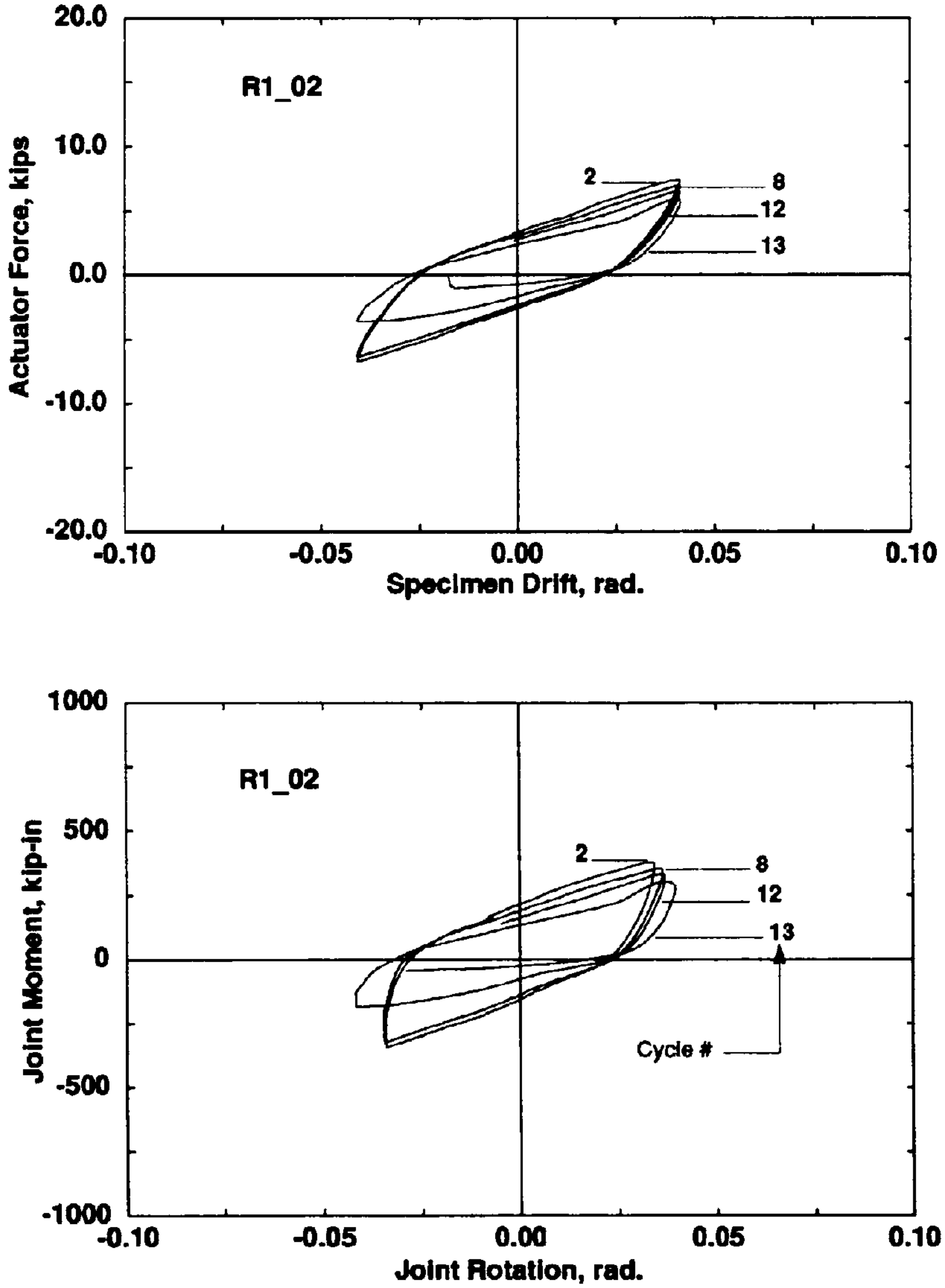

Figure 3-11 Experimental Results for ± 4% Drift Specimen R1_02

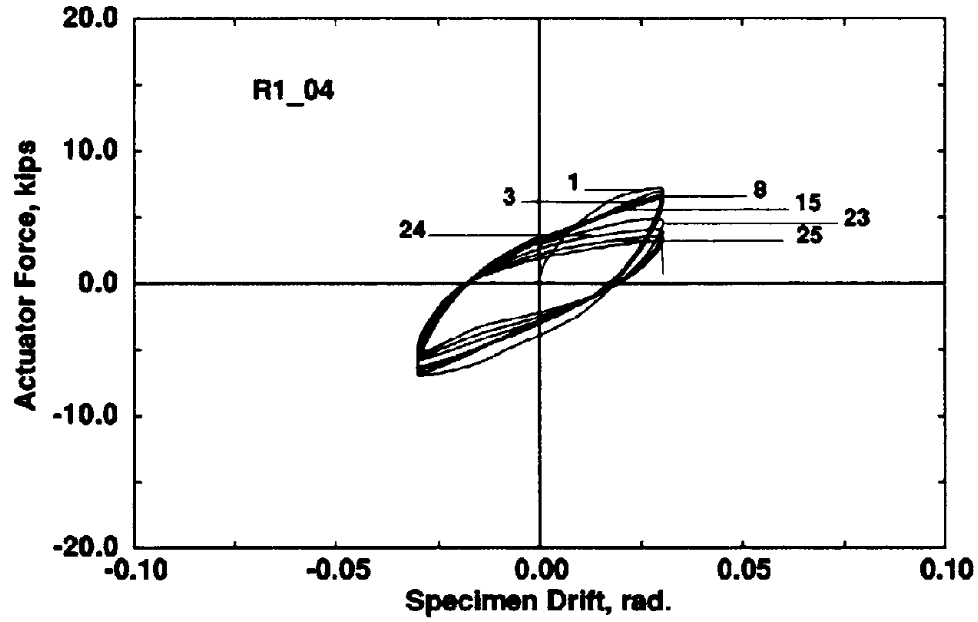

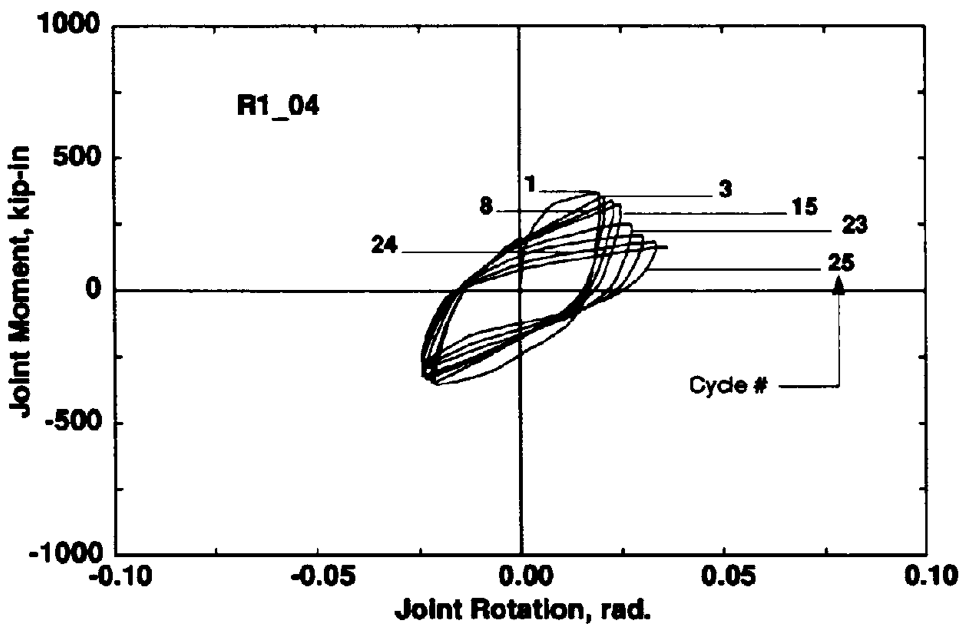

Figure 3-12 Experimental Results for ± 3% Drift Specimen R1_04

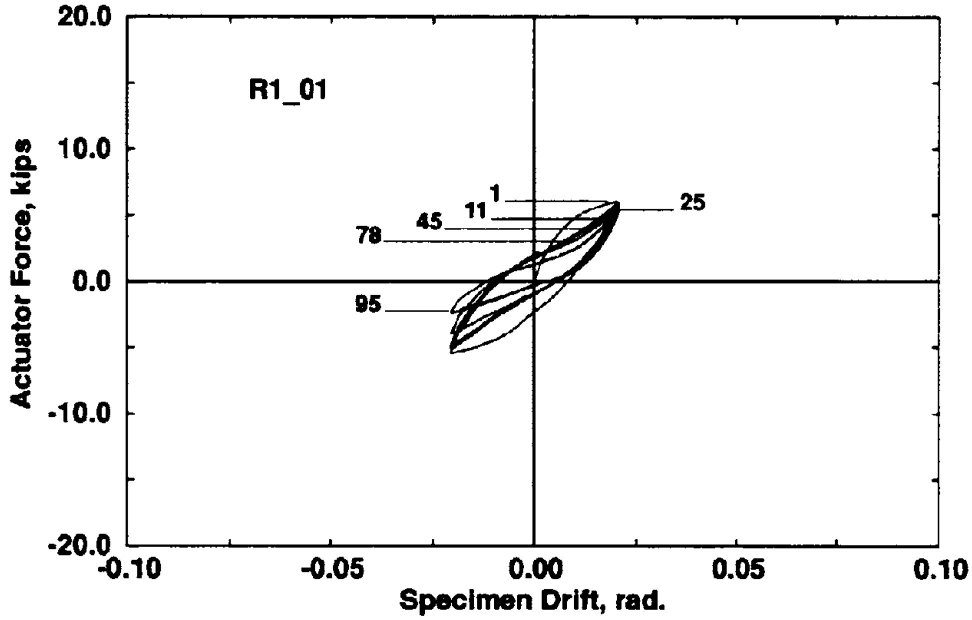

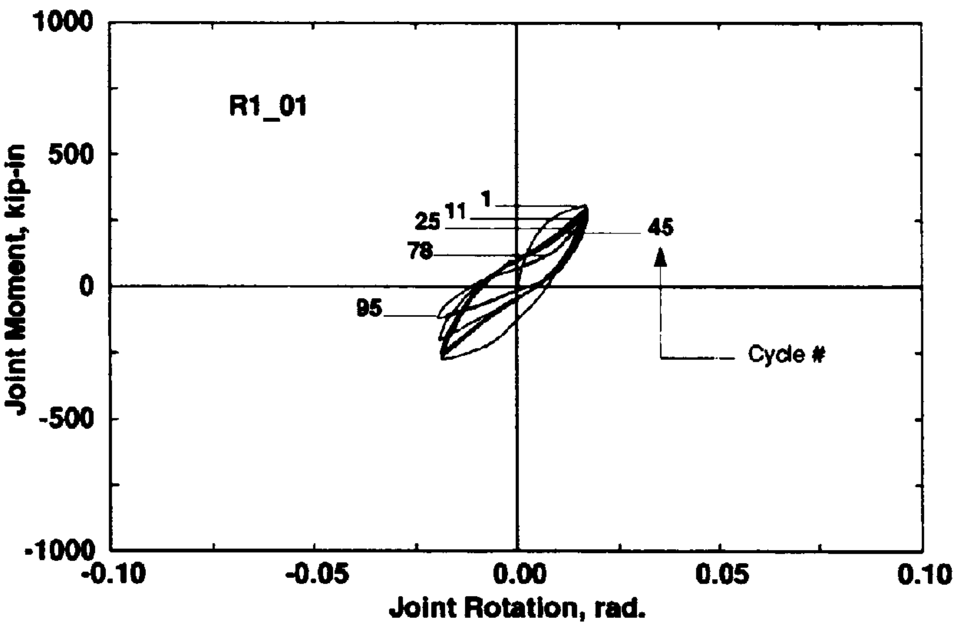

Figure 3-13 Experimental Results for ± 2% Drift Specimen R1_01

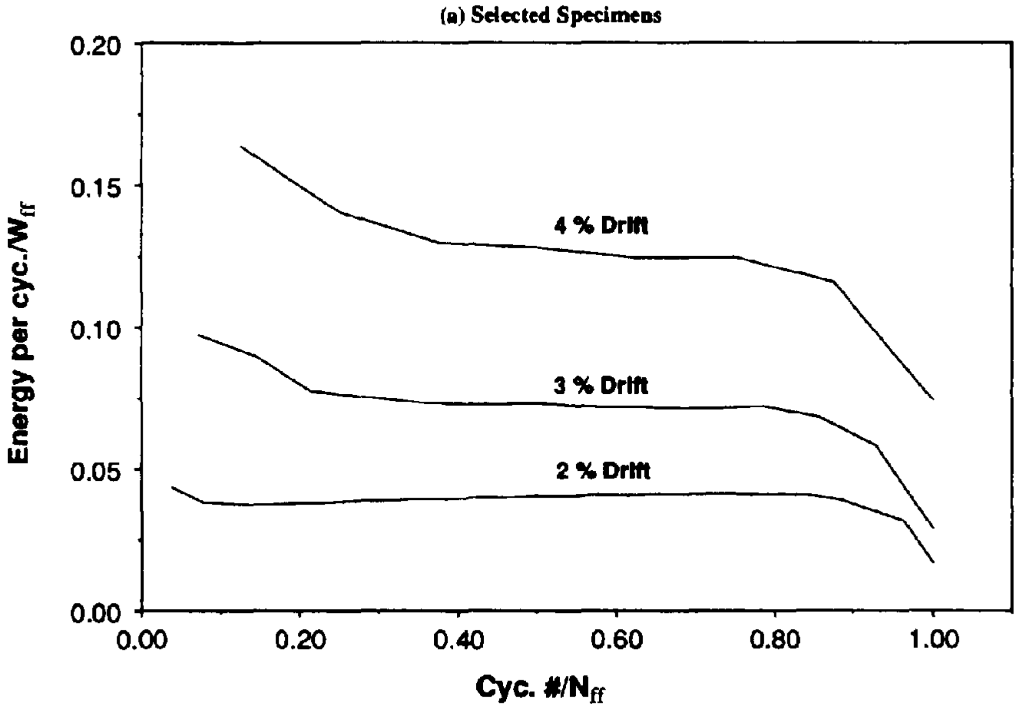

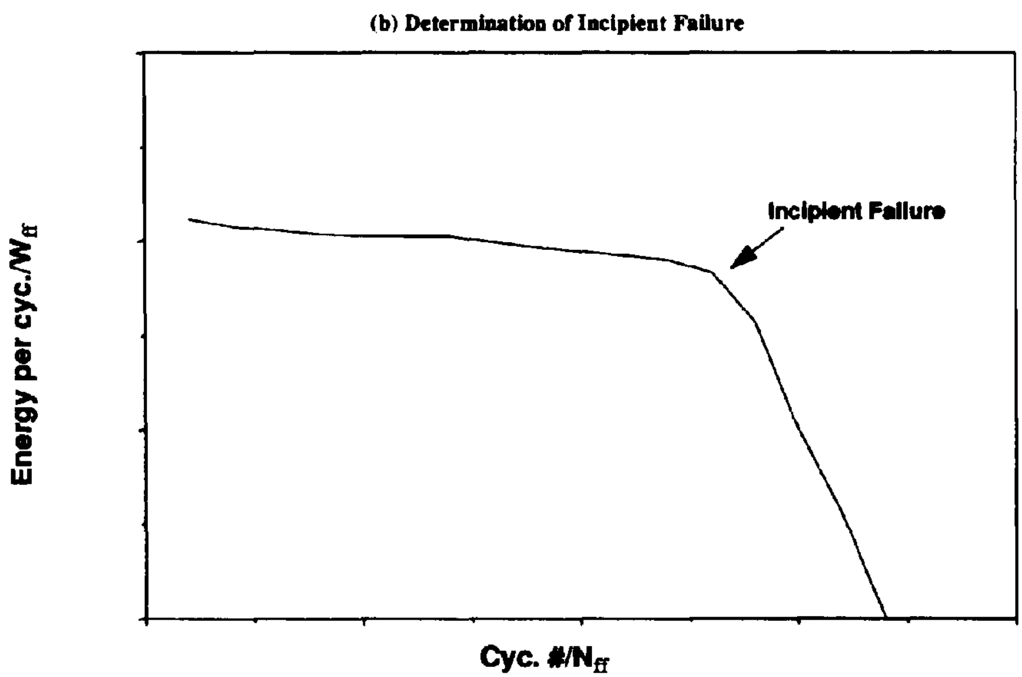

Figure 3-14 Energy vs. Cycle

fatigue crack extended only through about 70% of the angle thickness on the beam flange. In such cases, failure was defined when the moment capacity reduced to a small (but non-zero) value.

3.5 Constant Amplitude (R=0) Cyclic Test Results

Two specimens were tested under constant amplitude cyclic loading with $R \approx 0$, in order to investigate the effect of the type of stress reversals on the connection behavior. Testing procedures are as explained in Section 2 and the testing parameters for the specimens R0_10 and R0_11 are given in Table 2-I. Specific test results are summarized in Table 3-I. M-θ_j and Force-Drift plots are given in Figures 3-15 and 3-16. It should be noted that for these tests, an equivalent equi-amplitude rotation is defined as $\theta_j = \dfrac{\theta_{maxj} - \theta_{minj}}{2}$. This is necessary to make a meaningful comparison with the other (R=-1) constant amplitude tests.

Failure occurred in the angle which was on the tension side.

3.6 Variable Amplitude Test Results

A total of five specimens were tested under variable amplitude displacement histories. Three specimens (V_16, V_17, V_18) were subjected to step histories in which the connection was initially cycled at a certain drift for a specified number of cycles. After this, the amount of drift was either increased or decreased and the test was resumed until the complete fracture failure occurred. Two specimens (V_14, V_15) were tested under sinusoidally increasing or decreasing displacement amplitudes. A summary of the testing parameters are given in Table 2-I.

M-θ_j, Force-Drift, relationships obtained from the variable amplitude tests are given in Figures 3-17 to 3-21. The test results are summarized in Table 3-II. The table includes the actuator displacement, the total number of cycles applied at each displacement block, test frequency and cumulative number of cycles. The range of rotation and the range of moment are also given with the single and cumulative loop areas. Single hysteresis loop areas were calculated as the average of the loop areas at a particular displacement block for step tests. However, exact loop areas were reported for sinusoidally increasing or decreasing amplitude tests.

From the constant amplitude test results, fatigue life relationships have been developed (see Section 5 and 6) for application to appropriate cumulative damage models in order to predict total fatigue lives of connections subjected to variable amplitude displacement histories. The variable amplitude tests thus provide initial data to check the proposed damage models.

The results for the variable amplitude step tests are summarized in Table 3-II. One of the specimens (V_16) was subjected to low-to-high constant amplitude displacement blocks; first 2% drift for 50 cycles and then 4% drift until complete fracture failure, for a total of 58 cycles (Figure 3-17). Specimen V_17 and V_18 were tested under high-to-low constant amplitude displacement blocks. V_17 was first subjected to 4% drift for 8 cycles after which it sustained 173 cycles at 2% drift before failure (Figure 3-18). V_18 was tested under three different displacement blocks; first 4% drift for 5 cycles and then 3% drift for 10 cycles. Complete failure occurred during the 152th cycle at 2% drift (Figure 3-19). For these tests, the number of applied cycles for the initial displacement blocks was so chosen to consume approximately half the estimated life based on range of rotation observed from the equi-amplitude tests.

Finally, specimens V_14 and V_15 were subjected to sinusoidally increasing or decreasing displacement amplitudes between 0% and 4% within 20 cycles with a cycling frequency of 0.1 Hz. Specimen V_14 was tested by varying the drift amplitude initially from 0% to 4%. The fracture failure occurred during 64th cycle. Incipient failure was observed at the 60th cycle. Some selected cycles are shown in Figure 3-20. Specimen V_15, however, was subjected to initially decreasing drift amplitudes. The first surface crack was visually observable after the 46th cycle, and failure occurred at the 75th cycle. Figure 3-21 shows hysteretic loops at various stages of the test. Test results are reported in Table 3-III. The table includes moment and connection rotation range, total drift, area of single hysteresis loop and the cumulative area of the hysteresis loops.

3.7 Discussion

The moment-rotation relationship was observed to be nonlinear early in the loading sequence. For the monotonic test, the connection was loaded to complete fracture failure which occurred at approximately 12% drift (corresponding to 0.1 rad. connection rotation). After 1% drift (0.008 rad. joint rotation) was reached, the connection stiffness did not change significantly until before the failure.

Figure 3-5 shows a brittle fracture failure which is possibly because of the orientation of rolling direction of the steel, i.e. it is perpendicular to the tensile stresses, as explained in Section 2.6. Although it has not been investigated in the present study, the effect of the hole size and geometry

Table 3-II Variable Amplitude - Step Test Results[a]

Spec. Id.	Actuator Displ. (in.)	% Nominal Drift	Freq. (Hz.)	Cyc. #	Range of Moment (kip.in)	Range of Connection Rotation, θ_j (rad)	Area of Single Hysteresis Loop[b] (kip.in)	Cumulative Area of Hysterisis Loops (kip.in)	Remarks
V_16	1.02	2	0.1	1	613.7	0.0272	6.3	6.3	First crack observed at 55th cycle.
				50	542.9	0.0275	4.7	234.8	
	2.04	4	0.1	51	721.3	0.0638	20.9	255.7	
				58	450.4	0.0695	16.0	393.6	
V_17	2.04	4	0.1	1	906.6	0.0644	21.2	21.2	First crack observed at 96th cycle.
				8	694.4	0.0661	17.3	148.3	
	1.02	2	0.1	9	402.7	0.0346	5.7	154.0	
				181	268.5	0.0357	2.4	781.5	
V_18	2.04	4	0.1	1	680.7	0.0740	23.0	23.0	First crack observed at 80th cycle.
				5	617.7	0.0580	11.8	96.1	
	1.53	3	0.1	6	546.5	0.0500	9.4	105.5	
				14	541.0	0.0502	9.4	180.2	
	1.02	2	0.1	15	483.5	0.0413	5.8	185.9	
				152	278.0	0.0286	1.2	646.6	

a. To convert in. to cm. multiply by 2.544, kip.in to kN.m by 0.11225.
b. Includes the area under fractional final cycles.

Table 3-III Other Variable Amplitude Test Results[a]

Spec. Id.	Freq. (Hz.)	% Drift	Cyc. #	Range of Moment (kip.in)	Range of Connection Rotation, θ_j (rad)	Area of Single Hysteresis Loop[b] (kip.in)	Cumulative Area of Hysterisis Loops (kip.in)	Remarks
V_15	0.1	3.96	1	816.3	0.0614	20.2	20.2	First crack observed at 60th cycle. Complete failure at 74th cycle.
		2.95	6	593.1	0.0462	8.2	78.0	
		1.93	12	349.3	0.0317	2.5	105.9	
		3.15	35	631.4	0.0488	8.1	150.7	
		2.54	46	436.9	0.0420	8.0	283.9	
		2.13	68	323.2	0.0366	1.5	319.0	
		1.97	74	321.9	0.0329	4.5	341.7	
V_14	0.1	1.69	8	549.2	0.0196	2.4	6.7	First crack observed at 18th cycle. Complete failure at 64th cycle
		2.75	14	679.3	0.0397	8.1	40.8	
		3.57	18	756.0	0.0538	13.9	87.6	
		1.53	33	301.3	0.0260	1.9	224.9	
		2.55	53	493.1	0.0405	5.7	253.2	
		3.57	63	471.2	0.0604	10.2	375.0	

a. To convert in. to cm. multiply by 2.544, kip.in to kN.m by 0.11225

b. Includes the area under fractional final cycles on the moment capacity of the connection is significant, since the plastic yield line pattern would change with those geometric properties.

It is evident that the total energy dissipated during the course of a cyclic loading is not constant for different range of connection rotations and fatigue lives. However, it was observed that for a given connection rotation, the per-cycle hysteresis energy was nearly constant after a few cycles till incipient failure. The energy-fatigue life relationship is discussed in detail in Section 5. From Tables 3-I to 3-II, it can be concluded that the total hysteretic energy accumulation increases at the longer fatigue lives corresponding to smaller per cycle loop areas. Total hysteretic energy ranged between 206.0 kip-in (23.3 kN-m) for ±8 % drift (N_f = 0.5 cyc., N_{ff} = 1.75 cyc.) and 1043 kip-in (117.9 kN-m) for ±1.5 % drift test (N_f = 397 cyc.,N_{ff} =446 cyc.) for constant amplitude tests. For the two tests at ±0.6 % (N_f = 14461 cyc., N_{ff} = 17064 cyc.) and ±0.8 % (N_f = 4379 cyc., N_{ff} = 5341 cyc.) drift, these values were 10900 kip-in (1220.6 kN-m) and 3250 kip-in (365.3 kN-m), respectively.

It can be observed that the R factor does not have a significant effect on joint behavior. In order to make a direct comparison, if one considers the equi-amplitude 2% drift test with R=-1 (R1_01) and 4% with R=0 (R0_10), in the 2% drift test with complete stress reversals (R=-1), the fatigue life till complete fracture failure (N_{ff}) came out to be approximately 96 cycles whereas, for the R=0 test with the corresponding drift value, fatigue life was 76 cycles. Moreover, in terms of hysteretic energy, cumulative energy up to fracture failure was within 10% (Table 3-I). However, parameters related to the incipient failure can give a better comparison as shown in Table 3-I. Fatigue lives (N_f) for R=-1 and R=0 tests are 73 and 62 cycles, respectively. It should also be noted that the average area for single hysteresis loop has a comparable value for the two tests. This comparison is also given in Section 5, on the fatigue-life plots.

The general purpose of the cyclic tests was to quantify the cyclic moment-rotation characteristics of this specific type of top-and-seat angle connection. In order to establish the fatigue-life relationships, constant amplitude test results have been used in the rest of this report. These relationships are mainly based on the total and plastic connection rotation as well as energy absorption capacities and later applied to a damage model for predicting the low-cycle fatigue behavior of the connection which is subjected to variable amplitude displacement histories.

As can be seen in Table 3-II, the fatigue life for the low-to-high step test (V_16) is 55 cycles whereas for the high-to-low step test (V_17), it is 96 cycles. At each test, the number of cycles for the first displacement block was chosen to be almost one half of the fatigue life for the constant amplitude test with the same amplitude. The cyclic behavior of the connection under low-to-high rotation amplitudes is observed to be quite different than that under high-to-low rotation amplitude.

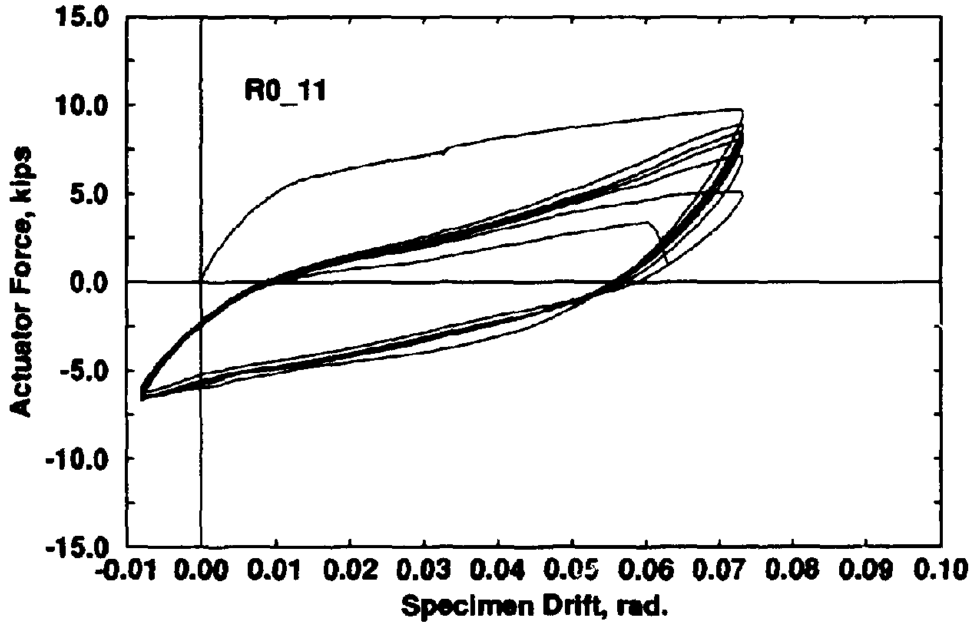

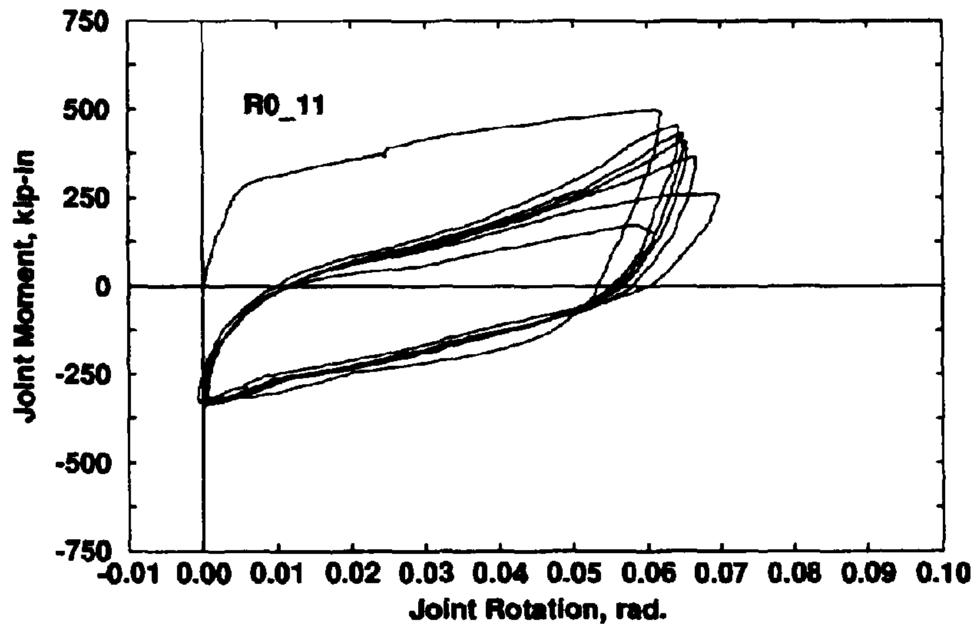

Figure 3-15 Experimental Results for the One-Sided Test (R=0) at +8% Drift Specimen R0_11

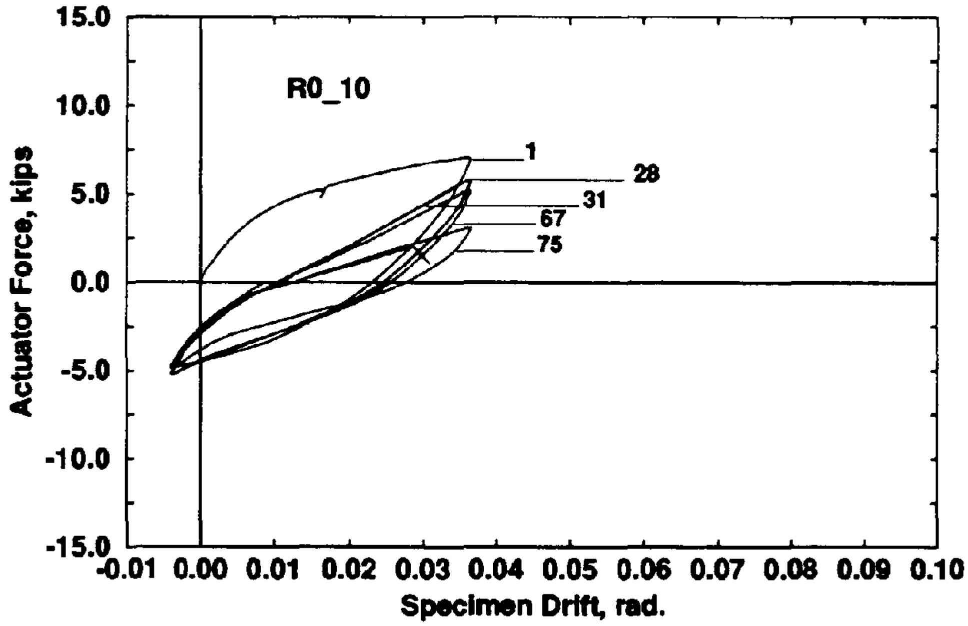

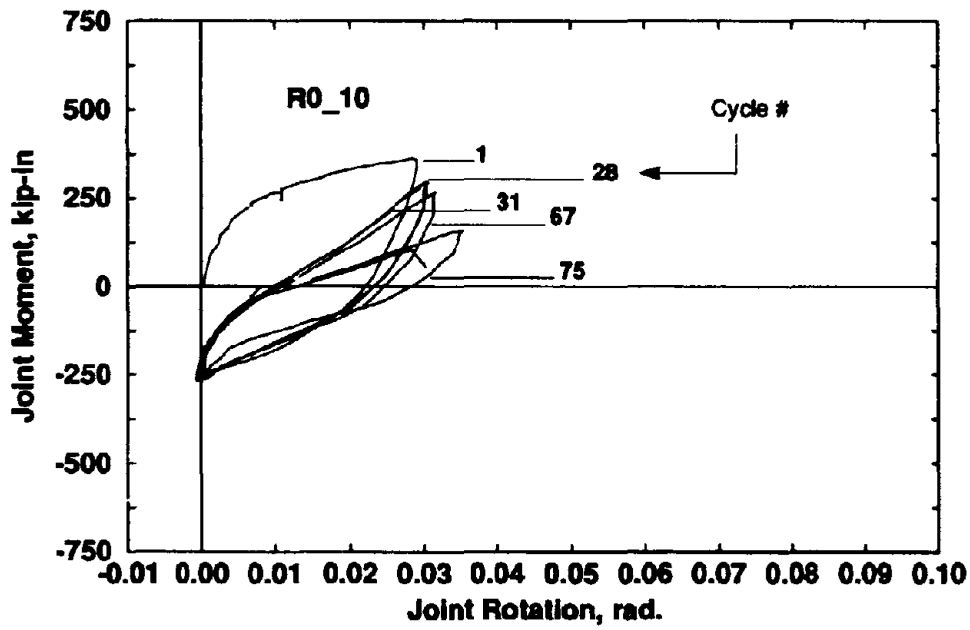

Figure 3-16 Experimental Results for the One- Sided Test (R=0) at +4% Drift Specimen R0_10

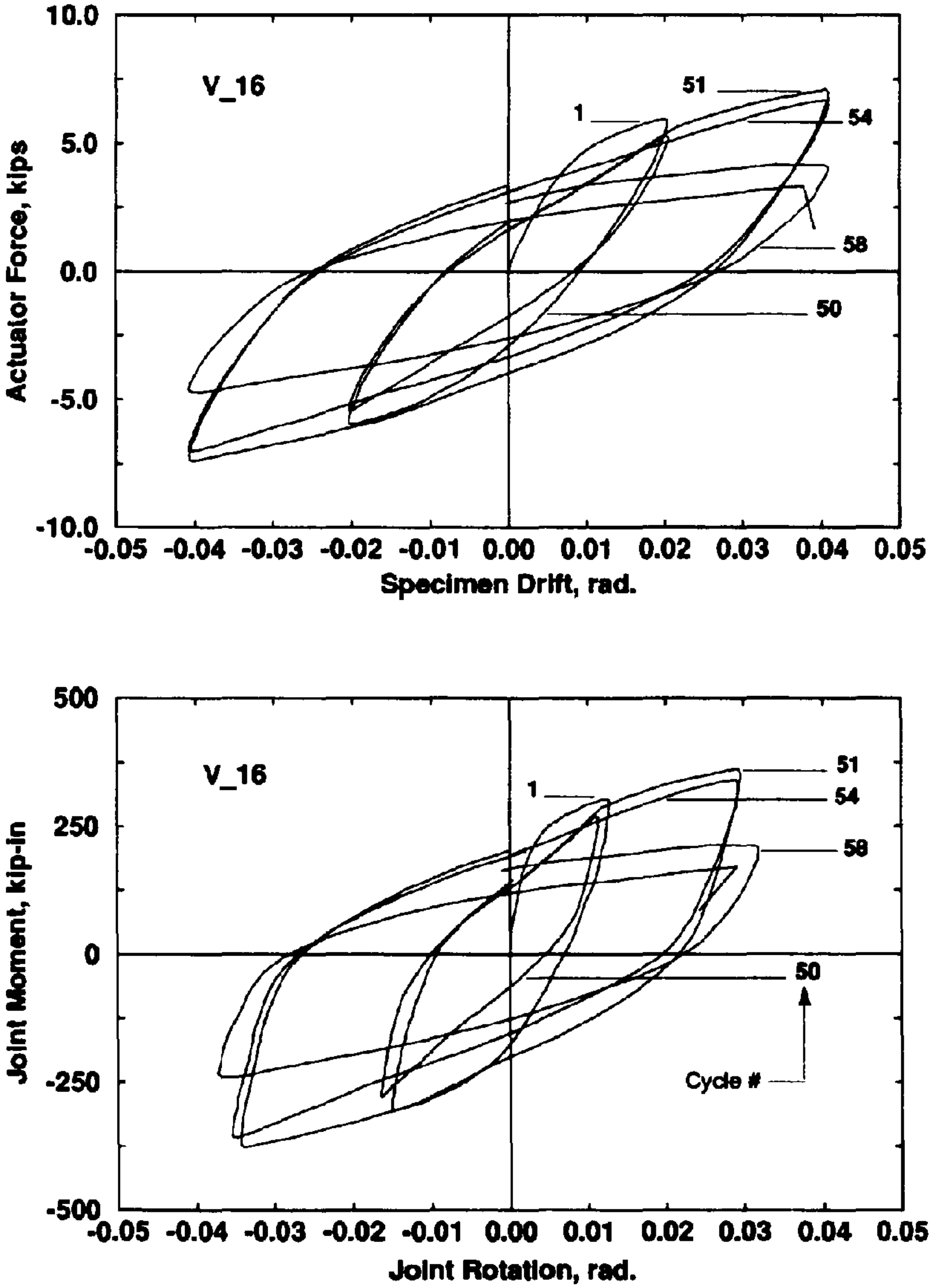

Figure 3-17 Experimental Results for the Step-Test at ± 2%, ± 4% Drift Specimen V_16

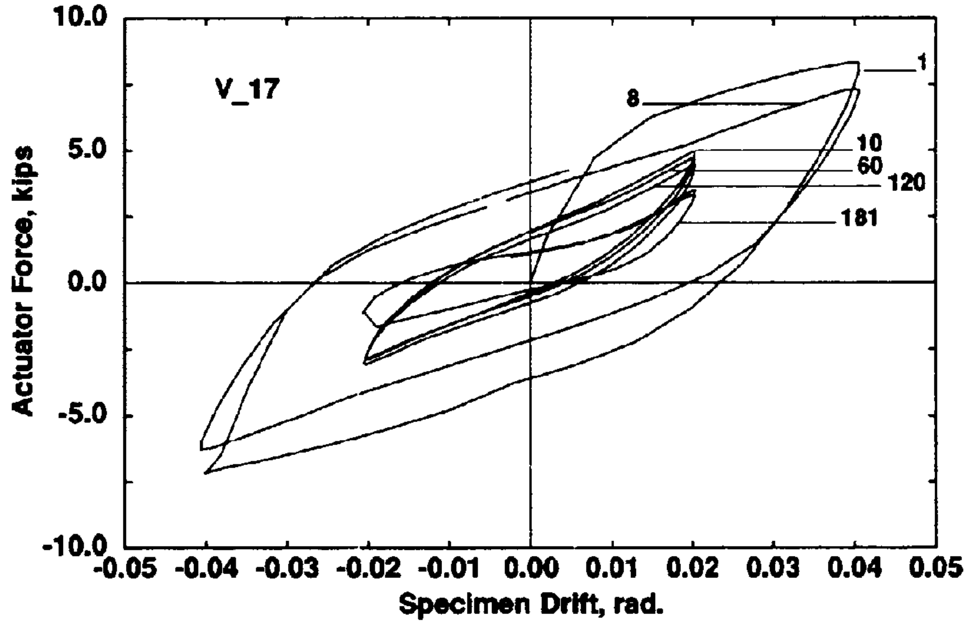

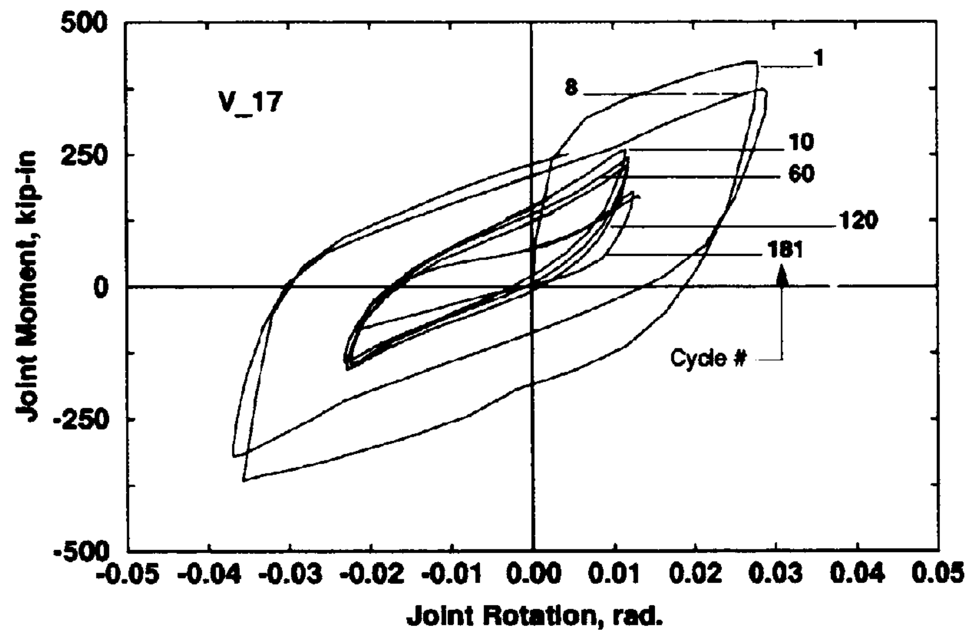

Figure 3-18 Experimental Results for the Step-Test at ± 4%, ± 2% Drift Specimen V_17

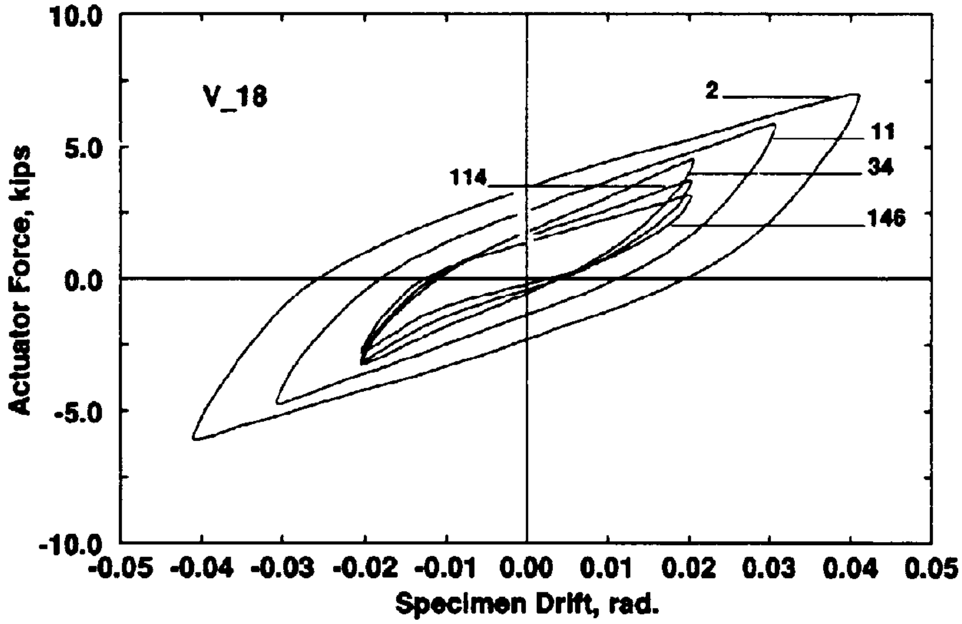

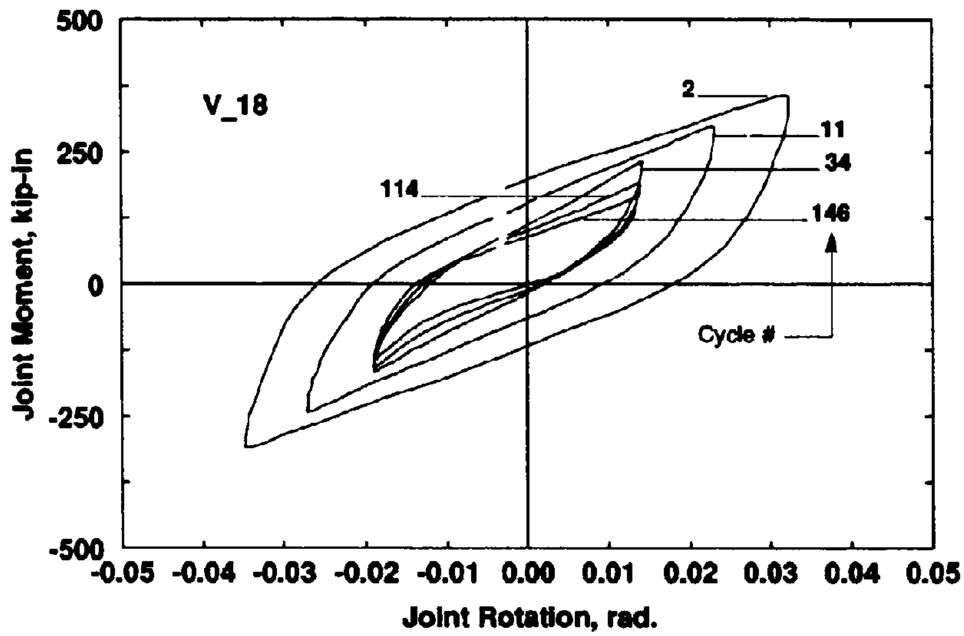

Figure 3-19 Experimental Results for the Step-Test at ± 4%, ± 3%, ± 2% Drift Specimen V_18

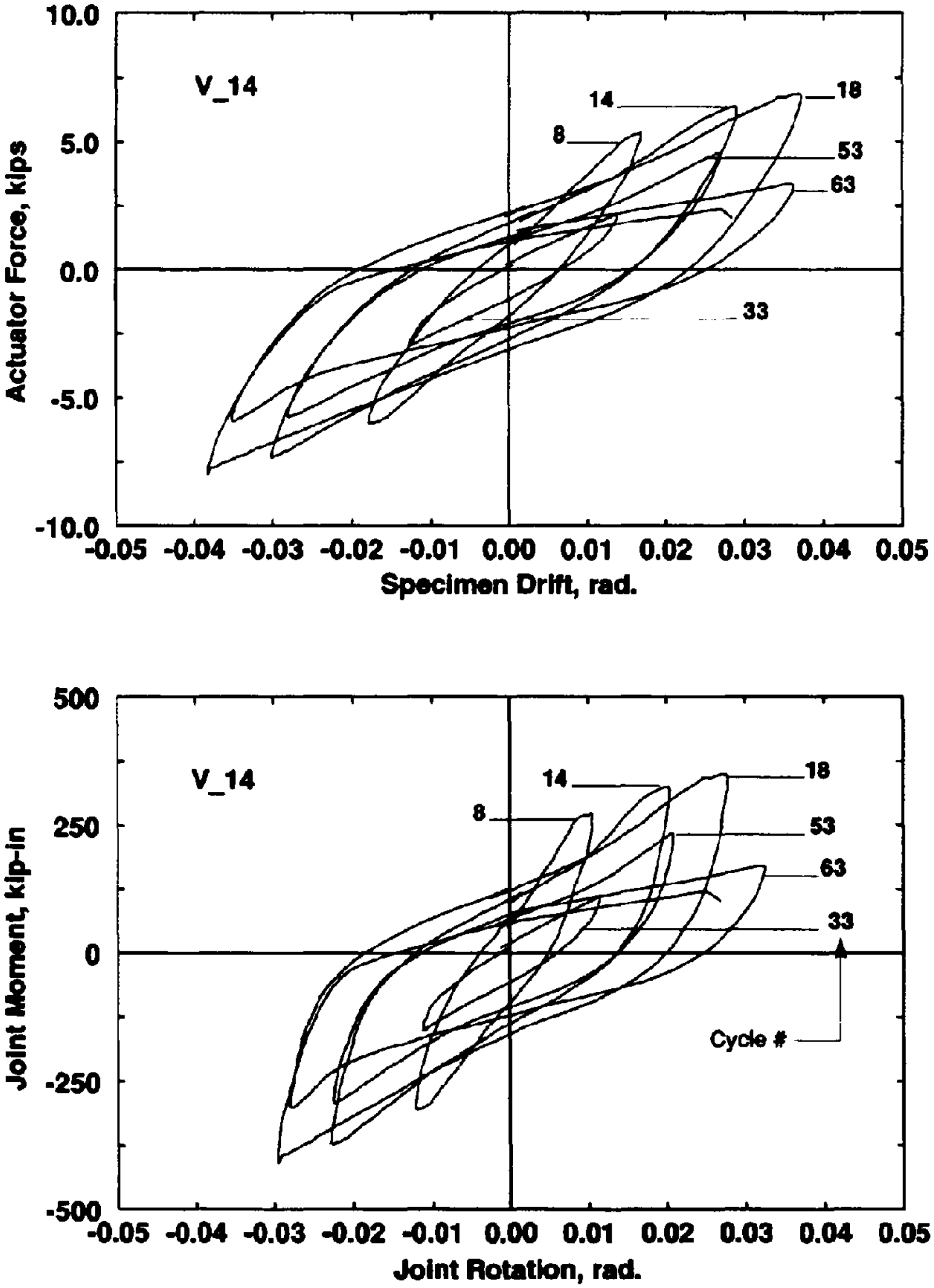

Figure 3-20 Experimental Results for the Incremental-Decremental Test ± 0 to 4% Drift, Specimen V_14

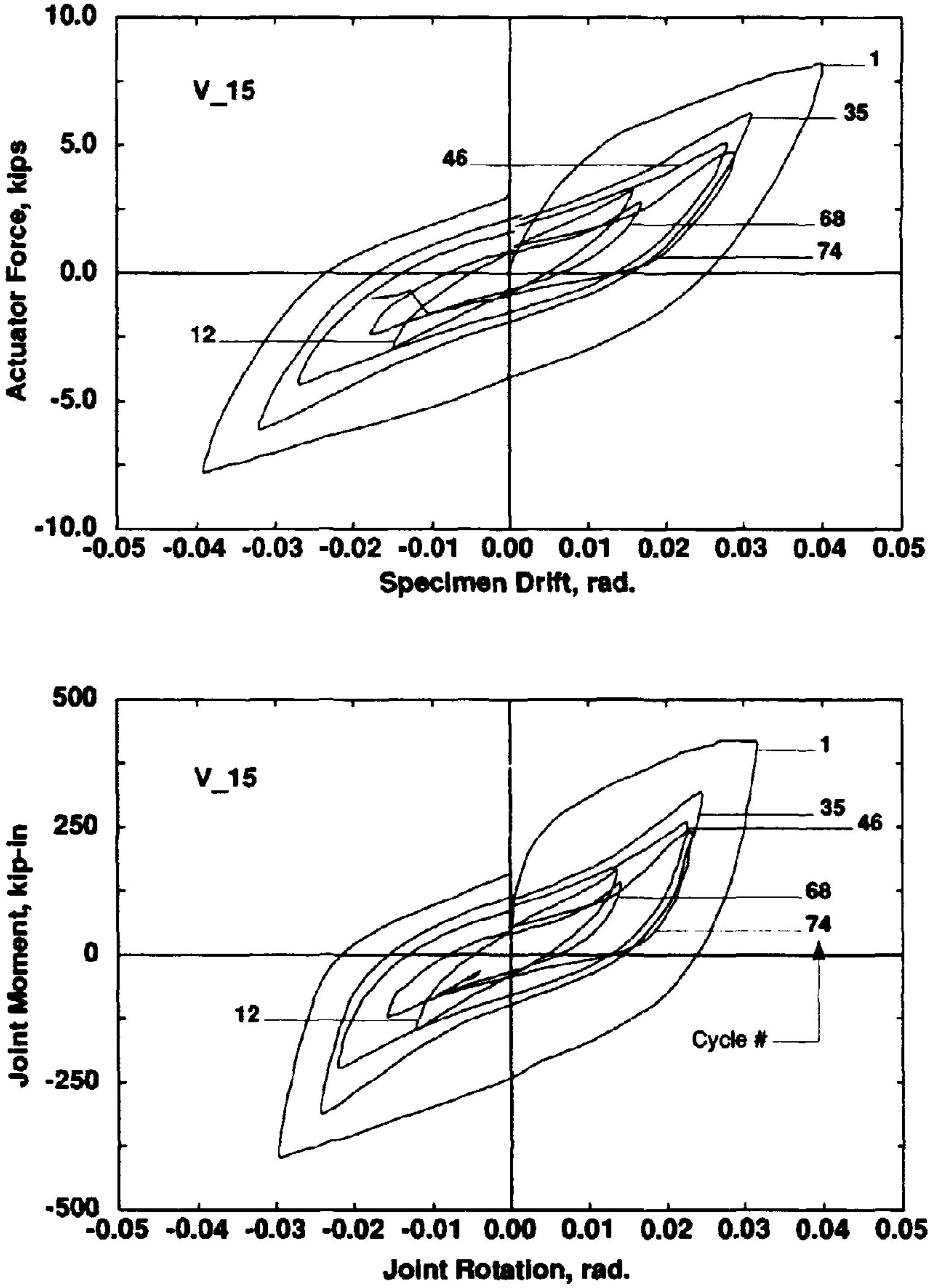

Figure 3-21 Experimental Results for the Decremental-Incremental Test ± 4 to 0% Drift, Specimen V_15

SECTION 4

MONOTONIC BEHAVIOR AND CHARACTERIZATION

4.1 Introduction

This section seeks to characterize the moment-drift and moment-rotation relationship of the monotonic behavior for the top-and-seat angle connection. An analytical investigation is presented in order to predict the initial connection stiffness, mechanism moment capacity and plastic connection rotation. Predictions are compared with those of previous researchers. The complete moment-rotation curve is calibrated for the Menegotto-Pinto (1973) analytical model which incorporates the plastic and elastic connection stiffness ratio, yield moment and a shape factor.

The moment-rotation characteristics for both experimental and analytical studies are determined from the graphs given in Figure 3-6 to 3-21. The comparisons of the test results with the predicted values are discussed in Section 4.4.

4.2 Modeling Monotonic Performance

The following analytical study has been performed in order to predict the initial connection stiffness, plastic rotation capacity and the plastic mechanism moment capacity. The relationship between moment and overall joint rotation was derived using basic equilibrium principles. The model used for this purpose is given in Figure 4-1a and Figure 4-1b.

4.2.1 Elastic Stiffness and Deformation Modeling

Figure 4-1a shows the center lines of the beam and column sections and the moment diagram for the given loading. Joint equilibrium requires that

$$V_c L_c = V_b L \tag{4-1}$$

in which V_c= end reactions due to cantilever loading, V_b= actuator load, L= beam length plus one half the column section depth, L_c= total column length, L_b= total beam length. From the geometry of the deflected shape in Figure 4-1b,

$$\theta_{Te} = \frac{\Delta_{Te}}{L} \tag{4-2}$$

in which, θ_{Te}= overall elastic joint rotation = $\theta_{be}+\theta_{col}+\gamma_j+\theta_{je}$, and Δ_{Te}= total elastic displacement, where

$$\theta_{col} = \frac{V_c L_c^2}{12EI_c} \tag{4-3}$$

$$\theta_{be} = \frac{V_b L_b^2}{3EI_b} \tag{4-4}$$

Elastic rotation due to joint panel shear, γ_j can be easily determined considering the moment diagram in Figure 4-1a. The slope at the joint region, i.e. the joint shear force is

$$V_{jh} = \frac{\left(V_c\left(\frac{L_c}{h_b}-1\right)-\frac{V_b h_c}{2h_b}\right)}{h_b/2} \tag{4-5}$$

using the moment equilibrium given in Eq.(4-1),

$$V_{jh} = V_b\left(\frac{L_b}{h_b}-\frac{L}{L_c}\right) \tag{4-6}$$

and therefore, assuming constant shear force and elastic behavior, the joint panel rotation due to shear can be written as

$$\gamma_j = \frac{V_{jh}}{AG} = \frac{V_{jh}}{Gt_{wc}h_c} \tag{4-7}$$

Substituting Eq.(4-6) into (4-7),

$$\gamma_j = \frac{V_b}{Gt_{wc}h_c}\left(\frac{L_b}{h_b}-\frac{L}{L_c}\right) \tag{4-8}$$

in which h_b= beam depth, h_c= column depth, t_{wc}= column web thickness. Consequently, the expression for the total elastic joint rotation takes the following form,

$$\theta_{Te} = \theta_{col}+\theta_{be}+\theta_{je}+\gamma_j \tag{4-9}$$

in which θ_{je} is the elastic relative connection rotation. Substituting the corresponding expressions into Eq.(4-9),

$$\theta_{Te} = \frac{V_b L_b^2}{3EI_b}+\frac{V_c L_c^2}{12EI_c}+\frac{V_b}{Gt_{wc}h_c}\left(\frac{L_b}{h_b}-\frac{L}{L_c}\right)+\theta_{je} \tag{4-10}$$

In order to obtain an expression in terms of initial joint and connection stiffnesses, the above equation can be multiplied by $1/(V_b L_b L)$, noting that $\frac{1}{L_b K_{Te}} = \frac{\theta_{Te}}{V_b L L_b}$

$$\frac{1}{L_b K_{Te}} = \frac{\theta_{Te}}{V_b L L_b} = \frac{L_b}{3EI_b L} + \frac{L_c}{12EI_c L_b} + \frac{1/(h_b L) - 1/(L_b L_c)}{G t_{wc} h_c} + \frac{1}{L K_{je}} \tag{4-11}$$

After substituting the known geometric parameters and solving for initial connection stiffness, Eq. (4-11) takes the following form:

$$\frac{1}{(K_{je})_{exp}} = \frac{1.078}{(K_{Te})_{exp}} - \frac{1}{71,250} \tag{4-12}$$

in which $(K_{Te})_{exp}$= experimentally obtained initial joint stiffness (= $V_b L/\theta_{Te}$) and K_{je}= initial connection stiffness (= $V_b L_b/\theta_{je}$).

Kishi and Chen (1986) and Kishi et.al. (1987) have developed an expression for the initial connection stiffness of the top-and-seat angle connection based on kinematic and equilibrium principles, assuming a center of rotation as shown in Figure 4-2b. The resulting equation is

$$K_{je} = \frac{4EI_s}{l_{so}} + \frac{3EI_t}{1 + 0.78t_t^2/g_3^2}\left(\frac{d_1^2}{g_3^3}\right) \tag{4-13}$$

Subscripts 't' and 's' denotes top and seat angle respectively. The critical distance, l_{so} is defined as the distance from plastic hinge at the seat angle (center of rotation) to the tip of the angle leg on beam flange. Note that, in Eq. (4-13), $g_3 = g - \frac{t}{2} - \frac{H}{2}$ by Kishi and Chen's definition.

Further modeling for the plastic joint rotation can be carried out in a similar way. Figure 4-2a shows the mechanism for the model. Total joint rotation can be written in terms of its elastic and plastic components as,

$$\theta_T = \theta_{Te} + \theta_{Tp} \tag{4-14}$$

From geometry (Figure 4-2a), it can be shown that,

$$\theta_{Tp} = \frac{\theta_{jp} L_b}{L} \tag{4-15}$$

and elastic rotation is simply,

$$\theta_{Te} = \frac{P}{K_{Te}} \tag{4-16}$$

Substituting Eq.(4-15) and (16) into Eq.(4-14) and rearranging terms,

$$\theta_{jp} = \left(\theta_T - \frac{P}{K_{Te}}\right)\frac{L}{L_b} \tag{4-17}$$

in which, θ_{jp}= plastic connection rotation, θ_T= overall joint rotation, P= average actuator (applied) force, K_{Te}= overall total elastic joint stiffness.

4.2.2 Plastic Moment Capacity

The plastic moment capacity of the connection is determined using virtual work principles based on the plastic hinging in the connection elements as shown in Figure 4-2b and c.

External and internal work done can be written as

$$EWD = M_{jp}\theta_{jp} \tag{4-18}$$

$$IWD = m_1\theta_{jp} + m_2(\theta_{jp} + \alpha) + m_3\alpha \tag{4-19}$$

$$= 2m(\theta_{jp} + \alpha)$$

where m_1, m_2, m_3 are moment strengths per unit length, all equal m $(f_y bt^2/4)$ for this case, θ_{jp}= the plastic rotation of the semi-rigid joint connection, and α= rotation of the top angle yield line which from geometry may be defined as

$$\alpha = \frac{d_2}{g_1}\theta_{jp}$$

Equating Eq.(4-18) and (4-19) and solving for M_{jp},

$$M_{jp} = 2m\left(1 + \frac{d_2}{g_1}\right) \tag{4-20}$$

in which for a single yield line across the width of an angle

$$m = f_y \frac{bt^2}{4}$$

$$d_2 = \frac{t}{2} + h_b + k$$

$$g_1 = g - \frac{H}{2} - k$$

where b= width of the angle, t= thickness of the angle and g= distance between the yield lines in the top angle, k= distance from heel to toe of fillet of angle, g= distance from heel of the angle to the bolt center line, H= diameter of the washer or bolt head. By substituting the known parameters into Eq. (4-20),

$$M_{jp} = \frac{f_y bt^2}{2}\left(1 + \frac{t/2 + h_b + k}{g_1}\right) = 0.457 f_y\left(1 + \frac{9.3425}{g_1}\right) \tag{4-21}$$

Note that for the above equation, the plastic mechanism moment capacity of the top-and-seat angle connection is very sensitive to the value of g_1. This value can be defined in different ways depending on the geometrical orientation of the bolt head and/or nut and washers. Hence, in the present experimental study, it was observed that orientation of the bolt head had a significant effect on the distance between plastic hinges as well as the modes of hinging. To examine the sensitivity of g_1 on the plastic moment capacity, three scenarios are explained in what follows:

a. Upper Bound Strength:

If one of the apexes of the bolt head is pointing toward the yield line m_3, (Figure 4-2b) then the distance g_1 becomes a minimum with the yield line passing directly beneath the hardened washer. However, it should be noted that in the limit as $g_1 \to 0$, shear capacity rather than the flexural capacity of the angle governs the plastic moment capacity, which yields the following equation:

$$M_{jp} = 2m\left(1 + \frac{h_b + k}{t}\right) = 11.6 f_y$$

For the present specimen this gives M_{jp} = 491 kip-in based on f_y = 42.3 ksi, and at fracture where f_{su} = 64.7 ksi, M_{jp} = 751 kip-in.

b. Lower Bound Strength:

If load indicator washer are used, then the yield line m_3 is able to penetrate up underneath the bolt, approaching the center of the bolt hole. In this case,

$$g_1 = g - k = 2 - 0.875 = 1.125 \text{ in.}$$

This gives M_{jp} = 180 kip-in.

c. Nominal Plastic Strength:

Post-test inspection revealed that in most cases a radial fan yield line formed beneath the bolt head and washer connecting the angles to the column. Such a yield line pattern is shown in Fig 4.4(d). Using the principles of virtual work for this pattern gave a plastic joint capacity of M_{jp}= 280 kip-in.

4.2.3 Shear Effects on Joint Strength Capacity

Kishi and Chen also developed an expression for the mechanism moment capacity of top-and-seat angle connections (For details, refer to Kishi and Chen 1986). In the following equation, the effect of shear force on the moment capacity is also taken into account.

$$M_{u1} = M_{os} + M_{pt} + V_{pt}d_2 \qquad (4\text{-}22)$$

V_{pt} is determined by solving the following equation:

$$\left(\frac{V_{pt}}{\left(\frac{f_y bt}{2}\right)}\right)^4 + \frac{g_1}{t}\left(\frac{V_{pt}}{\left(\frac{f_y bt}{2}\right)}\right) = 1$$

then M_{pt} becomes

$$M_{pt} = \frac{V_{pt}g_1}{2}$$

and M_{os} is the plastic moment capacity of the seat angle,

$$M_{os} = \frac{f_y bt^2}{4}$$

In Section 4.4, moment capacities calculated using above formulation and compared for various failure modes discussed earlier.

4.2.4 Modeling the Moment-Rotation Behavior

An analytical model to describe the moment-rotation behavior of the connection is incorporated in the present study, which uses the Menegotto-Pinto (Menegotto and Pinto, 1973) equation. This is a powerful means for describing a curve between two tangents that has a variable radius of curvature at the intersections. The basic form of the equation for a monotonic loading is

$$M = K_{je}\theta_j\left[Q + \frac{1-Q}{\left[1+\left|\frac{K_{je}\theta_j}{M_y}\right|^R\right]^{1/R}}\right] \tag{4-23}$$

in which, K_{je}= initial elastic stiffness of the joint, θ_j= connection rotation, M_y= yield strength which is at the intersection of the elastic and plastic tangents, Q= ratio of the post-yield plastic to elastic tangents K_{jp}/K_{je}, and R= a curvature parameter which may vary between 1 and 25 (the higher value giving a bilinear curve). The graphical determination of the parameters K_{je}, K_{jp}, θ_{jy} and M_y is shown on Figure 4-3

Strictly, the values of K_{je}, M_y, Q and R should be determined using nonlinear regression analysis. However, in view of the significant scatter in the results K_{je} and K_{jp} (and hence Q) may be determined from the average of a series of experiments, and M_y may be found graphically as the intersection of the two tangents (Figure 4-3). Experimental values for these parameters are assessed in Table 4-I.

The value for the parameter R may be determined from a graphical construction such that

$$R = \frac{ln2}{ln\left[\frac{1-Q}{(M(\theta_{jy})/M_y)-Q}\right]} \tag{4-24}$$

in which $M(\theta_{jy})$= experimental moment capacity observed at the "theoretical" yield rotation, θ_j= θ_{jy}. From the present study $M(\theta_{jy})/M_y = 0.72$, thus $R \approx 2$.

4.3 Monotonic Test Results

Figure 4-4 shows the experimentally observed moment-rotation curves which are extracted from the first cycle of the cyclic test results as well as the monotonic test itself.

In order to investigate the repeatability and reliability of the monotonic behavior, initial

Table 4-I Comparison of Monotonic Behavior[a]

Spec. Id	Total Drift %	Actuator force kips	K_{Te} kip-in/rad	Expt. K_{je} kip-in/rad	K_{je}[b] kip-in/rad	Expt. θ_{je} rad	Expt. θ_{jp} rad	θ_{jp}[c] rad	θ_{jT} rad	M_{jp} kip-in
M_19	11.85	14.71	49,500	122,500	129,300	0.004	0.096	0.107	0.100	337.3
R1_06	8.50	15.80	50,900	138,500	140,000	0.003	0.068	0.070	0.071	454.5
R1_09	7.20	15.09	48,600	123,600	122,600	0.003	0.057	0.056	0.060	372.5
R1_05	6.10	14.61	50,000	137,600	132,900	0.003	0.049	0.045	0.052	504.5
R1_04	3.00	7.18	49,400	122,800	128,700	0.004	0.018	0.022	0.022	343.5
R1_01	2.10	5.63	44,800	95,300	99,700	0.007	0.011	0.014	0.018	226.1
R0_10	1.98	6.23	45,400	93,300	102,900	0.003	0.016	0.017	0.018	267.9
R0_11	4.06	8.18	45,900	106,700	105,800	0.004	0.034	0.038	0.038	325.6

a. To convert kip.in to kN.m, multiply by 0.11225
b. Inferred experimental value from Eq.(4-12)
c. Inferred experimental value from Eq.(4-17)

stiffnesses, elastic, plastic rotations and plastic moment capacities from some of the cyclic tests are compared on Table 4-I. The initial connection stiffness was determined both from the M-θ_j plots and using Eq. (4-12) derived in the following section. A secant slope was to allow comparisons to be made among the different tests and to indicate the early connection stiffness. Since the initial tangent slope is highly sensitive to any irregularities in the first few data points, the secant slope may better represent the initial connection stiffness. As can be seen from Table 4-I, initial connection stiffnesses ranged between 138,500 kip-in/rad (15,700 kN-m/rad) for specimen R1_06 and 93,000 kip-in/rad (10,500 kN-m/rad) for specimen R0_10. However, except for specimens R1_05 and R1_06, connection stiffnesses stayed in an acceptable range. These results are used in modeling the moment-rotation behavior in subsection 4.3.3.

Monotonic test results are also used in determining the low-cycle fatigue behavior. In this case, it is assumed that the test results for specimen M_19 correspond to 1/4 cycle fatigue life. Details of the fatigue results are given in Section 5.

4.4 Discussion

An analytical investigation was carried out in order to predict the monotonic characteristics of this specific type of top-and-seat angle connection.

First, an analytical study was perfonned on the model test setup shown in Figure 4-1a. Since the shear deformation in the panel zone of a joint would affect the overall behavior of the connection, it has been realized that the rotation due to that effect must also be included in the formulation assuming an elastic behavior at the column web. Figure 4-1a shows the correct moment diagram which accounts for the large horizontal shear force at the joint region. Consequently, Eq.(4-12) was derived using the equilibrium condition to predict the initial connection stiffness based on the Force-Drift behavior of the joint.

The main purpose of this experimental study was to investigate the low-cycle fatigue behavior which requires the post-elastic behavior to be studied. Therefore, in order to predict the plastic connection rotation, simple failure mechanism was used for the model setup as shown in Figure 4-2. From the geometry of the mechanism, total drift could be easily related to plastic connection rotation by Eq.(4-17) as explained in Section 4.3.1. The predicted values are evaluated for the constant amplitude cyclic tests and monotonic test. The comparison of the predicted initial stiffnesses and plastic connection rotations with the experimentally obtained values, Table 4-I, indicates that the initial stiffnesses predicted by Eq.(4-12) are generally greater than those obtained experimentally. However, this difference is not larger than 10% (10% for R1_06, 9% for R1_05) which is quite acceptable.

Kishi and Chen (1986, 1987) obtained an expression for the initial stiffness of top-and-seat angle connections (Eq. (4-13)) by modeling the flange angles as assemblies of beam segments (Figure 4-2b and c). This equation is simply the sum of the stiffness contributions of two flange angles under a monotonic loading. In Eq.(4-13), a small change in g_3, which is defined as "the length of the vertical leg that acted as a cantilever beam "(see deformed shape of top angle on column flange in Figure 4-2b) would change the overall stiffness a considerable amount. In order to demonstrate the effect of g_3, Table 4-II gives three different stiffness values that may be obtained using three different possible g_3 values. These values were determined by considering the possible bolt head orientations.

The first term in the equation which was assumed to represent the seat angle contribution to the stiffness is insignificant compared to the second term.

Table 4-II Comparison of Predicted Initial Connection Stiffnesses (Eq.4-13)

l_{so} (in)	d_1 (in)	g_3 (in)	Predicted Stiffness (seat angle) (kip-in)	Predicted Stiffness (top angle) (kip-in)	Total Predicted Stiffness, K_{je} (kip-in)
5.25	9.03	1.06250	631	154,000	154,500
5.25	9.03	1.18750	631	112,000	113,000
5.25	9.03	1.09375	631	142,000	142,500

It is obvious from Table 4-II that even the position of bolt head affects the initial connection stiffness up to 25%. Therefore, assuming an average value of g_1 as 1.1146 in (2.83 mm), the initial stiffness comes out to be 134,500 kip-in. (15,000 kN.m) using the Chen and Kishi model.

Further analysis was carried out for the mechanism moment capacity of the connection. The value of g_1, which represents the distance between yield lines in Eq. (4-21), also depends on the orientation of the bolt head and washer which was found to affect the yield line pattern as explained in Subsection 4.3.2. Hence, three possible values are reported herein as upper, lower bounds and nominal strength. Capacity ranges between 180 kip-in (20.2 kN-m) and 501 kip-in (56.2 kN-m) based on yield strength of the angle material taken as 41.4 ksi (285.4 MPa) assuming an average value of those reported in Table 2-I for transverse coupon specimens.

Chen and Kishi (1986, 1987) also developed an expression, Eq.(4-22), to predict the mechanism moment of a top-and-seat angle connection. This model consists of considering each angle individually and determining the plastic moment contributions of the assembly angles. In this model, effect of shear is also included. This equation also involves the g_1 value which was mentioned above. Table 4-III summarizes the possible predicted mechanism moments for upper and lower bounds as discussed earlier, depending on the value of g_1. As can be seen in Table 4-III, the Chen and Kishi model underestimates the upper bound mechanism moment. However, for the lower bound, the model is accurate.

The values for different yield line spacing and failure modes, cover the range of the experimentally obtained moment capacities as shown in Figure 4-4. This implies that the capacity of bolted semi-rigid connections could be more reliably controlled if the location of hinging in the angle adjacent to the column is fixed.

Table 4-III Comparison of Predicted Mechanism Moments (Eq. 4-22)

g_1 (in)	M_{os} (kip-in)	M_{pt} (kip-in)	V_{pt} (kip)	M_{u1} (Chen & Kishi) (kip-in)
0.375	9.46	6.85	36.56	357
1.125	9.46	9.34	16.62	174

Finally, the experimental moment-rotation curve is calibrated for an analytical model (Eq.(4-23)) which incorporates the plastic, elastic connection stiffness ratio, yield moment and a shape factor. This model is compared with experimentally obtained M-θ_r relationships on Figure 4-4. In a recent publication by Kishi, et al. (1993), it was asserted that the Richard and Abbot equation is suitable for describing moment-rotation behavior of semi-rigid connections. This equation is identical to the more general Menegotto-Pinto equation, but with Q=0. This conservatively assumes that there is no strain-hardening in the connection. For comparative purposes, the Richard and Abbot (1975) equation is shown with the Menegotto-Pinto equation in Figure 4-4. It is evident that the top-and-seat angle connection does indeed exhibit significant strain-hardening which should thus be accounted for in the analytical modeling.

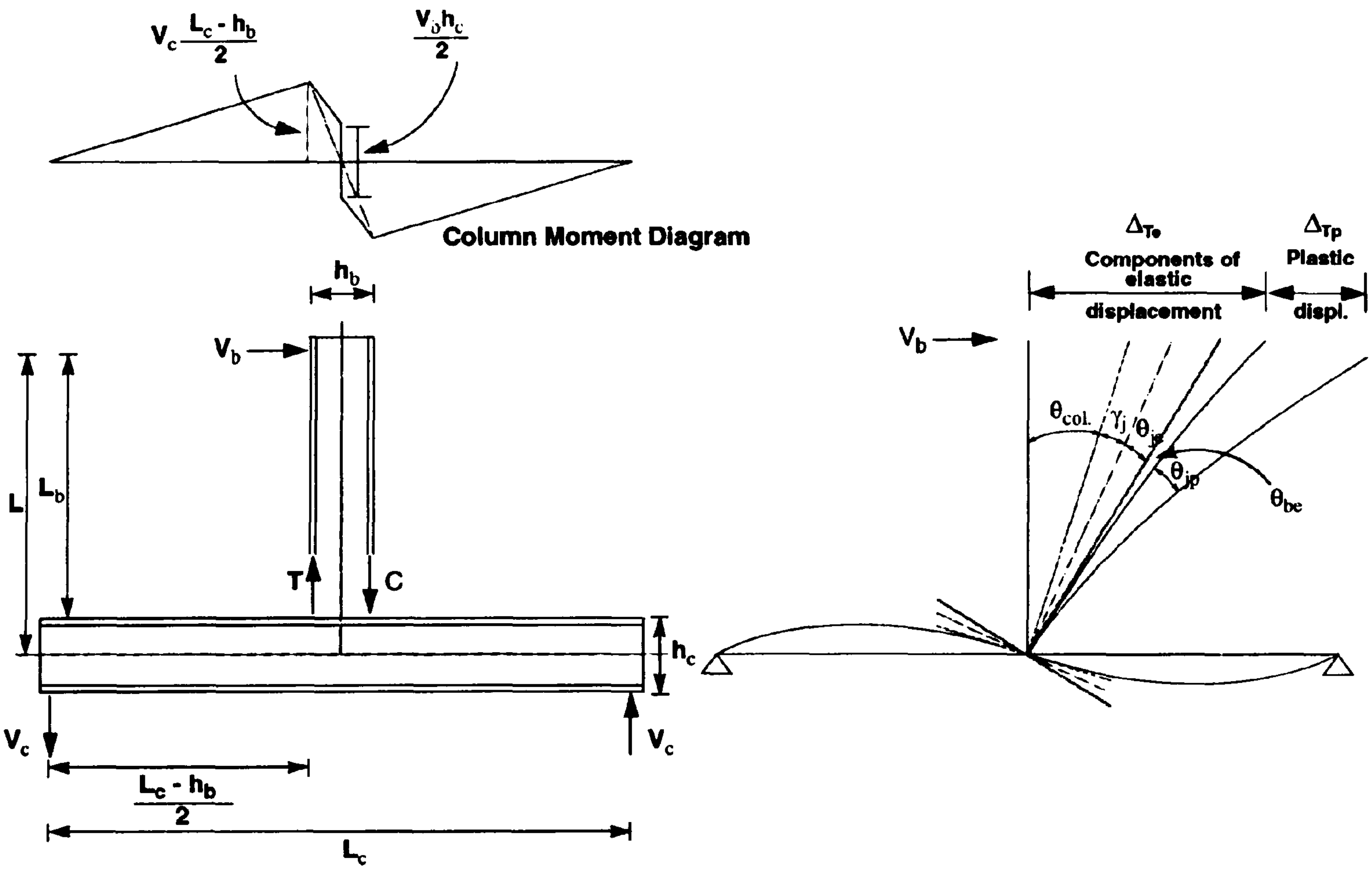

(a) Reactions and Moment Diagram for the Model Setup **(b) Deflected Shape and Components of Rotation**

Figure 4-1

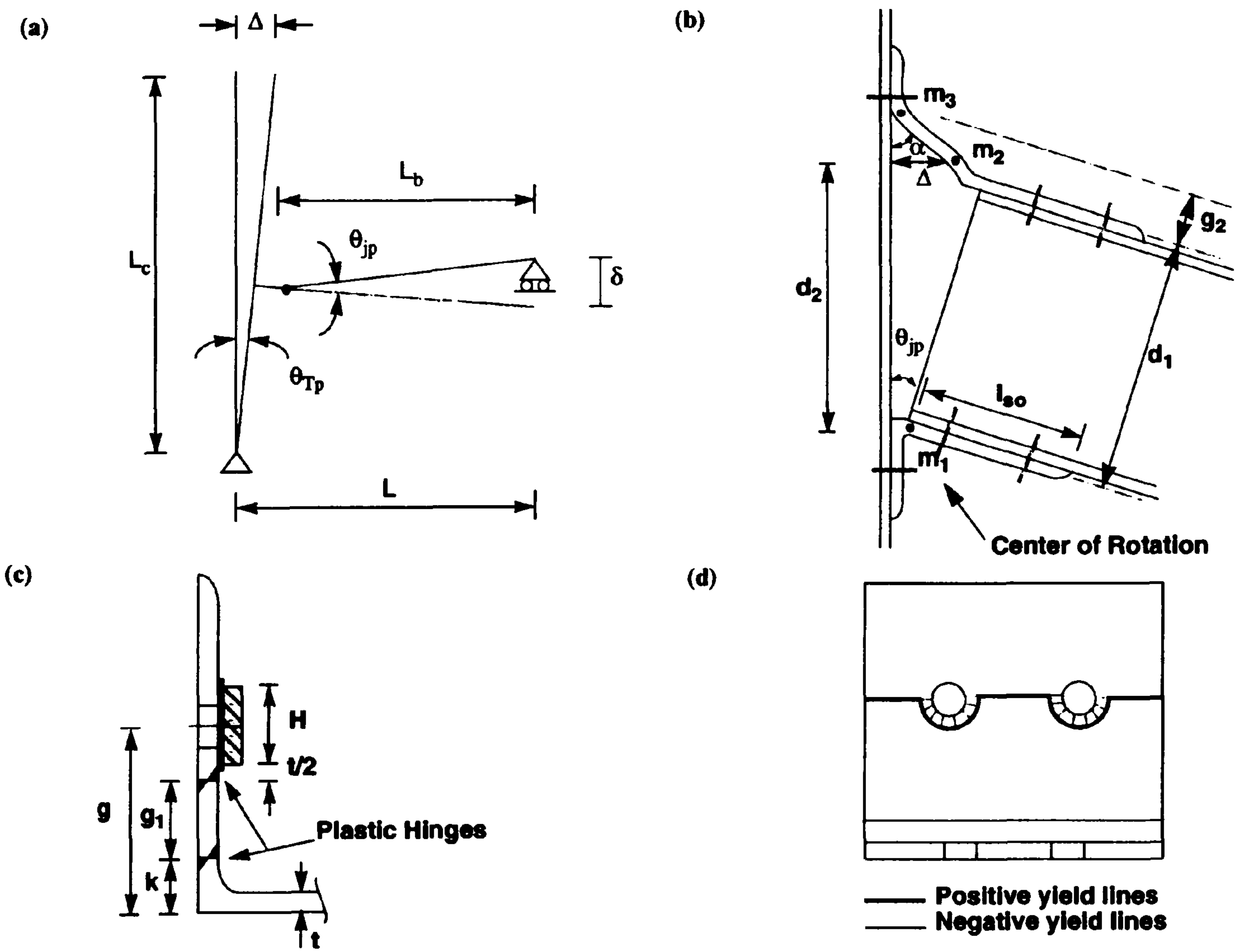

Figure 4-2 Plastic Mechanism and Yield Lines

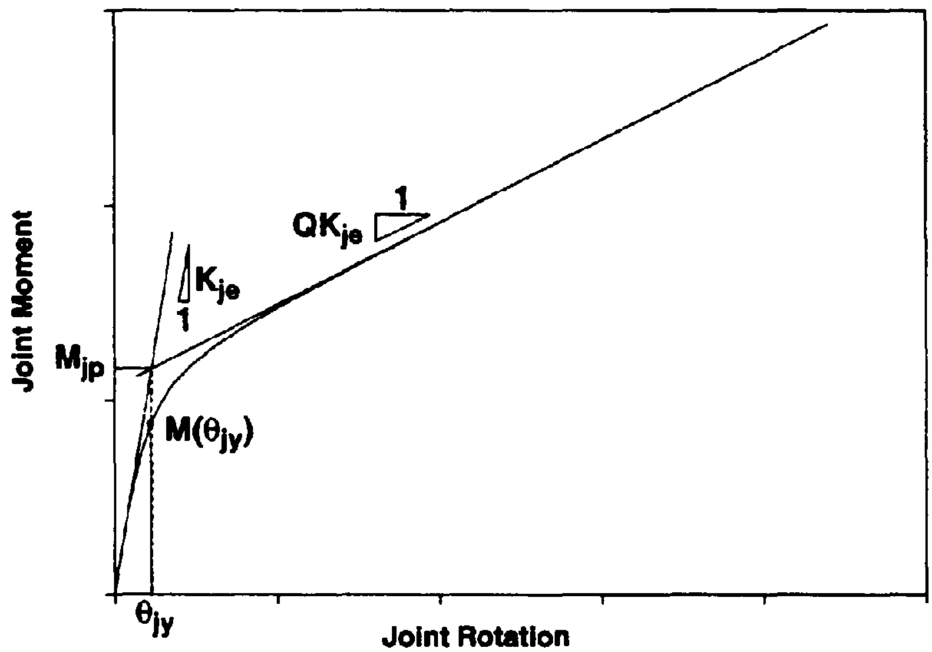

Figure 4-3 Menegotto-Pinto Idealization

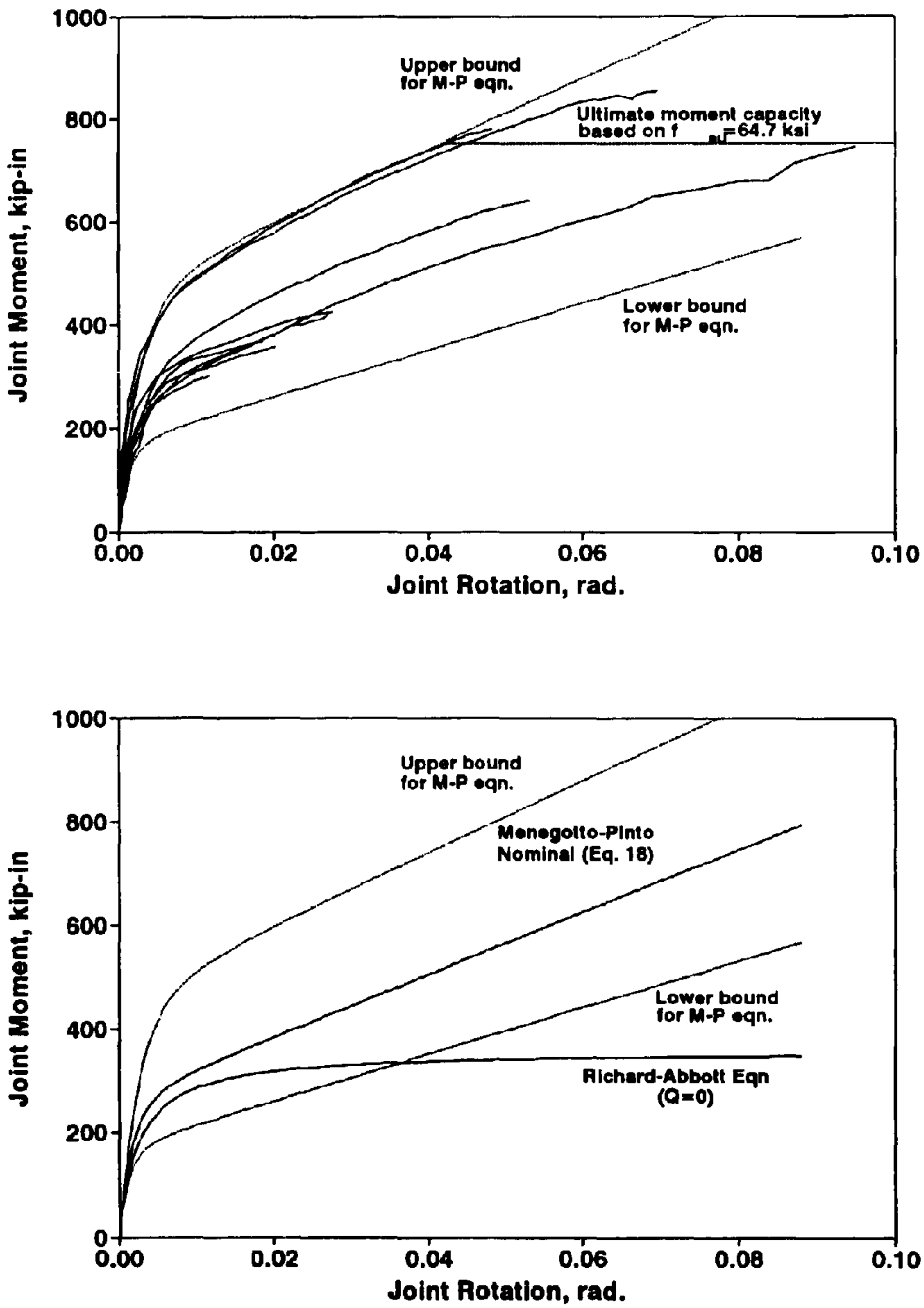

Figure 4-4 Comparison of First Quarter Cycles

SECTION 5

LOW-CYCLE FATIGUE RELATIONSHIP BASED ON DRIFT AND HYSTERETIC ENERGY

5.1 Introduction

In this section, low-cycle fatigue relationships are developed for the top-and-seat angle connection, based on both total and plastic connection rotations and cyclic energy, using the experimental data from the constant amplitude tests. It was found that these parameters versus the number of cycles to failure each produces a linear relationship on a log-log plot which is similar to the classical S-N curves used for metals. Equations for these linearized relationships are determined using a least squares regression analysis.

Various fatigue models are derived relating the following: (i) plastic connection rotation (θ_{jp}) to number of reversals till incipient failure ($2N_f$), (ii) θ_{jp} to number of cycles to final fatigue fracture ($2N_{ff}$), (iii) total connection rotation (θ_j) to ($2N_f$), (iv) θ_j to $2N_{ff}$, (v) cumulative cyclic hysteresis energy till incipient failure (W_f) to ($2N_f$), (vi) cumulative cyclic hysteresis energy to fracture (W_{ff}) to $2N_{ff}$, and (vii) average cyclic hysteresis energy (ΔW_f) to ($2N_f$).

5.2 Low-Cycle Fatigue (LCF) Models

In experimental low-cycle fatigue studies, fatigue life is commonly expressed as a function of the total and/or plastic strain. If the strain at critical locations in a structural element could be measured, then in conjunction with a suitable cycle counting method and an appropriate S-N type of fatigue model, the fatigue life under random cyclic loading could be predicted. However, structural elements are often rather complex systems, and it is not practical and indeed generally impossible to make strain measurements at the critical locations of a connection. Instead of using strain versus number of cycles relationship, analogous models based on total and plastic connection rotations are developed herein.

Cyclic loading involves a certain amount of energy dissipation for a certain displacement amplitude. Therefore, it is also reasonable to relate cyclic hysteresis energy to fatigue life. From Figure 3-14b, it can be observed that there is not much of a variation in the hysteresis energy absorbed per cycle during the fatigue life. For this reason, a relationship between average cyclic hysteresis energy and number of cycles can also be studied as discussed in what follows.

Fatigue terminology often differs slightly from one study to another. Therefore, it is considered worthwhile to summarize the basic terminology which is employed herein.

The fatigue life, N_f is defined as the number of cycles to the point of incipient failure at which the first surface crack was observed. However, the number of cycles to complete final fatigue fracture (separation) is defined as N_{ff}. Average cyclic hysteresis energy, ΔW_f is determined as the area of single hysteresis loop at half-life: at cycle number $n \approx 0.5N_f$. Total hysteretic energy is denoted as W_f and W_{ff} for incipient failure (first crack) and complete fracture, respectively. These values are reported in Table 5-I for constant amplitude tests and the monotonic test. Table 5-I also includes total drift and the plastic rotation of the connection.

The linear log-log relationship of plastic strain to the number of reversals ($2N_f$) to failure was first developed by Coffin (1954) and Manson (1953). This concept can be adopted and extended for semi-rigid connections using plastic connection rotation instead of plastic strain:

$$\theta_{jp} = \theta'_{Nf}(2N_f)^b \tag{5-1}$$

where θ'_{Nf} = fatigue ductility coefficient and b = fatigue ductility exponent. These coefficients are determined by fitting a linearized log-log model to the experimental data. Another variation of the Coffin-Manson relationship suggested by Koh and Stephens (1991) uses total strain instead of plastic strain only:

$$\theta_j = \theta'_{jf}(2N_f)^c \tag{5-2}$$

The fatigue life of a material subjected to a given strain range can also be estimated by superposition of elastic and plastic components, given by another variation of the Coffin-Manson relationship as follows:

$$\theta_j = \theta'_{Nf}(2N_f)^b + \frac{M'}{K_e}(2N_f)^c \tag{5-3}$$

where M' = a moment related coefficient and K_e= initial connection stiffness.

Table 5-I Summary of Fatigue Test Results[a]

Specimen Id.	θ_T (radx100)	θ_j (radx100)	θ_{jp} (radx100)	ΔW_f (kip-in)	W_f (kip-in)	W_{ff} (kip-in)	N_f	N_{ff}
M_19*	0.119	0.100	0.096	197.7	49.4	49.4	0.25	0.25
R1_06	0.085	0.071	0.068	106.0	57.7	206.0	0.5	1.75
R1_09	0.072	0.060	0.057	91.7	112.4	274.1	1.15	3.25
R1_05	0.061	0.052	0.049	72.7	146.3	295.5	2	4.25
R1_03	0.050	**	**	30.1	189.2	233.6	6	7.75
R1_02	0.040	0.036	0.027	21.4	198.8	279.3	9	13.75
R1_04	0.030	0.022	0.017	13.8	308.7	345.8	22	25.25
R1_07	0.025	0.021	0.018	6.2	315.8	358.3	47	54
R1_01	0.021	0.018	0.011	4.2	316.3	396.6	73	95.75
R1_08	0.014	0.010	0.007	2.4	944.1	1043	397	446
R1_12	0.009	0.008	0.005	1.4	2662	3255	4379	5341
R1_13	0.006	0.005	0.003	1.0	8963	10874	14461	17064
R0_11*	0.041	0.038	0.034	17.8	84.5	127.4	3.75	6.5
R0_10*	0.020	0.018	0.016	4.6	290.8	352.4	62	75.5

a. To convert kip-in to kN-m, multiply by 0.11225.
*. Not included in regression analysis.
**. Not available experimentally.

The average cyclic energy, ΔW_f can be related to fatigue life in the following form

$$\Delta W_f = \Delta C_f M_{jp} (2N_f)^d \tag{5-4}$$

where ΔC_f and d are material constants.

Similar to the above models, Tong, Wang and Xu (1989) related cyclic hysteresis energy W_f, to fatigue life using the relationship

$$W_f = C_f M_{jp} (2N_f)^e \tag{5-5}$$

where C_f and e are material constants. The relationship between total energy absorbed during the fatigue life of a specimen till failure and number of reversals has the following form,

$$W_{ff} = C_{ff} M_{jp} (2N_{ff})^f \tag{5-6}$$

where C_{ff} and f are material constants.

By combining Eqs (5-1) and (5-5) to eliminate $2N_f$, a relationship between the total work capacity and the constant plastic amplitude is obtained,

$$W_f = C_{\theta f} M_{jp} (\theta_{jp})^{e/b} \tag{5-7}$$

where $C_{\theta f} = C_f / (\theta'_{Nf})^{-e/b}$

The value of this relationship will become evident when utilized in the damage model described subsequently in Section 6. In Eqs (5-4) to (5-7) M_{jp} is used to keep the fatigue relationships independent of size (geometry and material strength).

Table 5-I also lists the fatigue results for both monotonic and one-sided constant amplitude (R=0) tests. However, these results are not used in the least squares regression analyses performed on the constant equi-amplitude (R=-1) test results to determine the best fit for the above mentioned relationships. They are included in the fatigue plots for comparison purposes only. In the following subsections, various fatigue models are discussed.

5.3 Results of Linearized Regression Analysis

Regression analyses were performed on the nonlinear data sets by taking logarithms of the

(x, y) pairs such that $X = \log x$ and $Y = \log y$. Least squares regression analysis was then performed on the linearized (X,Y) data to find the coefficients a and B such that

$$Y = ax + B \tag{5-8}$$

Thus in terms of the original data the relationship becomes

$$y = bx^a \tag{5-9}$$

where $b = 10^B$.

Results of the linearized regression analysis are presented in Table 5-II for both incipient (first crack) failure and fatigue fracture (separation). It will be noted that the right hand column of this table lists the correlation coefficient r^2, where a perfect fit would be given by r^2=1, smaller values indicating an increasing degree of scatter.

Table 5-II Low Cycle Fatigue Relationships Determined From Linearized Log-Log Regression Analysis

Equation No.	Best Fit	r^2
5-1	$\theta_{jp} = 0.0672\,(2N_f)^{-0.308}$	0.977
5-1	$\theta_{jp} = 0.0816\,(2N_{ff})^{-0.324}$	0.962
5-2	$\theta_j = 0.0689\,(2N_f)^{-0.255}$	0.970
5-2	$\theta_j = 0.0810\,(2N_{ff})^{-0.269}$	0.955
5-4	$\Delta W_f = 0.257 M_{jp}\,(2N_f)^{-0.479}$	0.928
5-5	$W_f = 0.137 M_{jp}\,(2N_f)^{0.512}$	0.966
5-6	$W_{ff} = 0.175 M_{jp}\,(2N_{ff})^{0.492}$	0.946
5-7	$W_f = 0.0071 M_{jp}\,(\theta_{jp})^{-1.212}$	0.934
5-7	$W_{ff} = 0.0268 M_{jp}\,(\theta_{jp})^{-0.952}$	0.836

5.4 Proposed Form of Low-Cycle Fatigue Relationships

5.4.1 Theory

In the foregoing least squares analysis it was assumed that errors are present in the dependent variable and that the independent variable is error free. However, all the parameters used in the regression analysis were subjected to some degree of random error resulting from how the experiments are performed and the results interpreted. Therefore, the exponential coefficients derived above should not be regarded as absolutely fixed, but rather as indicative to what power can be adopted for a general expression. From Table 5-II. it is also evident that the exponents for the relationships relating number of reversals to incipient failure as well as final fatigue fracture are similar. If these exponents were forced to be the same, then the ratio of the coefficients can be used to relate the incremental proportion of work or number of cycles from incipient failure to complete fatigue failure (separation).

Because of the similarity of the results between N_f and N_{ff} the exponents have been fixed (guided by the results from Table 5-II) and coefficients were determined as follows.

Consider the general power relationship

$$y = cx^p \tag{5-10}$$

If the power p is fixed, then for a given experimental x and y value, the coefficient c can be calculated from

$$c = yx^{-p} \tag{5-11}$$

If this is repeated for all experimental data points and averaged, a single "best fit" equation can be derived. Unlike the aforementioned linearized regression analysis, this procedure implicitly assumes errors are present in both x and y values.

5.4.2 Proposed Cyclic Based Fatigue Relationships

Low-cycle fatigue is generally associated with a small number of cycles required for failure of a specimen subjected to cyclic loading. This requires relatively larger displacement amplitudes which causes a considerable amount of inelastic strain. Therefore, study of the plastic behavior becomes an important aspect of low-cycle fatigue analysis. Moreover, past research has shown that the low-cycle fatigue behavior can be modeled well with a plastic strain based approach. In the present study, plastic connection rotations were determined from the constant amplitude test results as discussed in Section 3 and presented in Table 5-I.

Figure 5-1 shows two different fatigue models based on the plastic connection rotation. A regression analysis was carried out using the number of reversals to failure versus plastic connection rotation. For the present study, the exponent b in Eq. (5-1) was found to be close to -1/3. By adopting this result, as explained in the previous section, the coefficient θ'_{Nf} was obtained giving the following expression:

$$\theta_{jp} = 0.070\,(2N_f)^{-0.333} \tag{5-12}$$

In a similar manner, the case for final fatigue fracture life ($2N_{ff}$), produced the following relation,

$$\theta_{jp} = 0.0849\,(2N_{ff})^{-0.333} \tag{5-13}$$

Eqs (5-12) and (5-13) are plotted against the experimentally obtained data in Figure 5-1. These results, along with the experimental data are shown in Figure 5-2. Also shown are +100% and -50% bounds with respect to the line of best fit. The significance of these bounds are discussed later in Section 5.5.

For the total joint rotation, the exponents were found to be close to -0.3, and by adopting this value expressions are derived based on the number reversals to incipient failure and to final fatigue fracture as follows:

$$\theta_j = 0.0768\,(2N_f)^{-0.3} \tag{5-14}$$

$$\theta_j = 0.0887\,(2N_{ff})^{-0.3} \tag{5-15}$$

Figure 5-3 shows the application of superposition of elastic and plastic joint rotation components on a log-log plot. As can be seen from the figure, the total joint rotation curve approaches the plastic rotation life curve at large rotation amplitudes whereas it approaches the elastic rotation life curve at low rotation amplitudes. In this plot, the values of material fatigue constants corresponding to the elastic rotation component, which were defined in Eq. (5-3), were found to be $M'/K_e = 0.0075$, c= -0.07 so the resulting equation is as follows:

$$\theta_j = 0.70\,(2N_f)^{-0.333} + 0.0075\,(2N_f)^{-0.07} \qquad (5\text{-}16)$$

The exponent c should really only be considered as approximate because too few data points were available in the medium to high cycle fatigue range.

5.4.3 Proposed Energy Based Fatigue Relationships

At high displacement amplitudes, plastic strain is the main reason for energy dissipation in semi-rigid connections. Therefore, in this study a low-cycle fatigue relationship is established based on the cyclic energy dissipation. The average cyclic hysteresis energy, ΔW_f is approximated as the area of a single hysteresis loop at approximately half life (N_f/ 2) of the specimen. Similarly, cumulative cyclic hysteresis energy is determined as the sum of the areas of hysteresis loops till the incipient failure for W_f, or sum of the areas of hysteresis loops until the final fatigue fracture for W_{ff}.

A large degree of variability of behavior exists among the identical connections tested due to bolt head orientation. As discussed in Section 4, this variation can be clearly observed in plastic moment capacities as well as stiffness values. Therefore, in order to eliminate this dimensional effect and to obtain a better fit of fatigue data, cyclic hysteresis energy was normalized with plastic moment capacities, and the following fatigue relationships were obtained.

To examine the effect of energy dissipation on low-cycle fatigue behavior during cyclic loading, the energy per cycle at approximately half life, $\Delta W_f/M_{jp}$ was plotted versus the number of cycles to incipient failure. Guided by the least squares equation given in Table 5-II, the exponent was fixed at -0.5 and the following relationship which is plotted in Figure 5-4 was obtained:

$$\Delta W_f = 0.303 M_{jp}\,(2N_f)^{-0.5} \qquad (5\text{-}17)$$

Multiplying both sides of this equation by N_f gives the total energy dissipated until incipient failure. This changes the exponent to +0.5 which is relatively close to the value obtained directly based on the least squares analysis given in Table 5-II. By adopting an exponent of 0.5, the best fit relationship is

$$W_f = 0.144 M_{jp}\,(2N_f)^{0.5} \qquad (5\text{-}18)$$

An alternative fatigue relationship can be developed in a similar fashion that relates energy and fatigue life at final fatigue fracture (separation):

$$W_{ff} = 0.169 M_{jp} (2N_{ff})^{0.5} \tag{5-19}$$

Figure 5-5 plots Eqs (5-18) and (5-19) along with the experimental data.

As discussed previously in Section 5.2, it is possible to derive relationships that relate plastic rotation to the energy absorption capacity either at incipient failure or final fatigue fracture (Eq. 5.7). It will be noted that for the results of the linearized least squares regression analysis given in Table 5-II, the correlation coefficients obtained for these relationships indicate inferior agreement with the test results. This appears to be due to the high cycle results where little plastic rotation is obtained. Omitting these results from evaluations and setting the exponent to -1.0, the following equations are obtained

$$W_f = 0.0151 M_{jp} (\theta_{jp})^{-1.0} \tag{5-20}$$

$$W_{ff} = 0.0229 M_{jp} (\theta_{jp})^{-1.0} \tag{5-21}$$

5.5 Comparison of Fatigue Models with Previous Research by Harper et al.

Azizinamini et al. (1985) and Harper et.al. (1990) performed static and cyclic experimental studies on various types of semi-rigid connections. The specimens included bolted, bolted-welded top-and-seat angle with double web angle connections. In the test program, the angle thickness, length and gage (in the leg attached to the column flange) were varied, together with the beam depth. In these studies, in order to take varying geometries of specimens into account, a parameter R called "the nominal flange angle chord rotation index" was introduced. This parameter was intended to represent the degree of deformation (and thus strain) in the tension flange and was defined as follows:

$$R = 2\left[\frac{(d+t)\tan\theta_j}{g - 0.5d_w - t}\right] \tag{5-22}$$

in which d = beam depth, t= flange angle thickness, d_w= diameter of washer, g= gage in the flange angle; distance from the heel of the angle to the center of the bolt hole in the leg of the flange angle attached to the column face.

The chord rotation index R, was then used in the low-cycle fatigue models related N_{ff}, the number of cycles to failure. It should be noted here that Harper et al. defined the fatigue failure as having occured when the longest fatigue crack had extended over approximately 3/4 of the width of the flange angle. Fatigue lives ranged from 10^1 to 10^4 cycles. The following regression results were reported for all-bolted specimens:

$$N_{ff} = 1.227\,(R)^{-3.7857} \tag{5-23}$$

Similar expressions were derived for mixed connections that contained both bolted and welded elements.

A comparison can be made with the present results by substituting Eq. (5-22) into Eqs (5-23). The values for the geometric parameters defined in Eq. (5-22) are reported in Section 2. It should also be noted that $\tan\theta_j = \theta_j$ for small rotation angles. Therefore, Eqs (5-23) can be rewritten as:

$$\theta_j = 0.0643\,(2N_{ff})^{-0.264} \tag{5-24}$$

The fatigue-life relationship for total connection rotation (Figure 5-2) is compared with that of Harper et al. (1990). Slight difference in the definition of fatigue failure between the present study and Harpers' should be noted. Thus, in Figure 5-2, Eq. (5-28) plotted on both θ_j vs $2N_f$ and θ_j vs $2N_{ff}$ graphs.

5.6 Discussion

It is evident from the foregoing presentation of experimental results that there is an appreciable amount of scatter in the plotted data. This poses problems in making predictions of failure using the analytical relationships. However, most fatigue researchers consider experimental results to be of good quality if a failure prediction can be made within +100% or -50% of the line of best fit. These upper and lower bounds approximately correspond to the 95 percentile range with a lognormal distribution in experimental scatter. These bounds have been plotted in Figures 5-1, 5-2 and 5-4 to 5-6. In all cases, with the exception of the high cycle data in Figure 5-6, the experimental results fall well within this range of acceptability.

Also plotted in the above mentioned figures are the data points for the one-sided tests when $R \approx 0$. It appears that in the low cycle fatigue regime the results are not affected by so called "mean stress" effects. This finding is in agreement with the Koh and Stephens

(1991) observations for uniaxial low cycle fatigue in metals.

Comparison of Eqs (5-25) to (5-27) with corresponding relationships reported in Table 5-II and Eqs (5-14) and (5-15) shows that a universal slope (i.e. exponent) of -0.333 can be used for the types of semi-rigid connections tested, as it is -0.264 for the fatigue relationship in Eq. (5-24) which was derived based on the data for both all-bolted and bolted-welded specimens. It should be noted that the coefficients in the above mentioned equations are dependent on the monotonic rotation capacity of a specific type of connection. In fact, considering this, a set of fatigue design curves with a slope of -0.3 can be derived for semi-rigid connections. In Figure 5-2, Eq. (5-24) is plotted for comparison.

It is also of interest to compare the predicted fatigue lives based on incipient failure and final fatigue fracture. From the results obtained, using Eqs (5-12) and (5-13) $N_{ff}/N_f = 1.78$. Alternatively, using Eqs (5-14) and (5-15) $N_{ff}/N_f = 1.62$. Therefore, it appears that the cyclic life beyond incipient failure is extended by around 60% following which separation fracture will result. In terms of energy, by comparing Eqs (5-20) and (5-21) the ratio of the total work done until final fatigue fracture to incipient failure is $W_{ff}/W_f = 1.52$. These margins may be considered to be factors of safety with respect to assessment based on incipient (first crack) failure.

Bearing in mind this factor of safety, dependable fatigue relationships may be generated for design such that first crack may be predicted that utilizes available energy absorption capacity while ensuring that complete separation failure has not taken place. Thus, reassessing the experimental results, it is recommended that the following dependable fatigue relationships be used for design purposes:

$$\theta_{jp} = 0.062\,(2N_f)^{-0.333} \tag{5-25}$$

$$\theta_j = 0.06\,(2N_f)^{-0.3} \tag{5-26}$$

$$W_f = 0.0138 M_{jp}\,(\theta_{jp})^{-1.0} \tag{5-27}$$

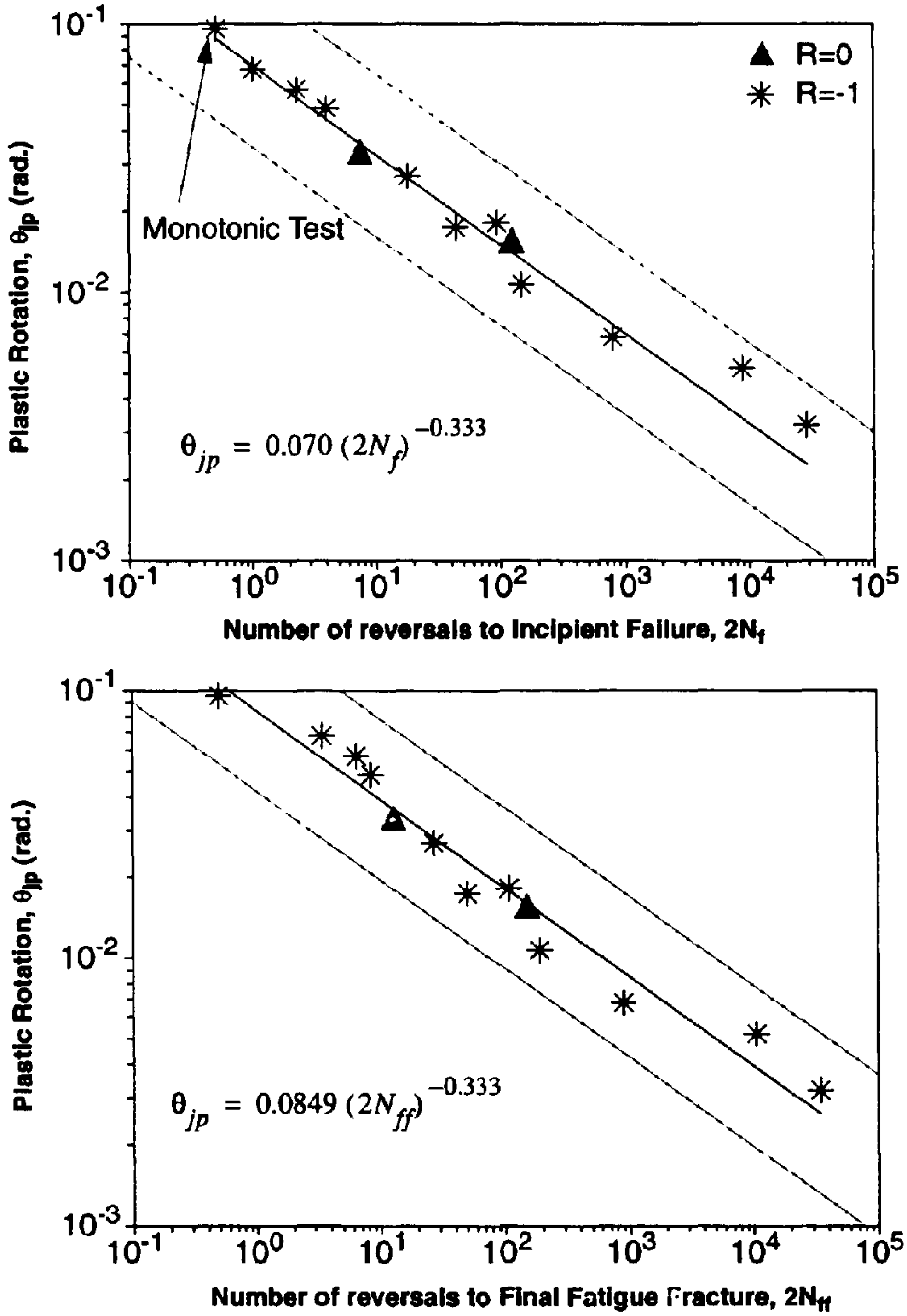

Figure 5-1 Fatigue Relationships-Plastic Rotation vs Fatigue Life

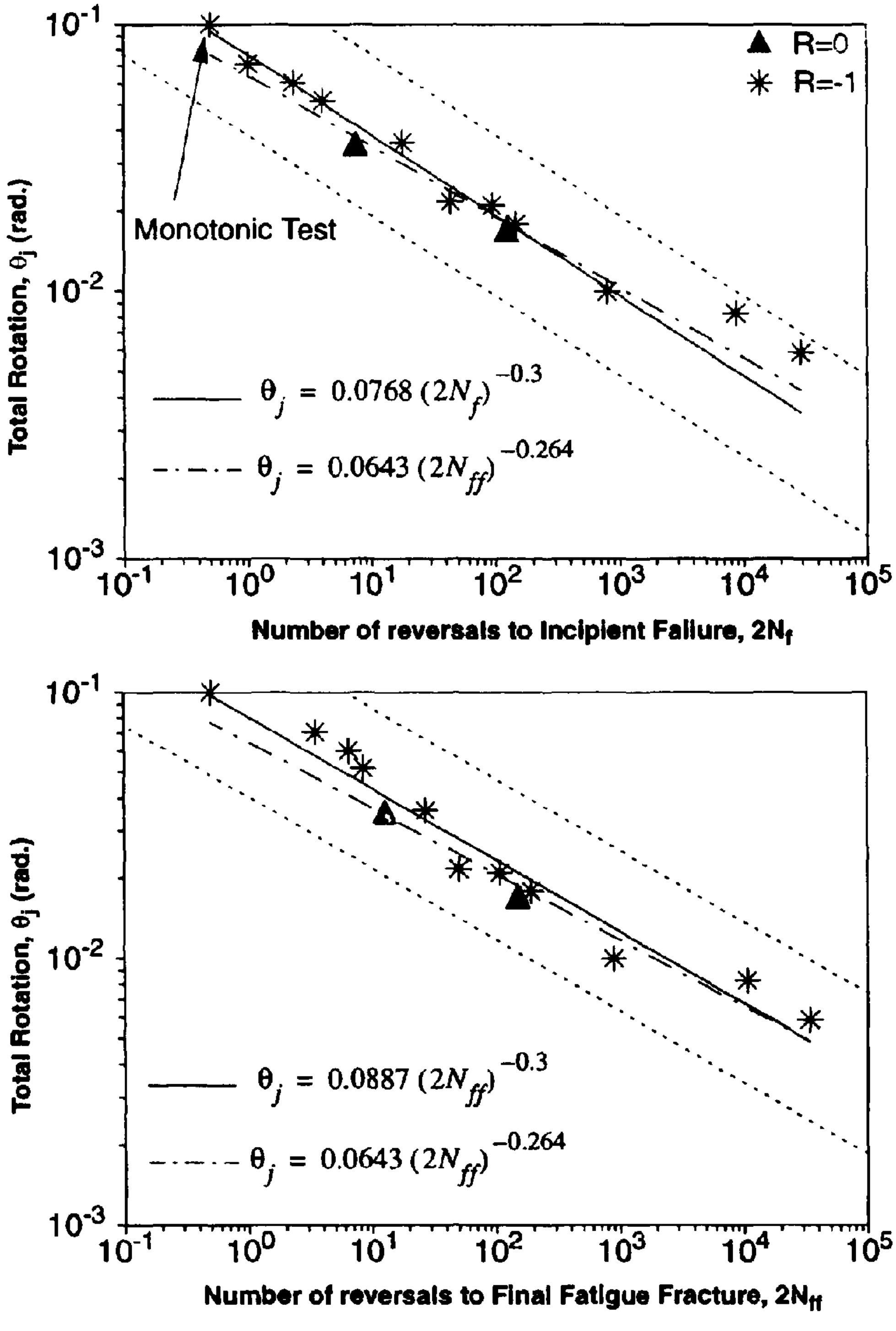

Figure 5-2 Fatigue Relationships-Total Joint Rotation vs Fatigue Life

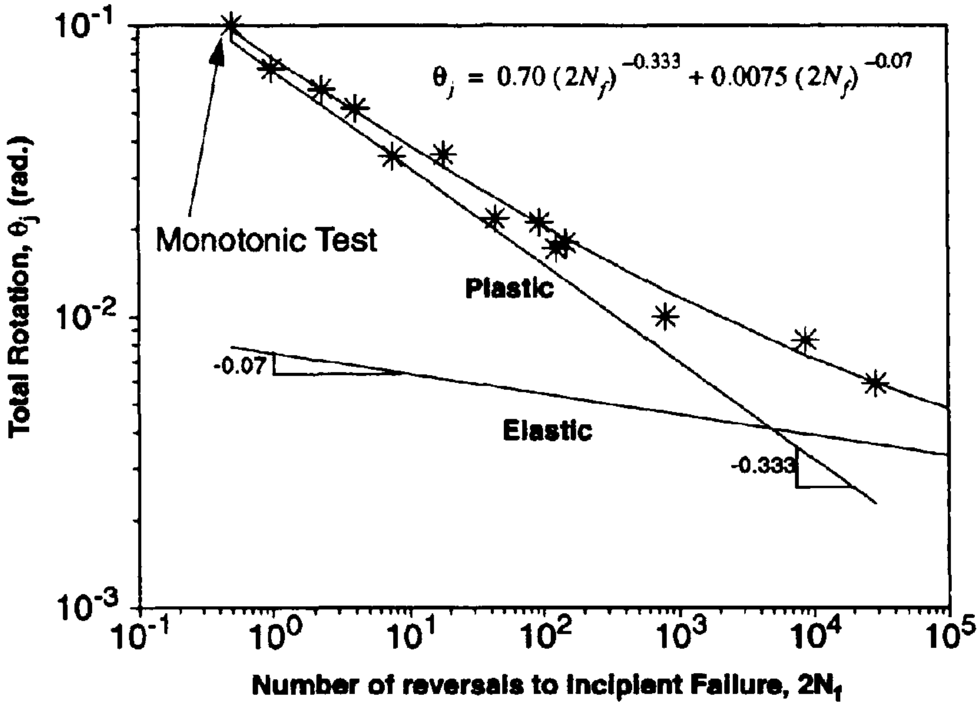

Figure 5-3 Coffin-Manson Model for Total Strain

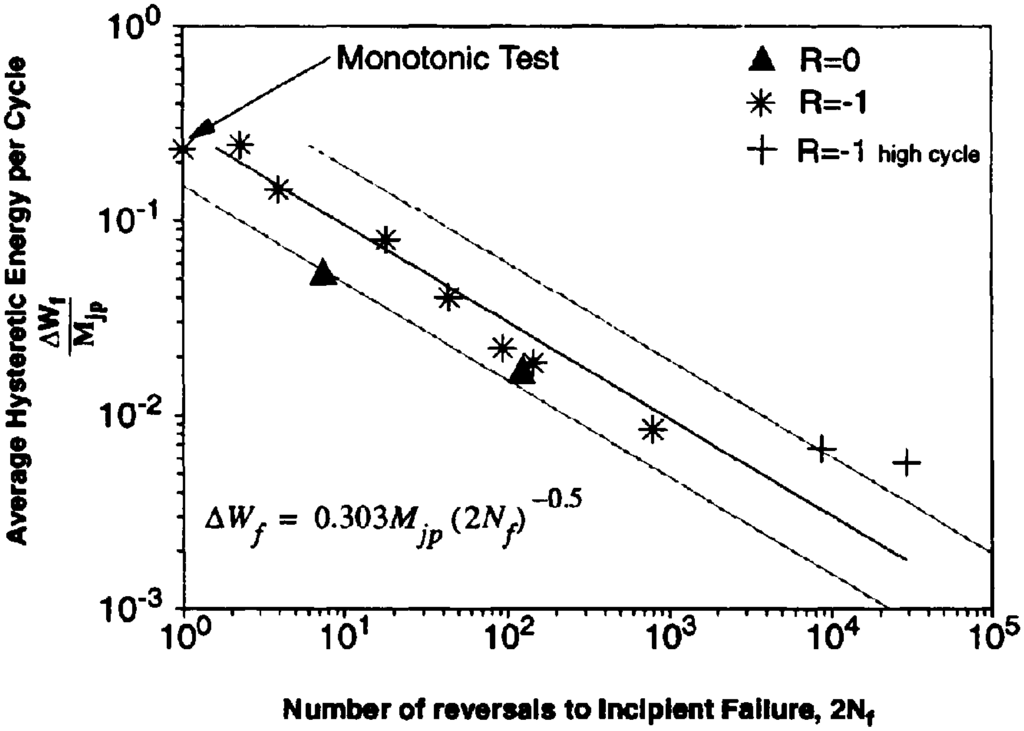

Figure 5-4 Fatigue Relationship-Energy per Cycle vs Fatigue Life

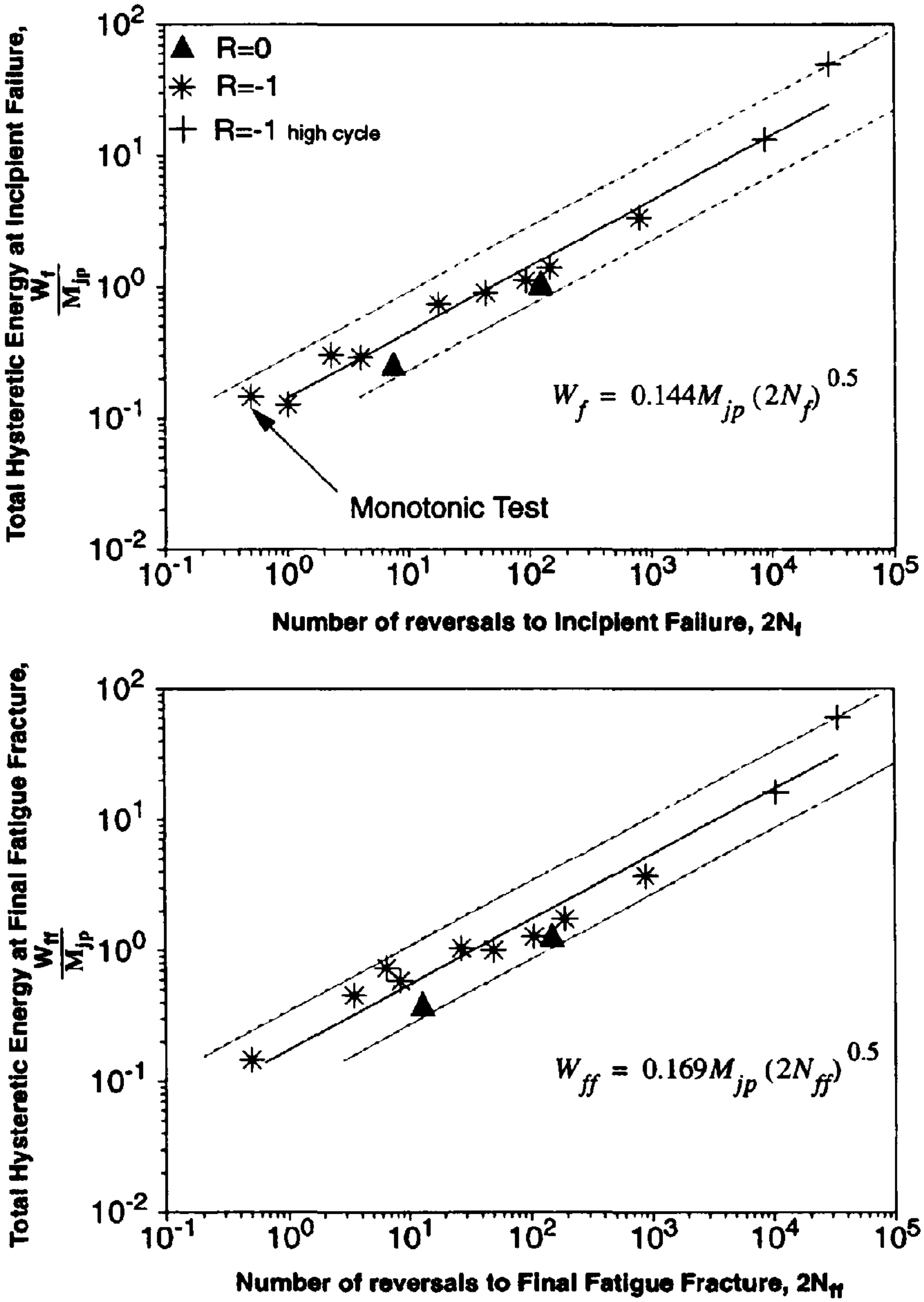

Figure 5-5 Fatigue Relationships-Energy vs Fatigue Life

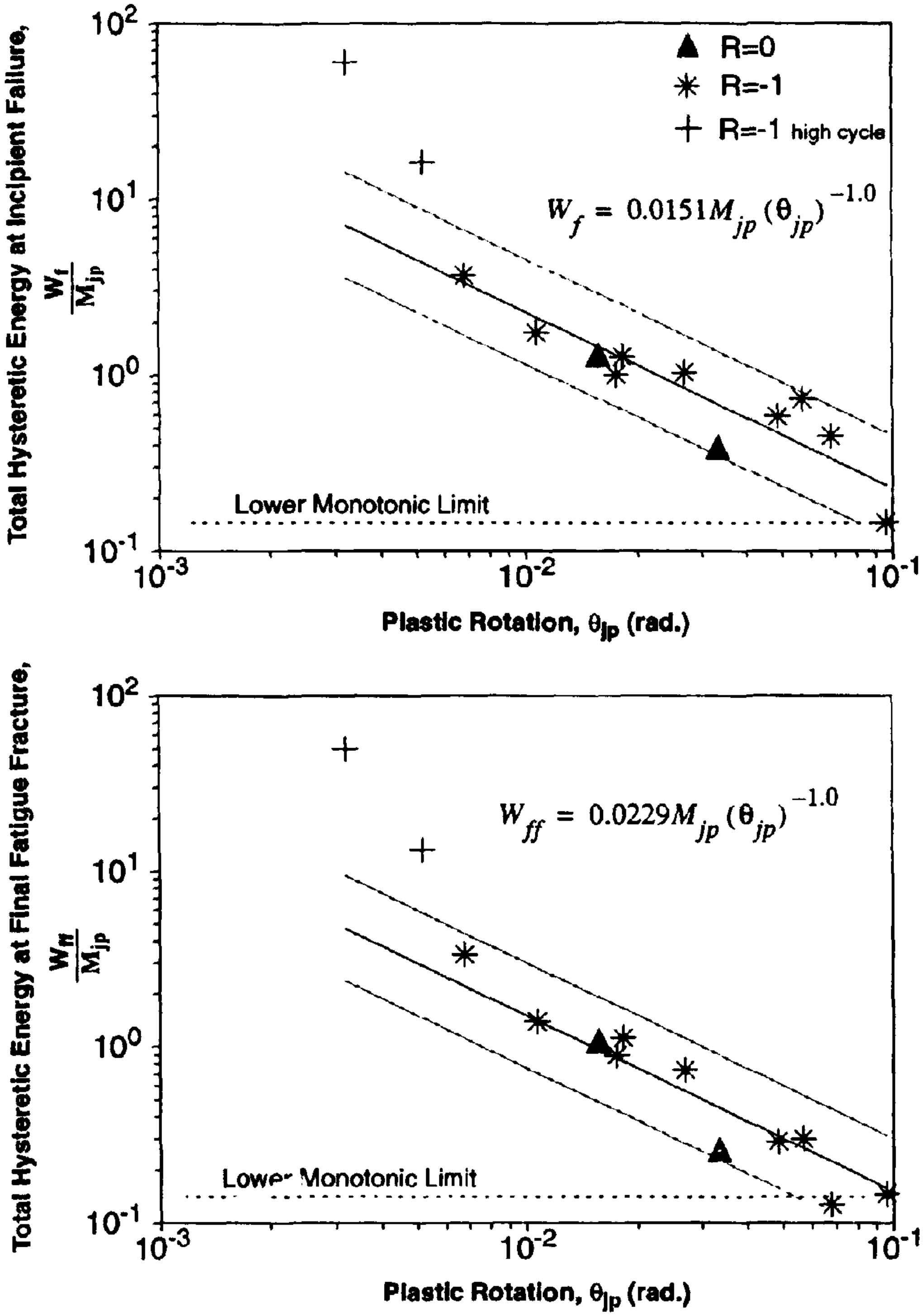

Figure 5-6 Fatigue Relationships-Energy vs Plastic Rotation

SECTION 6

DAMAGE MODELING FOR VARIABLE AMPLITUDE TESTS

6.1 Introduction

An energy based fatigue damage model is developed and applied to the variable amplitude fatigue tests. The model utilizes the constant amplitude relationships derived in Section 5. The energy based fatigue model is also compared with the more traditional fatigue life model, that is Miner's Rule coupled with the rainflow counting technique (Matsuishi and Endo 1968). The section first outlines this traditional approach and goes on to extend it to an energy based model.

6.2 Miner's Rule

The basis for the linear cumulative damage model consists of converting random cycles (displacement histories) into an equivalent number of constant amplitude cycles. Hence, damage fractions due to each individual cycle are summed until failure occurs.

Independently, Palmgren (1924) and Miner (1945) were first to propose a method which employs the linear damage accumulation law commonly known nowadays as Miner's Rule. In this method, the damage fraction D_i for the i^{th} cycle is defined as the life used up by the i^{th} event. Failure is assumed to occur when these damage fractions sum up to or exceed 1,

$$D_T = \sum D_i = \sum \left(\frac{1}{N_f}\right)_i \geq 1 \tag{6-1}$$

where $D_i = (1/N_f)_i$ is the damage fraction for the i^{th} cycle and $(N_f)_i$ = fatigue life at rotation amplitude θ_{ji}.

As discussed in the previous section, due to experimental scatter results of Miner's rule, damage fractions $\sum D_i$ are expected to fall between 0.5 and 2.0 at incipient failure. The difficulty in applying this method to variable amplitude loading arises from the fact that the loading histories in seismic events or other random loading such as wind or traffic often do not have well-defined cycles. To overcome the irregularities of real load histories, several cycle counting methods have been developed. One of the most widely used methods - the well known "rainflow cycle counting method" was used in this part of the study.

6.3 Effective Rotation

By employing Miner's Rule, an effective (or equivalent) constant amplitude rotation can be derived for a variable amplitude history. Eq. (5-2) can be rewritten as follows,

$$N_f = C\theta_j^{1/c} \tag{6-2}$$

The damage fraction D_i, according to Miner's Rule, for the i^th^ cycle of loading can be expressed as $D_i = 1/N_f$ where N_f is given by Eq. (6-2) for a certain rotation amplitude. Total damage, therefore can be written as in Eq. (6-1):

$$D_T = \sum D_i = \sum\left(\frac{1}{N_f}\right)_i = \sum\left(\frac{1}{C\theta_j^{1/c}}\right)_i \tag{6-3}$$

Damage at incipient failure, for N_f cycles at effective rotation amplitude, $\theta_{j\,\mathrm{eff}}$, is given by

$$D_{\mathrm{constant}} = N_f\left(\frac{1}{C\theta_{j\,eff}^{1/c}}\right) = 1 \tag{6-4}$$

Equivalent rotation amplitude can be determined by equating the total damage due to random loading with that due to constant-equivalent amplitudes (Eq. 6-4), which yields the following relation:

$$\frac{D_{\mathrm{random}}}{D_{\mathrm{constant}}} = \frac{\sum_{i=1}^{N_f}\left(\theta_j^{-1/c}\right)_i}{N_f\,\theta_{j\,eff}^{-1/c}} = 1 \tag{6-5}$$

Solving the above equation for $\theta_{j\,\mathrm{eff}}$,

$$\theta_{j\,eff} = \left(\frac{1}{N_f}\sum_{1}^{N_f}\theta_j^{-1/c}\right)^{-c} \tag{6-6}$$

Then effective plastic rotation (assuming R=-1) can be defined as,

$$\theta_{jp\,eff} = \theta_{j\,eff} - \frac{M(\theta_{j\,eff})}{K_e} \tag{6-7}$$

methods - the well known "rainflow cycle counting method" was used in this part of the study.

6.3 Effective Rotation

By employing Miner's Rule, an effective (or equivalent) constant amplitude rotation can be derived for a variable amplitude history. Eq. (5-2) can be rewritten as follows,

$$N_f = C\theta_j^{1/c} \tag{6-2}$$

The damage fraction D_i, according to Miner's Rule, for the i^{th} cycle of loading can be expressed as $D_i = 1/N_f$ where N_f is given by Eq. (6-2) for a certain rotation amplitude. Total damage, therefore can be written as in Eq. (6-1):

$$D_T = \sum D_i = \sum\left(\frac{1}{N_f}\right)_i = \sum\left(\frac{1}{C\theta_j^{1/c}}\right)_i \tag{6-3}$$

Damage at incipient failure, for N_f cycles at effective rotation amplitude, $\theta_{j\,eff}$, is given by

$$D_{\text{constant}} = N_f\left(\frac{1}{C\theta_{j\,eff}^{1/c}}\right) = 1 \tag{6-4}$$

Equivalent rotation amplitude can be determined by equating the total damage due to random loading with that due to constant-equivalent amplitudes (Eq. 6-4), which yields the following relation:

$$\frac{D_{\text{random}}}{D_{\text{constant}}} = \frac{\sum_{i=1}^{N_f}\left(\theta_j^{-1/c}\right)_i}{N_f\,\theta_{j\,eff}^{-1/c}} = 1 \tag{6-5}$$

Solving the above equation for $\theta_{j\,eff}$,

$$\theta_{j\,eff} = \left(\frac{1}{N_f}\sum_{1}^{N_f}\theta_j^{-1/c}\right)^{-c} \tag{6-6}$$

Then effective plastic rotation (assuming R=-1) can be defined as,

$$\theta_{jp\,eff} = \theta_{j\,eff} - \frac{M(\theta_{j\,eff})}{K_e} \tag{6-7}$$

where $\theta_{j\,eff}$ = effective rotation amplitude determined from Eq. (6-6) for the entire history, M = connection moment on the cyclic moment-rotation envelope corresponding to $\theta_{j\,eff}$ and K_c = initial connection stiffness (Section 4). Eq. (6-6) is related to the root mean cube of the response for a value of $c = -1/3$ where θ_j is taken as the peak amplitude for each cycle ($\theta_j = (\theta_{jmax} - \theta_{jmin})/2$). However, it is generally difficult to identify the peaks and troughs in a highly irregular or random event. Instead, if the points at each time step (Δt) in an analysis or experiment are used and the motion is harmonic, it can be shown that

$$\theta_{j\,eff} = 1.33\left(\frac{t}{\Delta t}\sum_{i=1}^{t_f}(\theta_j - \bar{\theta}_j)_i^3\right)^{1/3} \tag{6-8}$$

where $\bar{\theta}_j$ = mean rotation angle, t= total time and Δt= experimental time step.

A cyclic moment-rotation envelope curve can be deduced from a cyclic decremental test. The Menegotto-Pinto equation was used to define this envelope as explained in Section 4 and is given by

$$M = K_{je}\theta_j\left[Q + \frac{1-Q}{\left[1 + \left|\frac{K_{je}\theta_j}{M_y}\right|^R\right]^{1/R}}\right] \tag{6-9}$$

with K_{jc}=120000 kip-in, M_y=200 kip-in, Q=0.0415 and R=2.

Equivalent amplitude data points determined using Eq. (6-7) are plotted in Figure 6-1 and compared with the constant amplitude tests at incipient failure as well as final fatigue failure. This compares favorably with the constant amplitude test curves and the data points are well within the upper (+100%) and lower (-50%) envelopes.

6.4 Energy Based Modeling

Miner's rule, which is defined in Eq (6-1), can be modified as follows. Again, in this case the failure is assumed to occur when the summation of damage fractions equals or exceeds 1:

$$D_{wT} = \sum D_{wi} = \sum \frac{w_i}{W_{fi}} \geq 1 \tag{6-10}$$

in which w_i = total work done for the i^{th} cycle at rotation amplitude θ_{ji}, and W_{fi} = total work done as a function of the current rotation amplitude θ_{ji}. Furthermore, Eq. (6-10) can be rewritten to obtain the damage fraction as the ratio of incremental energy for the i^{th} time step to the current total energy as follows:

$$D_{wT} = \sum D_{wi} = \sum \frac{\delta w_i}{W_f(\theta_{\mathrm{jp\,eff}})} \geq 1 \qquad (6\text{-}11)$$

where δw = instantaneous incremental energy for the time interval (Δt) and is given by

$$\delta w_i = 0.5\,(M_i + M_{i-1})\,(\theta_{ji} - \theta_{j\,i-1}) \qquad (6\text{-}12)$$

$W_f\,(\theta_{\mathrm{jp\,eff}})$= total energy corresponding to the current effective plastic connection rotation $\theta_{\mathrm{jp\,eff}}$ of the i^{th} time step. For the variable amplitude tests described in Section 3, Figure 6-2 shows the total energy plotted against the effective plastic rotation $\theta_{\mathrm{jp\,eff}}$ (Eq. 6-7). These test results are compared with the constant amplitude relationships described in Section 5. The results demonstrate that the concept of converting variable amplitude history into an equivalent constant amplitude history appears viable for at least the investigated class of semi-rigid connections.

The advantage of employing an energy based model is that memory (sequence) effects can be taken into account by using the effective plastic rotation in determining the total energy until incipient failure, W_f. The value of W_f at a certain plastic rotation amplitude can be calculated using a low-cycle fatigue relationship in the form of Eq. (5-20), derived in Section 5. It should also be noted that W_f in Eq. (6-10) can be replaced by W_{ff}, in which case using the fatigue relationship of Eq. (5-21) total damage can be calculated at final fatigue failure.

6.5 Application

Table 6-1 summarizes the damage analysis results based on Eq. (5-20). In each case, the denominator in Eq. (6-10) was updated after each experimentally observed time step using corresponding effective connection rotation which was determined from Eq. (6-8).

Figures 6-3 through 6-7 show the rotation and moment time-histories for each variable amplitude test. The effective connection rotation ($\theta_{j\,\mathrm{eff}}$) is also plotted on the connection rotation graph in order to demonstrate the sequence effects on connection behavior. The accumulation of damage for both Miner's Rule and the proposed energy based model are also shown in these figures. For the latter model, damage at time t is computed by substituting Eq. (6-12) in the numerator and Eq. (5-20) into Eq. (6-11):

$$D(t) = \sum_{i=1}^{t} \left[\left(\frac{M_i + M_{i-1}}{2} \right) (\theta_{j\,i} - \theta_{j\,i-1}) \frac{\theta_{jp\,i}}{0.0151 M_{jp}} \right] \tag{6-13}$$

where $\theta_{jp\,i}$ is given by Eq. (6-7) and i = data point number.

Table 6-I Summary of Damage Analysis Results for Variable Amplitude Tests

Spec Id.	Experimental Results				Effective Amplitudes (rad)				Damage Rules			
					$\theta_{j\,eff}$		$\theta_{jp\,eff}$		Miner's		Energy Based	
	N_f	N_{ff}	W_f (kip-in)	W_{ff} (kip-in)	Incipient	Failure	Incipient	Failure	at N_f	at N_{ff}	at N_f	at N_{ff}
V_18	80	152	415.2	646.6	0.0202	0.0187	0.0177	0.0163	1.89	2.73	1.87	2.62
V_17	18	181	187.7	781.5	0.0274	0.0191	0.0246	0.0167	1.08	3.32	1.01	3.11
V_16	55	59	334.8	393.6	0.0181	0.0198	0.0158	0.0174	0.89	1.29	0.97	1.19
V_15	46	75	284.0	341.7	0.0220	0.0200	0.0195	0.0176	1.36	1.65	1.09	1.30
V_14	60	64	332.3	375.0	0.0204	0.0213	0.0179	0.0188	1.40	1.71	0.99	1.15

It can be observed from Table 6-I and Figures 6-3 and 6-4 that for high-low step tests, both models produce a similar type of damage accumulation, i.e. the damage rate as well as the cumulative damage at N_f and N_{ff} are similar. However, for the other test specimens the damage accumulation patterns are different for the two models, with the energy based model giving improved results for both N_f and N_{ff}. Rotation, moment and cumulative damage plots for decreasing-increasing and increasing-decreasing tests (V_15, V_14), are as shown in Figures 6-6 and 6-7, respectively. It appears from the cumulative damage plots that the energy based damage model is more capable of reflecting the effect of past rotation histories due to the use of the effective plastic rotation amplitude. Moreover, the area within the moment-rotation loops (energy) is directly affected by the sequence of loading which in turn is reflected in the rate of damage accumulation.

6.6 Discussion

The proposed energy based low-cycle fatigue damage model was validated by the variable amplitude test results on top-and-seat angle connections. This validation is over the range of amplitudes expected in the response of relatively weak steel structures in an extreme earthquake excitation ($\theta j < 0.04$ radians). This model monitors the incremental damage via hysteretic energy absorption. This was found to be a convenient way of characterizing the energy capacity under both constant and variable amplitude histories since cyclic energy dissipation mainly depends on the plastic rotation. For analysis with real earthquake time histories, cycle counting as required by Miner's Rule may become quite cumbersome. Hence, an important advantage of the energy-based approach is that no cycle counting is necessary for damage evaluation purposes.

The results demonstrate that the concept of converting variable amplitude history into an equivalent constant amplitude history appears viable for at least the investigated class of semi-rigid connections. The advantage of employing an energy based model is that the memory effects can be taken into account by using the effective plastic rotation in determining the total energy till incipient failure, W_f. The value of W_f at a certain plastic rotation amplitude can be calculated using a low-cycle fatigue relationship in the form of Eq. (5-18). Krawinkler and Zohrei (1983) used an implicit form of Miner's Rule of linear damage rule accumulation in conjunction with Eq. (5-12) using an exponent of -0.5 to -0.67 for welded steel connections. Mean rotation effects were ignored in the formulation whereas, in this study, linear damage accumulation has been extended using energy absorption concepts. Moreover, mean rotation effects have been taken into account by numerically integrating the dissipated energy as mentioned previously.

Effective total connection rotation instead of effective plastic rotation can also be used in the damage analysis. Although it is not reported herein, such an analysis was undertaken and the damage accumulation patterns yielded similar results within a ±5 % range.

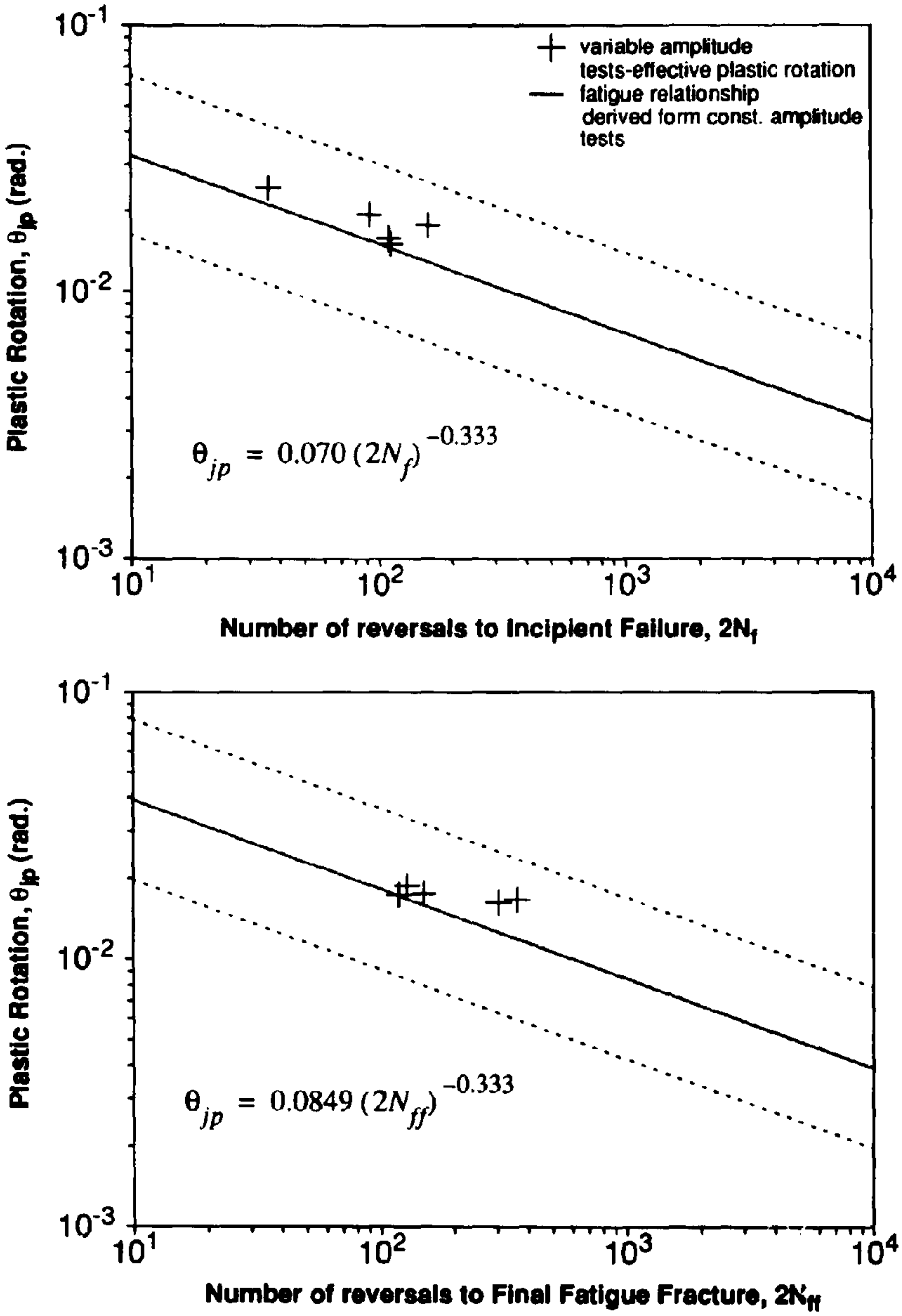

Figure 6-1 Fatigue Relationships-Plastic Rotation vs. Fatigue Life for Variable Amplitude Tests

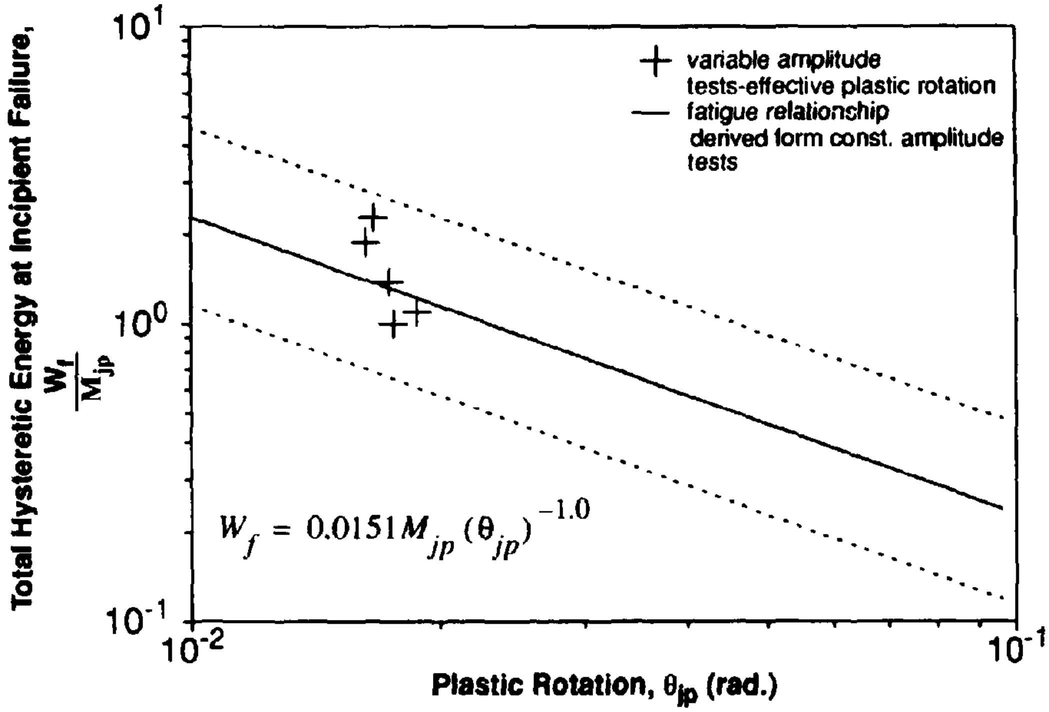

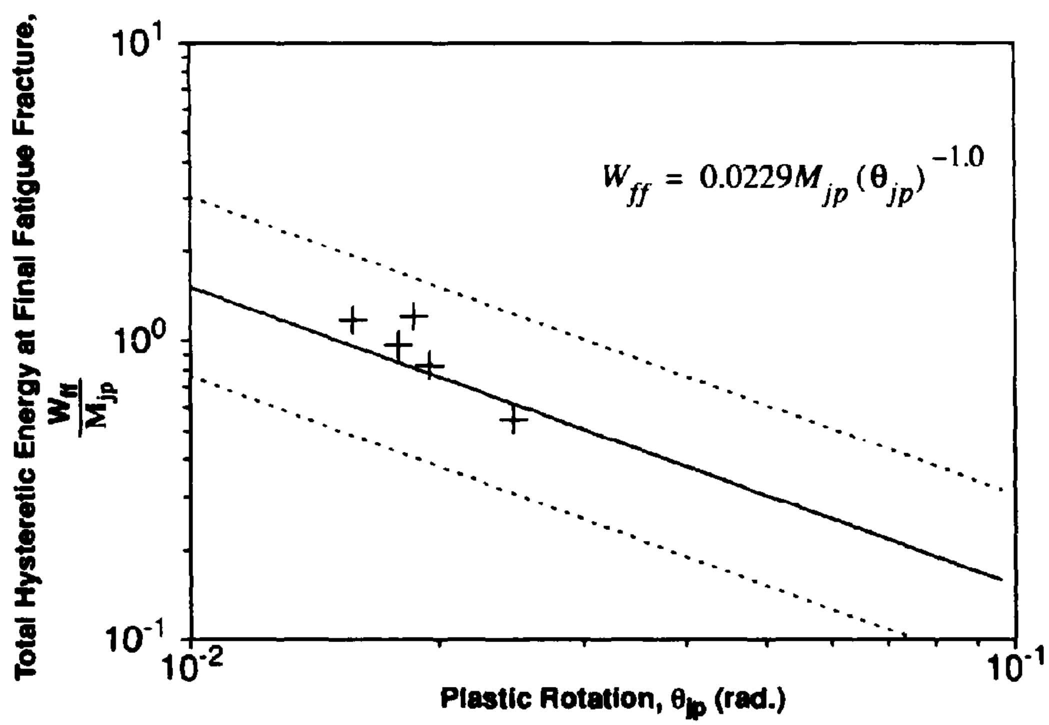

Figure 6-2 Fatigue Relationships-Energy vs. Effective Plastic Rotation for Variable Amplitude Tests

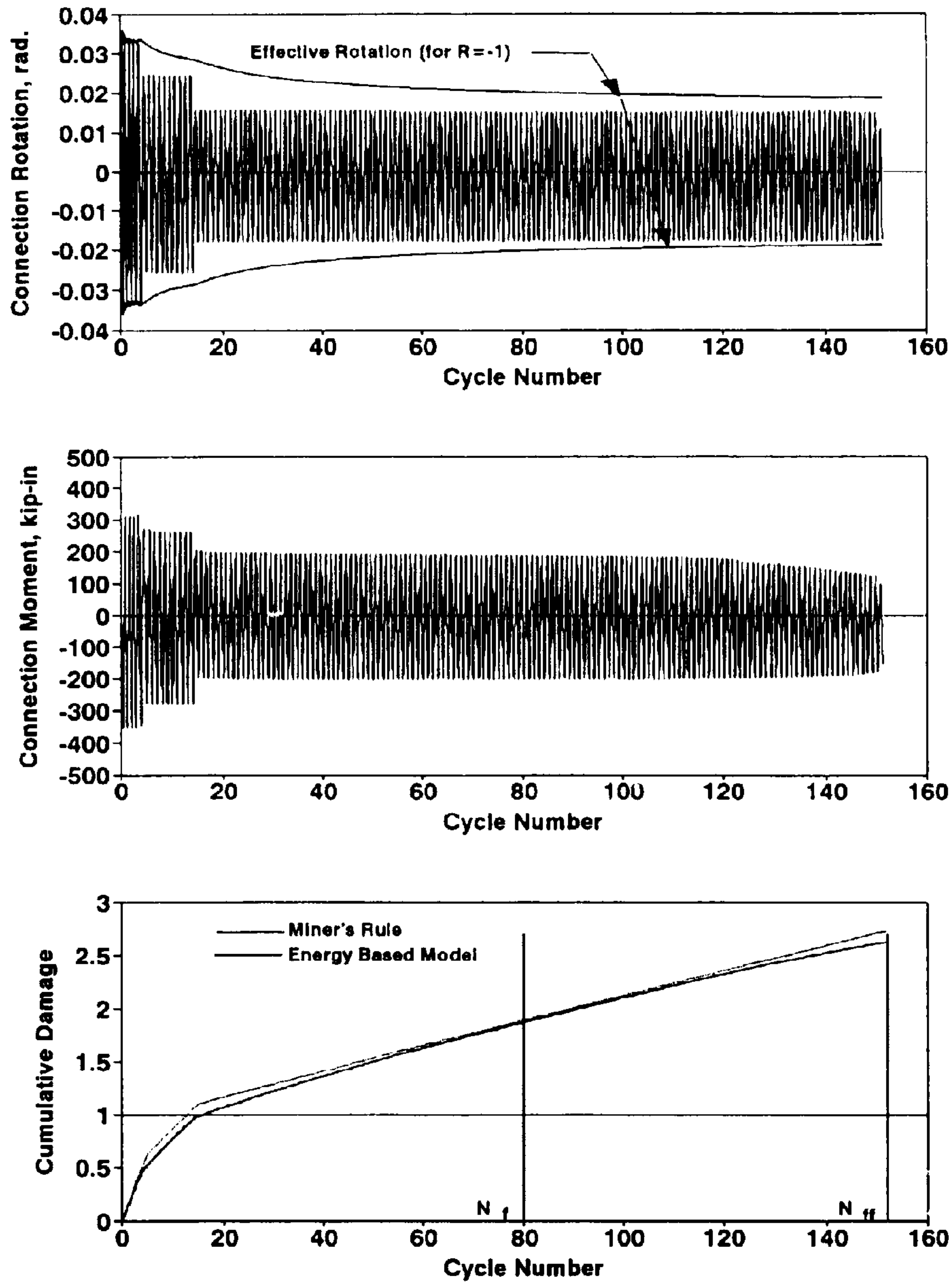

Figure 6-3 Rotation, Moment History and Cumulative Damage Fraction Specimen V_18

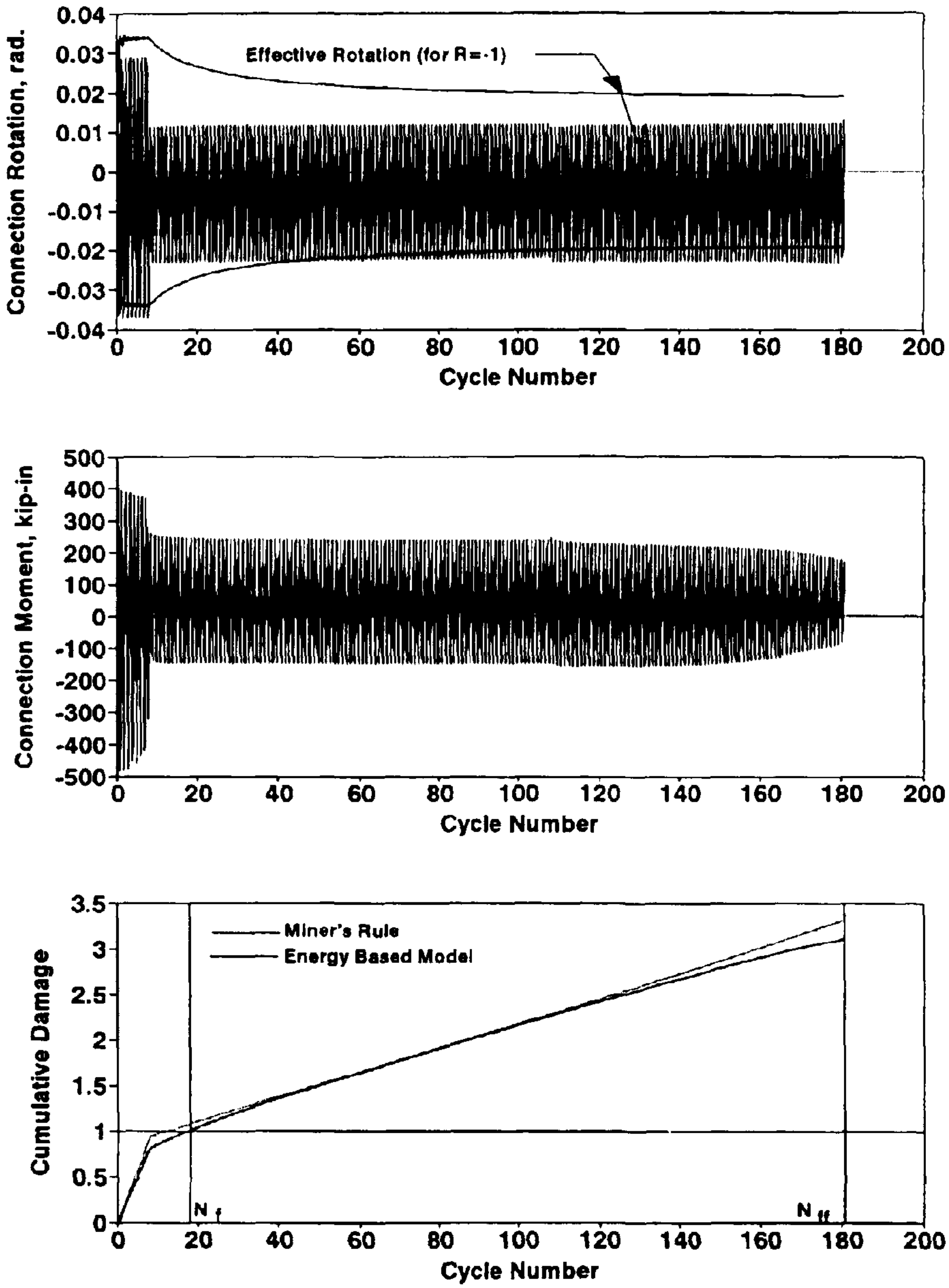

Figure 6-4 Rotation, Moment History and Cumulative Damage Fraction Specimen V_17

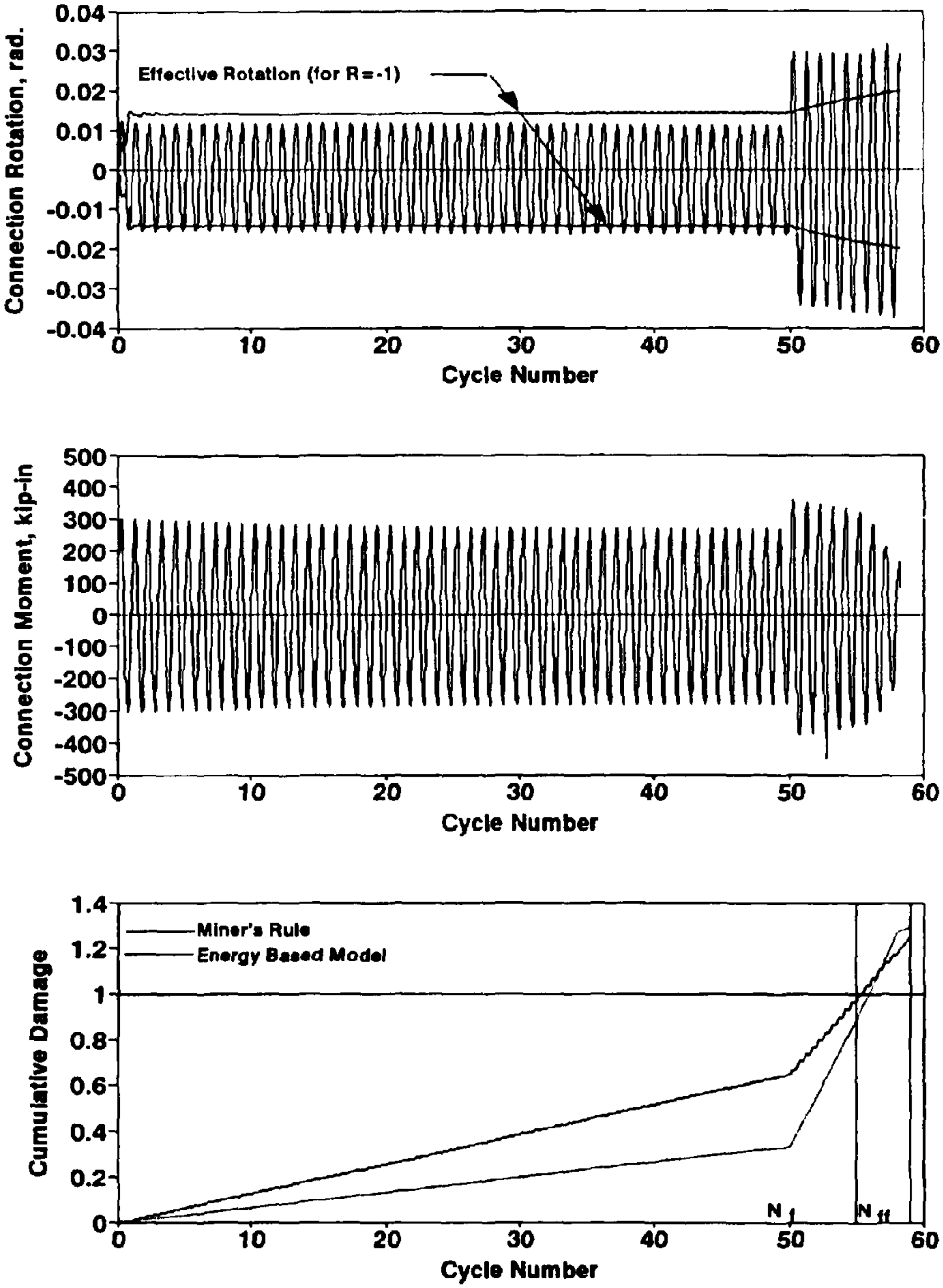

Figure 6-5 Rotation, Moment History and Cumulative Damage Fraction
Specimen V_16

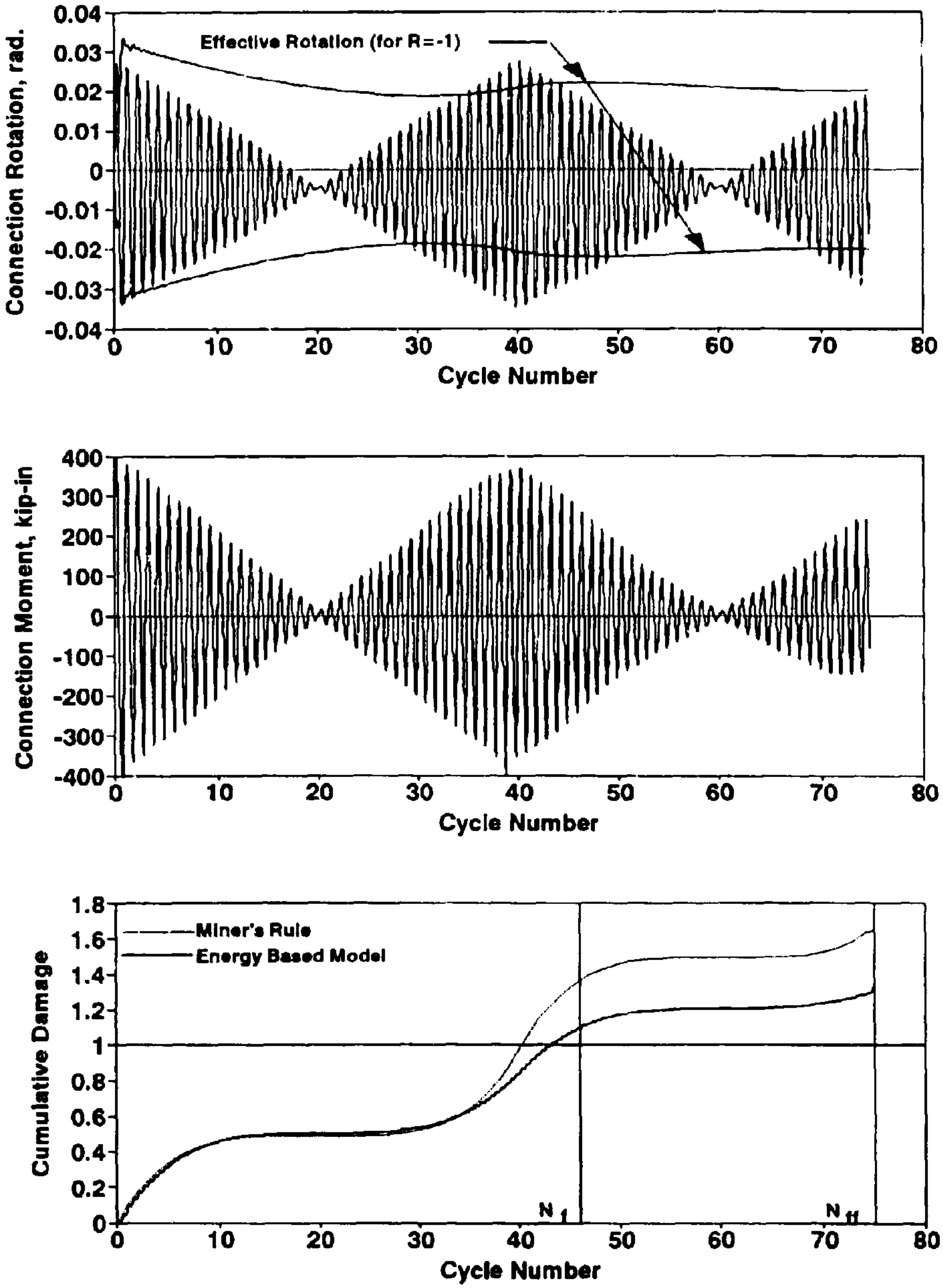

Figure 6-6 Rotation, Moment History and Cumulative Damage Fraction Specimen V_15

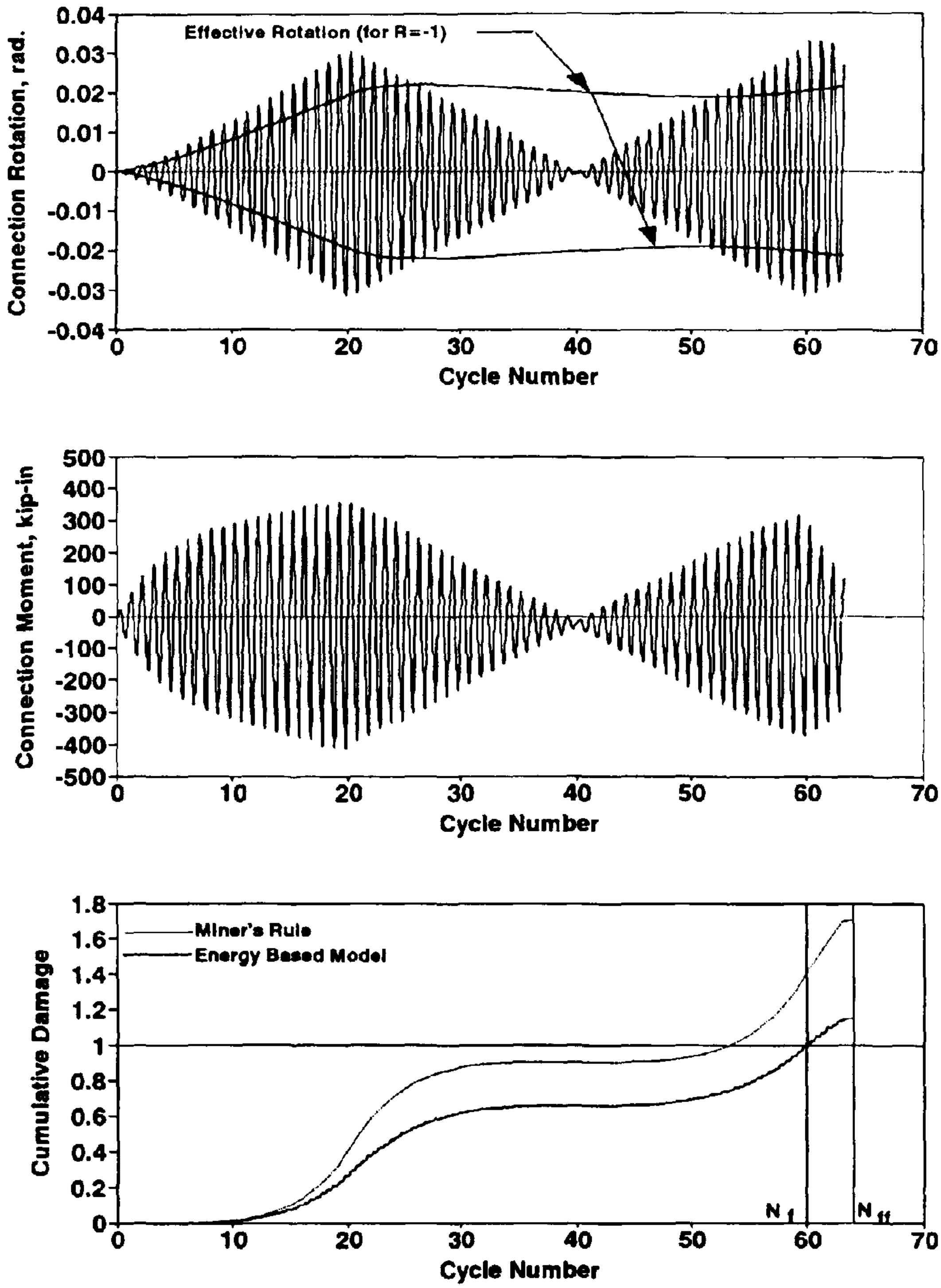

Figure 6-7 Rotation, Moment History and Cumulative Damage Fraction Specimen V_14

SECTION 7

SUMMARY AND CONCLUSIONS

7.1 Summary

The main purpose of this research was to experimentally observe the performance of a specific type of semi-rigid top-and-seat angle connection under static and cyclic loadings and to study the low-cycle fatigue characteristics. For this purpose, a total of nineteen identical pairs of connection angles were tested under various rotation amplitudes. The experimental test program consisted of three main groups; i) Static (monotonic) test, ii) Constant amplitude tests, iii) Variable amplitude tests.

An analytical investigation was carried out in order to predict the initial connection stiffness, mechanism moment capacity and plastic connection rotation. Predictions are compared with those of previous studies. The moment-rotation curve was calibrated for the Menegotto-Pinto analytical model which incorporates the plastic, elastic connection stiffness ratio, yield moment and a shape factor.

Variable amplitude tests included incremental-decremental and step tests to investigate the sequence effects on cyclic and low-cycle fatigue behavior of top-and-seat angle connections. An effective connection rotation concept was introduced as the characteristic feature of rotation history. In the light of the fatigue data generated from constant amplitude test results, various low-cycle fatigue relationships were developed. An energy based cumulative damage model was developed using effective plastic connection rotation along with the energy-life and energy-rotation relationships. The proposed damage model was employed in fatigue life and damage prediction analysis and compared with the classical Miner's linear damage model.

7.2 Conclusions

The following conclusions can be drawn based on the experimental and analytical study reported herein:

1. Although each specimen had identical material properties, the resultant apparent strength and stiffness varied markedly. A comparison of the experimentally observed values to the analytically predicted values have shown that initial connection stiffness and plastic moment capacity are very sensitive to the first yield (monotonic) line location due to the fact that the orientation of the bolt head and/or nut (fabrication) had a considerable effect on the failure mode and on the plastic hinging in the connection elements. Upper and lower bounds of strengths were obtained when the flats of the hexagonal nuts were oriented either parallel or at 30 degrees to the center line of column. This implies that the capacity of semi-rigid bolted connections could be more reliably controlled if the location of hinging in the angle adjacent to the column is fixed. It should be noted however, that the fatigue life appears independent of the nut orientation.

2. From the constant amplitude test results, it was concluded that the per-cycle hysteresis energy at a certain amplitude did not change significantly till the incipient failure. This fact can be better observed in relatively small amplitude tests.

3. Study of fatigue behavior showed that the commonly used hysteretic energy-life and rotation-life models can be employed in the low-cycle fatigue analysis of this specific type of top-and-seat angle connection. Therefore, a fatigue-life relationship was developed based on an analogy with the standard metal fatigue life relationship proposed by Manson and Coffin. This implication from this result for seismic design would indicate that if plastic hinge rotations are kept below 2 percent then at least 50 cycles of complete load reversals can be guaranteed. Furthermore, based on the recent fatigue analysis work carried out at SUNY at Buffalo (Mander et.al. 1992, Chang and Mander 1994), it can be shown that the equivalent number of equi-amplitude inelastic cycles at the maximum response displacement that may be expected for metal structures in a typical US earthquake is N_f = 7. Thus, from Eq. (5-12) the maximum plastic rotation capacity for such top-and-seat angle connections considered in this study is 0.029 radians. This large fatigue-based rotation capacity would generally well exceed expected demands for most structural steel systems where total drifts rarely exceed 2 percent.

4. Real earthquake response however, is concerned with variable amplitude behavior of members. One way in which seismic induced damage can be assessed is to compare hysteretic energy capacity to hysteretic demand induced by earthquakes. Therefore, energy as well as cyclic rotation based fatigue damage relationships were derived using the experimental data obtained in the present study. The relationships which were found to

represent the best fit to experimental data are as follows:

$$\theta_{jp} = 0.070\,(2N_f)^{-0.333} \tag{5-12}$$

$$\Delta W_f = 0.303 M_{jp}\,(2N_f)^{-0.5} \tag{5-17}$$

$$W_f = 0.0151 M_{jp}\,(\theta_{jp})^{-1.0} \tag{5-20}$$

5. Mean stress/rotation effects do not appear to have a significant effect on the low-cycle fatigue life of the class of top-and-seat angle connection tested herein, as can be observed from the fatigue plots.

6. It was observed from the step tests that the low-cycle fatigue life is considerably different for two step tests which have the same amplitude step blocks in reverse order (compare Figures 6-4 and 6-5). This squence dependence is due to the memory effects of the material. However, for the two incremental-decremental and decremental-incremental tests which were conducted at the same cycling frequency and maximum amplitude, low-cycle fatigue life as well as dissipated energy is comparable, i.e. sequence effects are not apparent in this case. All of the variable amplitude tests fall within the region bounded by damage index of **0.5** and **2.0** which corresponds to 95 percentile range with a lognormal distribution in experimental scatter.

7. From the low-cycle fatigue tests, it was observed that the specimen life may be continued by some 60%, following the first crack initiation (incipient failure), until complete seperation results. For design purposes, this reserve life may be considered as part of a factor of safety assuring that the complete separation will not take place.

8. An energy based cumulative damage model with incremental monitoring of the entire history was developed. An effective plastic connection rotation concept was introduced in the cumulative damage model. This was found to be a convenient way of characterizing the energy capacity under both constant and variable amplitude histories since the cyclic energy dissipation mainly depends on the plastic rotation. Sequence effects are taken into account by numerically integrating the dissipated energy and revising the denominator of the damage fraction at each time step. Hence, no cycle counting is necessary for damage evaluation purposes as opposed to Miner's Rule as it requires cycle counting which may become quite cumbersome for real earthquake time histories. However, although the model is general in nature, it should be validated for different top-and-seat angle bolting geometries. In order for the model to be utilized for different types of steel connections, such as welded connections or connections with web cleats, further tests should be conducted to calibrate the fatigue relationships reported in Section 6.

SECTION 8

REFERENCES

American Institute of Steel Construction, *Load and Resistance Factor Design Seismic Provisions for Structural Steel Buildings*, Chicago, 1992.

American Institute of Steel Construction, *Specifications for the Design, Fabrication and Erection of Structural Steel for Buildings (9th ed.)*, Chicago,1989.

Astaneh, A., Nader, M., and Malik, L., "Cyclic Behavior of Double Web Angle Connections," *Journal of Structural Engineering*, Vol. 115, No. 5, pp. 1101-1118, 1989.

ASTM, "Standard Test Methods of Tension Testing of Metallic Materials," Vol. 03.01, 1992, pp. 130-146

Azizinamini, A., Bradburn, J. H., and Radziminski, J. B., "Static and Cyclic Behavior of Semi-Rigid Steel Beam-Column Connections," *Technical Report*, Dept. of Civil Engineering, University of South Carolina, March 1985.

Chang, G. A., and Mander J. B., "Seismic Energy Based Fatigue Damage Analysis of Bridge Columns: Part II - Evaluation of Seismic Demand," *National Center for Earthquake Engineering Research, NCEER Technical Report No. 94-0013*, State University of New York at Buffalo, 1994.

Chasten, C. P., Fleischman, R. B., Driscoll, G. C., and Lu, L. W., "Top and Seat Angle Connections and End-Plate Connections: Behavior and Strength Under Monotonic and Cyclic Loading," *Proceedings, 1989 National Steel Construction Conference*, AISC, Nashville, TN., pp. 6-1 to 6-32.

Coffin, L. F. Jr., "A Study of the Effects of Cyclic Thermal Stresses on a Ductile Metal," *Trans. ASME*, Vol. 76, August 1954, pp. 931-950.

Dunai, L., and Lu, L. W., "Analytical Modeling of Bolted Semi-Rigid Connections," *in*

Bjorhovde, R., ed., Connections in Steel Structures II: Behavior, Strength and Design, AISC, 1992.

Harper, W. L., Jr., Dickerson, J. R., Bradburn, J. H., and Radziminski, J. B., "Static and Cyclic Behavior of Semi-Rigid Bolted and Welded Beam-Column Connections," *Structural Research Studies, Technical Report*, Dept. of Civil Engineering, University of South Carolina, May 1990.

Huang, J., and Morris, G., "Analysis of Flexibly Connected Frames under Non-Proportional Loading," *in Bjorhovde, R., ed., Connections in Steel Structures II: Behavior, Strength and Design*, AISC, 1992.

Kishi, N., and Chen, W. F., "Moment-Rotation Relation of Top-and-Seat Angle Connections," *Structural Engineering Report No. CE-STR-86-26*, School of Civil Engineering, Purdue University, 1986, West Lafayette, Ind.

Kishi, N., and Chen, W. F., et.al., "Moment-Rotation Relation of Top-and-Seat Angle with Double Web Angle Connections," *Proceedings of the State-of-Art Workshop on Connections and the Behavior, Strength and Design of Steel Structures*, Ecole Normale Superieure de Cachan, France, May 25-27, 1987, Elsevier, London, pp. 121-134.

Kishi, N., Chen, W. F., Goto, Y., and Matsuoka, K. G., "Design Aid of Semi-Rigid Connections for Frame Analysis," *AISC Engineering Journal*, Third Quarter, 1993, Vol. 30, No. 3, pp. 90-107.

Koh, S. K., Stephen, R. I., "Mean Stress Effects on Low-Cycle Fatigue for a High Strength Steel," *Fatigue Fracture of Engineering Materials and Structure*, Vol. 14, 1991, pp. 413-428.

Krawinkler, H., and Zohrei, M., "Cumulative Damage in Steel Structures Subjected to Earthquake Ground Motions", *Journal of Computers and Structures*, Vol. 16, No. 1-4, 1983, pp. 531-541.

Mander, J. B., Panthaki, F. D., and Chaudhary, M. T., "Evaluation of Seismic Vulnerability of Highway Bridges in the Eastern United States," *Lifeline Earthquake Engineering in the Central and Eastern U.S.*, ASCE Technical Council on Lifeline Earthquake Engineering, No. 5, pp. 72-86, 1992.

Manson, S. S., "Behavior of Materials under Conditions of Thermal Stress," *Heat Transfer Symposium*, University of Michigan Engineering Research Institute, 1953, pp. 9-75.

Matsuishi, M., and Endo, T., "Fatigue of Metals Subjected to Varying Stress", paper presented to Japan Society of Mechanical Engineers, Fukuoka, March 1968.

Menegotto, M. and Pinto, P. E., "Method of Analysis for Cyclically Loaded Reinforced Concrete Plane Frames Including Changes in Geometry and Non-Elastic Behavior of Elements Under Combined Normal Forces and Bending," *IABSE Symposium on the Resistance and Ultimate Deformability of Structures Acted on by Well-Defined Repeated Loads*, Lisbon, 1973.

Miner, M. A., "Cumulative Damage in Fatigue," Trans. ASME, Journal of Applied Mechanics, Vol. 67, 1945, pp. A159-A164.

Nader, N. M., Astaneh, A., "Seismic Behavior and Design of Semi-Rigid Steel Frames," *Technical Report No. UCB/EERC-92/06*, Earthquake Engineering Research Center, University of California at Berkeley, May 1992.

Palmgren, A., "Durability of Ball Bearings," ZVDI, Vol. 68, No. 14, 1924, pp. 339-341 (in German).

Richard, R. M., and Abbott, B. J., "Versatile elastic-plastic stress-strain formula," *Journal of Engineering Mechanics Division ASCE*, 101 (EM4), 1975, pp. 511-515.

Tong, X., Wang, D. and Xu, H., "Investigation of Cyclic Hysteresis Energy in Fatigue Failure Process," International Journal of Fatigue, Vol. 11, No. 5, September 1989, pp. 353-359.

NATIONAL CENTER FOR EARTHQUAKE ENGINEERING RESEARCH
LIST OF TECHNICAL REPORTS

The National Center for Earthquake Engineering Research (NCEER) publishes technical reports on a variety of subjects related to earthquake engineering written by authors funded through NCEER. These reports are available from both NCEER's Publications Department and the National Technical Information Service (NTIS). Requests for reports should be directed to the Publications Department, National Center for Earthquake Engineering Research, State University of New York at Buffalo, Red Jacket Quadrangle, Buffalo, New York 14261. Reports can also be requested through NTIS, 5285 Port Royal Road, Springfield, Virginia 22161. NTIS accession numbers are shown in parenthesis, if available.

NCEER-87-0001 "First-Year Program in Research, Education and Technology Transfer," 3/5/87, (PB88-134275).

NCEER-87-0002 "Experimental Evaluation of Instantaneous Optimal Algorithms for Structural Control," by R.C. Lin, T.T. Soong and A.M. Reinhorn, 4/20/87, (PB88-134341).

NCEER-87-0003 "Experimentation Using the Earthquake Simulation Facilities at University at Buffalo," by A.M. Reinhorn and R.L. Ketter, to be published.

NCEER-87-0004 "The System Characteristics and Performance of a Shaking Table," by J.S. Hwang, K.C. Chang and G.C. Lee, 6/1/87, (PB88-134259). This report is available only through NTIS (see address given above).

NCEER-87-0005 "A Finite Element Formulation for Nonlinear Viscoplastic Material Using a Q Model," by O. Gyebi and G. Dasgupta, 11/2/87, (PB88-213764).

NCEER-87-0006 "Symbolic Manipulation Program (SMP) - Algebraic Codes for Two and Three Dimensional Finite Element Formulations," by X. Lee and G. Dasgupta, 11/9/87, (PB88-218522).

NCEER-87-0007 "Instantaneous Optimal Control Laws for Tall Buildings Under Seismic Excitations," by J.N. Yang, A. Akbarpour and P. Ghaemmaghami, 6/10/87, (PB88-134333). This report is only available through NTIS (see address given above).

NCEER-87-0008 "IDARC: Inelastic Damage Analysis of Reinforced Concrete Frame - Shear-Wall Structures," by Y.J. Park, A.M. Reinhorn and S.K. Kunnath, 7/20/87, (PB88-134325).

NCEER-87-0009 "Liquefaction Potential for New York State: A Preliminary Report on Sites in Manhattan and Buffalo," by M. Budhu, V. Vijayakumar, R.F. Giese and L. Baumgras, 8/31/87, (PB88-163704). This report is available only through NTIS (see address given above).

NCEER-87-0010 "Vertical and Torsional Vibration of Foundations in Inhomogeneous Media," by A.S. Veletsos and K.W. Dotson, 6/1/87, (PB88-134291).

NCEER-87-0011 "Seismic Probabilistic Risk Assessment and Seismic Margins Studies for Nuclear Power Plants," by Howard H.M. Hwang, 6/15/87, (PB88-134267).

NCEER-87-0012 "Parametric Studies of Frequency Response of Secondary Systems Under Ground-Acceleration Excitations," by Y. Yong and Y.K. Lin, 6/10/87, (PB88-134309).

NCEER-87-0013 "Frequency Response of Secondary Systems Under Seismic Excitation," by J.A. HoLung, J. Cai and Y.K. Lin, 7/31/87, (PB88-134317).

NCEER-87-0014 "Modelling Earthquake Ground Motions in Seismically Active Regions Using Parametric Time Series Methods," by G.W. Ellis and A.S. Cakmak, 8/25/87, (PB88-134283).

NCEER-87-0015 "Detection and Assessment of Seismic Structural Damage," by E. DiPasquale and A.S. Cakmak, 8/25/87, (PB88-163712).

NCEER-87-0016 "Pipeline Experiment at Parkfield, California," by J. Isenberg and E. Richardson, 9/15/87, (PB88-163720). This report is available only through NTIS (see address given above).

NCEER-87-0017 "Digital Simulation of Seismic Ground Motion," by M. Shinozuka, G. Deodatis and T. Harada, 8/31/87, (PB88-155197). This report is available only through NTIS (see address given above).

NCEER-87-0018 "Practical Considerations for Structural Control: System Uncertainty, System Time Delay and Truncation of Small Control Forces," J.N. Yang and A. Akbarpour, 8/10/87, (PB88-163738).

NCEER-87-0019 "Modal Analysis of Nonclassically Damped Structural Systems Using Canonical Transformation," by J.N. Yang, S. Sarkani and F.X. Long, 9/27/87, (PB88-187851).

NCEER-87-0020 "A Nonstationary Solution in Random Vibration Theory," by J.R. Red-Horse and P.D. Spanos, 11/3/87, (PB88-163746).

NCEER-87-0021 "Horizontal Impedances for Radially Inhomogeneous Viscoelastic Soil Layers," by A.S. Veletsos and K.W. Dotson, 10/15/87, (PB88-150859).

NCEER-87-0022 "Seismic Damage Assessment of Reinforced Concrete Members," by Y.S. Chung, C. Meyer and M. Shinozuka, 10/9/87, (PB88-150867). This report is available only through NTIS (see address given above).

NCEER-87-0023 "Active Structural Control in Civil Engineering," by T.T. Soong, 11/11/87, (PB88-187778).

NCEER-87-0024 "Vertical and Torsional Impedances for Radially Inhomogeneous Viscoelastic Soil Layers," by K.W. Dotson and A.S. Veletsos, 12/87, (PB88-187786).

NCEER-87-0025 "Proceedings from the Symposium on Seismic Hazards, Ground Motions, Soil-Liquefaction and Engineering Practice in Eastern North America," October 20-22, 1987, edited by K.H. Jacob, 12/87, (PB88-188115).

NCEER-87-0026 "Report on the Whittier-Narrows, California, Earthquake of October 1, 1987," by J. Pantelic and A. Reinhorn, 11/87, (PB88-187752). This report is available only through NTIS (see address given above).

NCEER-87-0027 "Design of a Modular Program for Transient Nonlinear Analysis of Large 3-D Building Structures," by S. Srivastav and J.F. Abel, 12/30/87, (PB88-187950).

NCEER-87-0028 "Second-Year Program in Research, Education and Technology Transfer," 3/8/88, (PB88-219480).

NCEER-88-0001 "Workshop on Seismic Computer Analysis and Design of Buildings With Interactive Graphics," by W. McGuire, J.F. Abel and C.H. Conley, 1/18/88, (PB88-187760).

NCEER-88-0002 "Optimal Control of Nonlinear Flexible Structures," by J.N. Yang, F.X. Long and D. Wong, 1/22/88, (PB88-213772).

NCEER-88-0003 "Substructuring Techniques in the Time Domain for Primary-Secondary Structural Systems," by G.D. Manolis and G. Juhn, 2/10/88, (PB88-213780).

NCEER-88-0004 "Iterative Seismic Analysis of Primary-Secondary Systems," by A. Singhal, L.D. Lutes and P.D. Spanos, 2/23/88, (PB88-213798).

NCEER-88-0005 "Stochastic Finite Element Expansion for Random Media," by P.D. Spanos and R. Ghanem, 3/14/88, (PB88-213806).

NCEER-88-0006 "Combining Structural Optimization and Structural Control," by F.Y. Cheng and C.P. Pantelides, 1/10/88, (PB88-213814).

NCEER-88-0007 "Seismic Performance Assessment of Code-Designed Structures," by H.H-M. Hwang, J-W. Jaw and H-J. Shau, 3/20/88, (PB88-219423).

NCEER-88-0008 "Reliability Analysis of Code-Designed Structures Under Natural Hazards," by H.H-M. Hwang, H. Ushiba and M. Shinozuka, 2/29/88, (PB88-229471).

NCEER-88-0009 "Seismic Fragility Analysis of Shear Wall Structures," by J-W Jaw and H.H-M. Hwang, 4/30/88, (PB89-102867).

NCEER-88-0010 "Base Isolation of a Multi-Story Building Under a Harmonic Ground Motion - A Comparison of Performances of Various Systems," by F-G Fan, G. Ahmadi and I.G. Tadjbakhsh, 5/18/88, (PB89-122238).

NCEER-88-0011 "Seismic Floor Response Spectra for a Combined System by Green's Functions," by F.M. Lavelle, L.A. Bergman and P.D. Spanos, 5/1/88, (PB89-102875).

NCEER-88-0012 "A New Solution Technique for Randomly Excited Hysteretic Structures," by G.Q. Cai and Y.K. Lin, 5/16/88, (PB89-102883).

NCEER-88-0013 "A Study of Radiation Damping and Soil-Structure Interaction Effects in the Centrifuge," by K. Weissman, supervised by J.H. Prevost, 5/24/88, (PB89-144703).

NCEER-88-0014 "Parameter Identification and Implementation of a Kinematic Plasticity Model for Frictional Soils," by J.H. Prevost and D.V. Griffiths, to be published.

NCEER-88-0015 "Two- and Three- Dimensional Dynamic Finite Element Analyses of the Long Valley Dam," by D.V. Griffiths and J.H. Prevost, 6/17/88, (PB89-144711).

NCEER-88-0016 "Damage Assessment of Reinforced Concrete Structures in Eastern United States," by A.M. Reinhorn, M.J. Seidel, S.K. Kunnath and Y.J. Park, 6/15/88, (PB89-122220).

NCEER-88-0017 "Dynamic Compliance of Vertically Loaded Strip Foundations in Multilayered Viscoelastic Soils," by S. Ahmad and A.S.M. Israil, 6/17/88, (PB89-102891).

NCEER-88-0018 "An Experimental Study of Seismic Structural Response With Added Viscoelastic Dampers," by R.C. Lin, Z. Liang, T.T. Soong and R.H. Zhang, 6/30/88, (PB89-122212). This report is available only through NTIS (see address given above).

NCEER-88-0019 "Experimental Investigation of Primary - Secondary System Interaction," by G.D. Manolis, G. Juhn and A.M. Reinhorn, 5/27/88, (PB89-122204).

NCEER-88-0020 "A Response Spectrum Approach For Analysis of Nonclassically Damped Structures," by J.N. Yang, S. Sarkani and F.X. Long, 4/22/88, (PB89-102909).

NCEER-88-0021 "Seismic Interaction of Structures and Soils: Stochastic Approach," by A.S. Veletsos and A.M. Prasad, 7/21/88, (PB89-122196).

NCEER-88-0022 "Identification of the Serviceability Limit State and Detection of Seismic Structural Damage," by E. DiPasquale and A.S. Cakmak, 6/15/88, (PB89-122188). This report is available only through NTIS (see address given above).

NCEER-88-0023 "Multi-Hazard Risk Analysis: Case of a Simple Offshore Structure," by B.K. Bhartia and E.H. Vanmarcke, 7/21/88, (PB89-145213).

NCEER-88-0024 "Automated Seismic Design of Reinforced Concrete Buildings," by Y.S. Chung, C. Meyer and M. Shinozuka, 7/5/88, (PB89-122170). This report is available only through NTIS (see address given above).

NCEER-88-0025 "Experimental Study of Active Control of MDOF Structures Under Seismic Excitations," by L.L. Chung, R.C. Lin, T.T. Soong and A.M. Reinhorn, 7/10/88, (PB89-122600).

NCEER-88-0026 "Earthquake Simulation Tests of a Low-Rise Metal Structure," by J.S. Hwang, K.C. Chang, G.C. Lee and R.L. Ketter, 8/1/88, (PB89-102917).

NCEER-88-0027 "Systems Study of Urban Response and Reconstruction Due to Catastrophic Earthquakes," by F. Kozin and H.K. Zhou, 9/22/88, (PB90-162348).

NCEER-88-0028 "Seismic Fragility Analysis of Plane Frame Structures," by H.H-M. Hwang and Y.K. Low, 7/31/88, (PB89-131445).

NCEER-88-0029 "Response Analysis of Stochastic Structures," by A. Kardara, C. Bucher and M. Shinozuka, 9/22/88, (PB89-174429).

NCEER-88-0030 "Nonnormal Accelerations Due to Yielding in a Primary Structure," by D.C.K. Chen and L.D. Lutes, 9/19/88, (PB89-131437).

NCEER-88-0031 "Design Approaches for Soil-Structure Interaction," by A.S. Veletsos, A.M. Prasad and Y. Tang, 12/30/88, (PB89-174437). This report is available only through NTIS (see address given above).

NCEER-88-0032 "A Re-evaluation of Design Spectra for Seismic Damage Control," by C.J. Turkstra and A.G. Tallin, 11/7/88, (PB89-145221).

NCEER-88-0033 "The Behavior and Design of Noncontact Lap Splices Subjected to Repeated Inelastic Tensile Loading," by V.E. Sagan, P. Gergely and R.N. White, 12/8/88, (PB89-163737).

NCEER-88-0034 "Seismic Response of Pile Foundations," by S.M. Mamoon, P.K. Banerjee and S. Ahmad, 11/1/88, (PB89-145239).

NCEER-88-0035 "Modeling of R/C Building Structures With Flexible Floor Diaphragms (IDARC2)," by A.M. Reinhorn, S.K. Kunnath and N. Panahshahi, 9/7/88, (PB89-207153).

NCEER-88-0036 "Solution of the Dam-Reservoir Interaction Problem Using a Combination of FEM, BEM with Particular Integrals, Modal Analysis, and Substructuring," by C-S. Tsai, G.C. Lee and R.L. Ketter, 12/31/88, (PB89-207146).

NCEER-88-0037 "Optimal Placement of Actuators for Structural Control," by F.Y. Cheng and C.P. Pantelides, 8/15/88, (PB89-162846).

NCEER-88-0038 "Teflon Bearings in Aseismic Base Isolation: Experimental Studies and Mathematical Modeling," by A. Mokha, M.C. Constantinou and A.M. Reinhorn, 12/5/88, (PB89-218457). This report is available only through NTIS (see address given above).

NCEER-88-0039 "Seismic Behavior of Flat Slab High-Rise Buildings in the New York City Area," by P. Weidlinger and M. Ettouney, 10/15/88, (PB90-145681).

NCEER-88-0040 "Evaluation of the Earthquake Resistance of Existing Buildings in New York City," by P. Weidlinger and M. Ettouney, 10/15/88, to be published.

NCEER-88-0041 "Small-Scale Modeling Techniques for Reinforced Concrete Structures Subjected to Seismic Loads," by W. Kim, A. El-Attar and R.N. White, 11/22/88, (PB89-189625).

NCEER-88-0042 "Modeling Strong Ground Motion from Multiple Event Earthquakes," by G.W. Ellis and A.S. Cakmak, 10/15/88, (PB89-174445).

NCEER-88-0043 "Nonstationary Models of Seismic Ground Acceleration," by M. Grigoriu, S.E. Ruiz and E. Rosenblueth, 7/15/88, (PB89-189617).

NCEER-88-0044 "SARCF User's Guide: Seismic Analysis of Reinforced Concrete Frames," by Y.S. Chung, C. Meyer and M. Shinozuka, 11/9/88, (PB89-174452).

NCEER-88-0045 "First Expert Panel Meeting on Disaster Research and Planning," edited by J. Pantelic and J. Stoyle, 9/15/88, (PB89-174460).

NCEER-88-0046 "Preliminary Studies of the Effect of Degrading Infill Walls on the Nonlinear Seismic Response of Steel Frames," by C.Z. Chrysostomou, P. Gergely and J.F. Abel, 12/19/88, (PB89-208383).

NCEER-88-0047 "Reinforced Concrete Frame Component Testing Facility - Design, Construction, Instrumentation and Operation," by S.P. Pessiki, C. Conley, T. Bond, P. Gergely and R.N. White, 12/16/88, (PB89-174478).

NCEER-89-0001 "Effects of Protective Cushion and Soil Compliancy on the Response of Equipment Within a Seismically Excited Building," by J.A. HoLung, 2/16/89, (PB89-207179).

NCEER-89-0002 "Statistical Evaluation of Response Modification Factors for Reinforced Concrete Structures," by H.H-M. Hwang and J-W. Jaw, 2/17/89, (PB89-207187).

NCEER-89-0003 "Hysteretic Columns Under Random Excitation," by G-Q. Cai and Y.K. Lin, 1/9/89, (PB89-196513).

NCEER-89-0004 "Experimental Study of 'Elephant Foot Bulge' Instability of Thin-Walled Metal Tanks," by Z-H. Jia and R.L. Ketter, 2/22/89, (PB89-207195).

NCEER-89-0005 "Experiment on Performance of Buried Pipelines Across San Andreas Fault," by J. Isenberg, E. Richardson and T.D. O'Rourke, 3/10/89, (PB89-218440). This report is available only through NTIS (see address given above).

NCEER-89-0006 "A Knowledge-Based Approach to Structural Design of Earthquake-Resistant Buildings," by M. Subramani, P. Gergely, C.H. Conley, J.F. Abel and A.H. Zaghw, 1/15/89, (PB89-218465).

NCEER-89-0007 "Liquefaction Hazards and Their Effects on Buried Pipelines," by T.D. O'Rourke and P.A. Lane, 2/1/89, (PB89-218481).

NCEER-89-0008 "Fundamentals of System Identification in Structural Dynamics," by H. Imai, C-B. Yun, O. Maruyama and M. Shinozuka, 1/26/89, (PB89-207211).

NCEER-89-0009 "Effects of the 1985 Michoacan Earthquake on Water Systems and Other Buried Lifelines in Mexico," by A.G. Ayala and M.J. O'Rourke, 3/8/89, (PB89-207229).

NCEER-89-R010 "NCEER Bibliography of Earthquake Education Materials," by K.E.K. Ross, Second Revision, 9/1/89, (PB90-125352).

NCEER-89-0011 "Inelastic Three-Dimensional Response Analysis of Reinforced Concrete Building Structures (IDARC-3D), Part I - Modeling," by S.K. Kunnath and A.M. Reinhorn, 4/17/89, (PB90-114612).

NCEER-89-0012 "Recommended Modifications to ATC-14," by C.D. Poland and J.O. Malley, 4/12/89, (PB90-108648).

NCEER-89-0013 "Repair and Strengthening of Beam-to-Column Connections Subjected to Earthquake Loading," by M. Corazao and A.J. Durrani, 2/28/89, (PB90-109885).

NCEER-89-0014 "Program EXKAL2 for Identification of Structural Dynamic Systems," by O. Maruyama, C-B. Yun, M. Hoshiya and M. Shinozuka, 5/19/89, (PB90-109877).

NCEER-89-0015 "Response of Frames With Bolted Semi-Rigid Connections, Part I - Experimental Study and Analytical Predictions," by P.J. DiCorso, A.M. Reinhorn, J.R. Dickerson, J.B. Radziminski and W.L. Harper, 6/1/89, to be published.

NCEER-89-0016 "ARMA Monte Carlo Simulation in Probabilistic Structural Analysis," by P.D. Spanos and M.P. Mignolet, 7/10/89, (PB90-109893).

NCEER-89-P017 "Preliminary Proceedings from the Conference on Disaster Preparedness - The Place of Earthquake Education in Our Schools," Edited by K.E.K. Ross, 6/23/89, (PB90-108606).

NCEER-89-0017 "Proceedings from the Conference on Disaster Preparedness - The Place of Earthquake Education in Our Schools," Edited by K.E.K. Ross, 12/31/89, (PB90-207895). This report is available only through NTIS (see address given above).

NCEER-89-0018 "Multidimensional Models of Hysteretic Material Behavior for Vibration Analysis of Shape Memory Energy Absorbing Devices, by E.J. Graesser and F.A. Cozzarelli, 6/7/89, (PB90-164146).

NCEER-89-0019 "Nonlinear Dynamic Analysis of Three-Dimensional Base Isolated Structures (3D-BASIS)," by S. Nagarajaiah, A.M. Reinhorn and M.C. Constantinou, 8/3/89, (PB90-161936). This report is available only through NTIS (see address given above).

NCEER-89-0020 "Structural Control Considering Time-Rate of Control Forces and Control Rate Constraints," by F.Y. Cheng and C.P. Pantelides, 8/3/89, (PB90-120445).

NCEER-89-0021 "Subsurface Conditions of Memphis and Shelby County," by K.W. Ng, T-S. Chang and H-H.M. Hwang, 7/26/89, (PB90-120437).

NCEER-89-0022 "Seismic Wave Propagation Effects on Straight Jointed Buried Pipelines," by K. Elhmadi and M.J. O'Rourke, 8/24/89, (PB90-162322).

NCEER-89-0023 "Workshop on Serviceability Analysis of Water Delivery Systems," edited by M. Grigoriu, 3/6/89, (PB90-127424).

NCEER-89-0024 "Shaking Table Study of a 1/5 Scale Steel Frame Composed of Tapered Members," by K.C. Chang, J.S. Hwang and G.C. Lee, 9/18/89, (PB90-160169).

NCEER-89-0025 "DYNA1D: A Computer Program for Nonlinear Seismic Site Response Analysis - Technical Documentation," by Jean H. Prevost, 9/14/89, (PB90-161944). This report is available only through NTIS (see address given above).

NCEER-89-0026 "1:4 Scale Model Studies of Active Tendon Systems and Active Mass Dampers for Aseismic Protection," by A.M. Reinhorn, T.T. Soong, R.C. Lin, Y.P. Yang, Y. Fukao, H. Abe and M. Nakai, 9/15/89, (PB90-173246).

NCEER-89-0027 "Scattering of Waves by Inclusions in a Nonhomogeneous Elastic Half Space Solved by Boundary Element Methods," by P.K. Hadley, A. Askar and A.S. Cakmak, 6/15/89, (PB90-145699).

NCEER-89-0028 "Statistical Evaluation of Deflection Amplification Factors for Reinforced Concrete Structures," by H.H.M. Hwang, J-W. Jaw and A.L. Ch'ng, 8/31/89, (PB90-164633).

NCEER-89-0029 "Bedrock Accelerations in Memphis Area Due to Large New Madrid Earthquakes," by H.H.M. Hwang, C.H.S. Chen and G. Yu, 11/7/89, (PB90-162330).

NCEER-89-0030 "Seismic Behavior and Response Sensitivity of Secondary Structural Systems," by Y.Q. Chen and T.T. Soong, 10/23/89, (PB90-164658).

NCEER-89-0031 "Random Vibration and Reliability Analysis of Primary-Secondary Structural Systems," by Y. Ibrahim, M. Grigoriu and T.T. Soong, 11/10/89, (PB90-161951).

NCEER-89-0032 "Proceedings from the Second U.S. - Japan Workshop on Liquefaction, Large Ground Deformation and Their Effects on Lifelines, September 26-29, 1989," Edited by T.D. O'Rourke and M. Hamada, 12/1/89, (PB90-209388).

NCEER-89-0033 "Deterministic Model for Seismic Damage Evaluation of Reinforced Concrete Structures," by J.M. Bracci, A.M. Reinhorn, J.B. Mander and S.K. Kunnath, 9/27/89.

NCEER-89-0034 "On the Relation Between Local and Global Damage Indices," by E. DiPasquale and A.S. Cakmak, 8/15/89, (PB90-173865).

NCEER-89-0035 "Cyclic Undrained Behavior of Nonplastic and Low Plasticity Silts," by A.J. Walker and H.E. Stewart, 7/26/89, (PB90-183518).

NCEER-89-0036 "Liquefaction Potential of Surficial Deposits in the City of Buffalo, New York," by M. Budhu, R. Giese and L. Baumgrass, 1/17/89, (PB90-208455).

NCEER-89-0037 "A Deterministic Assessment of Effects of Ground Motion Incoherence," by A.S. Veletsos and Y. Tang, 7/15/89, (PB90-164294).

NCEER-89-0038 "Workshop on Ground Motion Parameters for Seismic Hazard Mapping," July 17-18, 1989, edited by R.V. Whitman, 12/1/89, (PB90-173923).

NCEER-89-0039 "Seismic Effects on Elevated Transit Lines of the New York City Transit Authority," by C.J. Costantino, C.A. Miller and E. Heymsfield, 12/26/89, (PB90-207887).

NCEER-89-0040 "Centrifugal Modeling of Dynamic Soil-Structure Interaction," by K. Weissman, Supervised by J.H. Prevost, 5/10/89, (PB90-207879).

NCEER-89-0041 "Linearized Identification of Buildings With Cores for Seismic Vulnerability Assessment," by I-K. Ho and A.E. Aktan, 11/1/89, (PB90-251943).

NCEER-90-0001 "Geotechnical and Lifeline Aspects of the October 17, 1989 Loma Prieta Earthquake in San Francisco," by T.D. O'Rourke, H.E. Stewart, F.T. Blackburn and T.S. Dickerman, 1/90, (PB90-208596).

NCEER-90-0002 "Nonnormal Secondary Response Due to Yielding in a Primary Structure," by D.C.K. Chen and L.D. Lutes, 2/28/90, (PB90-251976).

NCEER-90-0003 "Earthquake Education Materials for Grades K-12," by K.E.K. Ross, 4/16/90, (PB91-251984).

NCEER-90-0004 "Catalog of Strong Motion Stations in Eastern North America," by R.W. Busby, 4/3/90, (PB90-251984).

NCEER-90-0005 "NCEER Strong-Motion Data Base: A User Manual for the GeoBase Release (Version 1.0 for the Sun3)," by P. Friberg and K. Jacob, 3/31/90 (PB90-258062).

NCEER-90-0006 "Seismic Hazard Along a Crude Oil Pipeline in the Event of an 1811-1812 Type New Madrid Earthquake," by H.H.M. Hwang and C-H.S. Chen, 4/16/90(PB90-258054).

NCEER-90-0007 "Site-Specific Response Spectra for Memphis Sheahan Pumping Station," by H.H.M. Hwang and C.S. Lee, 5/15/90, (PB91-108811).

NCEER-90-0008 "Pilot Study on Seismic Vulnerability of Crude Oil Transmission Systems," by T. Ariman, R. Dobry, M. Grigoriu, F. Kozin, M. O'Rourke, T. O'Rourke and M. Shinozuka, 5/25/90, (PB91-108837).

NCEER-90-0009 "A Program to Generate Site Dependent Time Histories: EQGEN," by G.W. Ellis, M. Srinivasan and A.S. Cakmak, 1/30/90, (PB91-108829).

NCEER-90-0010 "Active Isolation for Seismic Protection of Operating Rooms," by M.E. Talbott, Supervised by M. Shinozuka, 6/8/9, (PB91-110205).

NCEER-90-0011 "Program *LINEARID* for Identification of Linear Structural Dynamic Systems," by C-B. Yun and M. Shinozuka, 6/25/90, (PB91-110312).

NCEER-90-0012 "Two-Dimensional Two-Phase Elasto-Plastic Seismic Response of Earth Dams," by A.N. Yiagos, Supervised by J.H. Prevost, 6/20/90, (PB91-110197).

NCEER-90-0013 "Secondary Systems in Base-Isolated Structures: Experimental Investigation, Stochastic Response and Stochastic Sensitivity," by G.D. Manolis, G. Juhn, M.C. Constantinou and A.M. Reinhorn, 7/1/90, (PB91-110320).

NCEER-90-0014 "Seismic Behavior of Lightly-Reinforced Concrete Column and Beam-Column Joint Details," by S.P. Pessiki, C.H. Conley, P. Gergely and R.N. White, 8/22/90, (PB91-108795).

NCEER-90-0015 "Two Hybrid Control Systems for Building Structures Under Strong Earthquakes," by J.N. Yang and A. Danielians, 6/29/90, (PB91-125393).

NCEER-90-0016 "Instantaneous Optimal Control with Acceleration and Velocity Feedback," by J.N. Yang and Z. Li, 6/29/90, (PB91-125401).

NCEER-90-0017 "Reconnaissance Report on the Northern Iran Earthquake of June 21, 1990," by M. Mehrain, 10/4/90, (PB91-125377).

NCEER-90-0018 "Evaluation of Liquefaction Potential in Memphis and Shelby County," by T.S. Chang, P.S. Tang, C.S. Lee and H. Hwang, 8/10/90, (PB91-125427).

NCEER-90-0019 "Experimental and Analytical Study of a Combined Sliding Disc Bearing and Helical Steel Spring Isolation System," by M.C. Constantinou, A.S. Mokha and A.M. Reinhorn, 10/4/90, (PB91-125385).

NCEER-90-0020 "Experimental Study and Analytical Prediction of Earthquake Response of a Sliding Isolation System with a Spherical Surface," by A.S. Mokha, M.C. Constantinou and A.M. Reinhorn, 10/11/90, (PB91-125419).

NCEER-90-0021 "Dynamic Interaction Factors for Floating Pile Groups," by G. Gazetas, K. Fan, A. Kaynia and E. Kausel, 9/10/90, (PB91-170381).

NCEER-90-0022 "Evaluation of Seismic Damage Indices for Reinforced Concrete Structures," by S. Rodriguez-Gomez and A.S. Cakmak, 9/30/90, PB91-171322).

NCEER-90-0023 "Study of Site Response at a Selected Memphis Site," by H. Desai, S. Ahmad, E.S. Gazetas and M.R. Oh, 10/11/90, (PB91-196857).

NCEER-90-0024 "A User's Guide to Strongmo: Version 1.0 of NCEER's Strong-Motion Data Access Tool for PCs and Terminals," by P.A. Friberg and C.A.T. Susch, 11/15/90, (PB91-171272).

NCEER-90-0025 "A Three-Dimensional Analytical Study of Spatial Variability of Seismic Ground Motions," by L-L. Hong and A.H.-S. Ang, 10/30/90, (PB91-170399).

NCEER-90-0026 "MUMOID User's Guide - A Program for the Identification of Modal Parameters," by S. Rodriguez-Gomez and E. DiPasquale, 9/30/90, (PB91-171298).

NCEER-90-0027 "SARCF-II User's Guide - Seismic Analysis of Reinforced Concrete Frames," by S. Rodriguez-Gomez, Y.S. Chung and C. Meyer, 9/30/90, (PB91-171280).

NCEER-90-0028 "Viscous Dampers: Testing, Modeling and Application in Vibration and Seismic Isolation," by N. Makris and M.C. Constantinou, 12/20/90 (PB91-190561).

NCEER-90-0029 "Soil Effects on Earthquake Ground Motions in the Memphis Area," by H. Hwang, C.S. Lee, K.W. Ng and T.S. Chang, 8/2/90, (PB91-190751).

NCEER-91-0001 "Proceedings from the Third Japan-U.S. Workshop on Earthquake Resistant Design of Lifeline Facilities and Countermeasures for Soil Liquefaction, December 17-19, 1990," edited by T.D. O'Rourke and M. Hamada, 2/1/91, (PB91-179259).

NCEER-91-0002 "Physical Space Solutions of Non-Proportionally Damped Systems," by M. Tong, Z. Liang and G.C. Lee, 1/15/91, (PB91-179242).

NCEER-91-0003 "Seismic Response of Single Piles and Pile Groups," by K. Fan and G. Gazetas, 1/10/91, (PB92-174994).

NCEER-91-0004 "Damping of Structures: Part 1 - Theory of Complex Damping," by Z. Liang and G. Lee, 10/10/91, (PB92-197235).

NCEER-91-0005 "3D-BASIS - Nonlinear Dynamic Analysis of Three Dimensional Base Isolated Structures: Part II," by S. Nagarajaiah, A.M. Reinhorn and M.C. Constantinou, 2/28/91, (PB91-190553).

NCEER-91-0006 "A Multidimensional Hysteretic Model for Plasticity Deforming Metals in Energy Absorbing Devices," by E.J. Graesser and F.A. Cozzarelli, 4/9/91, (PB92-108364).

NCEER-91-0007 "A Framework for Customizable Knowledge-Based Expert Systems with an Application to a KBES for Evaluating the Seismic Resistance of Existing Buildings," by E.G. Ibarra-Anaya and S.J. Fenves, 4/9/91, (PB91-210930).

NCEER-91-0008 "Nonlinear Analysis of Steel Frames with Semi-Rigid Connections Using the Capacity Spectrum Method," by G.G. Deierlein, S-H. Hsieh, Y-J. Shen and J.F. Abel, 7/2/91, (PB92-113828).

NCEER-91-0009 "Earthquake Education Materials for Grades K-12," by K.E.K. Ross, 4/30/91, (PB91-212142).

NCEER-91-0010 "Phase Wave Velocities and Displacement Phase Differences in a Harmonically Oscillating Pile," by N. Makris and G. Gazetas, 7/8/91, (PB92-108356).

NCEER-91-0011 "Dynamic Characteristics of a Full-Size Five-Story Steel Structure and a 2/5 Scale Model," by K.C. Chang, G.C. Yao, G.C. Lee, D.S. Hao and Y.C. Yeh," 7/2/91, (PB93-116648).

NCEER-91-0012 "Seismic Response of a 2/5 Scale Steel Structure with Added Viscoelastic Dampers," by K.C. Chang, T.T. Soong, S-T. Oh and M.L. Lai, 5/17/91, (PB92-110816).

NCEER-91-0013 "Earthquake Response of Retaining Walls; Full-Scale Testing and Computational Modeling," by S. Alampalli and A-W.M. Elgamal, 6/20/91, to be published.

NCEER-91-0014 "3D-BASIS-M: Nonlinear Dynamic Analysis of Multiple Building Base Isolated Structures," by P.C. Tsopelas, S. Nagarajaiah, M.C. Constantinou and A.M. Reinhorn, 5/28/91, (PB92-113885).

NCEER-91-0015 "Evaluation of SEAOC Design Requirements for Sliding Isolated Structures," by D. Theodossiou and M.C. Constantinou, 6/10/91, (PB92-114602).

NCEER-91-0016 "Closed-Loop Modal Testing of a 27-Story Reinforced Concrete Flat Plate-Core Building," by H.R. Somaprasad, T. Toksoy, H. Yoshiyuki and A.E. Aktan, 7/15/91, (PB92-129980).

NCEER-91-0017 "Shake Table Test of a 1/6 Scale Two-Story Lightly Reinforced Concrete Building," by A.G. El-Attar, R.N. White and P. Gergely, 2/28/91, (PB92-222447).

NCEER-91-0018 "Shake Table Test of a 1/8 Scale Three-Story Lightly Reinforced Concrete Building," by A.G. El-Attar, R.N. White and P. Gergely, 2/28/91, (PB93-116630).

NCEER-91-0019 "Transfer Functions for Rigid Rectangular Foundations," by A.S. Veletsos, A.M. Prasad and W.H. Wu, 7/31/91.

NCEER-91-0020 "Hybrid Control of Seismic-Excited Nonlinear and Inelastic Structural Systems," by J.N. Yang, Z. Li and A. Danielians, 8/1/91, (PB92-143171).

NCEER-91-0021 "The NCEER-91 Earthquake Catalog: Improved Intensity-Based Magnitudes and Recurrence Relations for U.S. Earthquakes East of New Madrid," by L. Seeber and J.G. Armbruster, 8/28/91, (PB92-176742).

NCEER-91-0022 "Proceedings from the Implementation of Earthquake Planning and Education in Schools: The Need for Change - The Roles of the Changemakers," by K.E.K. Ross and F. Winslow, 7/23/91, (PB92-129998).

NCEER-91-0023 "A Study of Reliability-Based Criteria for Seismic Design of Reinforced Concrete Frame Buildings," by H.H.M. Hwang and H-M. Hsu, 8/10/91, (PB92-140235).

NCEER-91-0024 "Experimental Verification of a Number of Structural System Identification Algorithms," by R.G. Ghanem, H. Gavin and M. Shinozuka, 9/18/91, (PB92-176577).

NCEER-91-0025 "Probabilistic Evaluation of Liquefaction Potential," by H.H.M. Hwang and C.S. Lee," 11/25/91, (PB92-143429).

NCEER-91-0026 "Instantaneous Optimal Control for Linear, Nonlinear and Hysteretic Structures - Stable Controllers," by J.N. Yang and Z. Li, 11/15/91, (PB92-163807).

NCEER-91-0027 "Experimental and Theoretical Study of a Sliding Isolation System for Bridges," by M.C. Constantinou, A. Kartoum, A.M. Reinhorn and P. Bradford, 11/15/91, (PB92-176973).

NCEER-92-0001 "Case Studies of Liquefaction and Lifeline Performance During Past Earthquakes, Volume 1: Japanese Case Studies," Edited by M. Hamada and T. O'Rourke, 2/17/92, (PB92-197243).

NCEER-92-0002 "Case Studies of Liquefaction and Lifeline Performance During Past Earthquakes, Volume 2: United States Case Studies," Edited by T. O'Rourke and M. Hamada, 2/17/92, (PB92-197250).

NCEER-92-0003 "Issues in Earthquake Education," Edited by K. Ross, 2/3/92, (PB92-222389).

NCEER-92-0004 "Proceedings from the First U.S. - Japan Workshop on Earthquake Protective Systems for Bridges," Edited by I.G. Buckle, 2/4/92, (PB94-142239, A99, MF-A06).

NCEER-92-0005 "Seismic Ground Motion from a Haskell-Type Source in a Multiple-Layered Half-Space," A.P. Theoharis, G. Deodatis and M. Shinozuka, 1/2/92, to be published.

NCEER-92-0006 "Proceedings from the Site Effects Workshop," Edited by R. Whitman, 2/29/92, (PB92-197201).

NCEER-92-0007 "Engineering Evaluation of Permanent Ground Deformations Due to Seismically-Induced Liquefaction," by M.H. Baziar, R. Dobry and A-W.M. Elgamal, 3/24/92, (PB92-222421).

NCEER-92-0008 "A Procedure for the Seismic Evaluation of Buildings in the Central and Eastern United States," by C.D. Poland and J.O. Malley, 4/2/92, (PB92-222439).

NCEER-92-0009 "Experimental and Analytical Study of a Hybrid Isolation System Using Friction Controllable Sliding Bearings," by M.Q. Feng, S. Fujii and M. Shinozuka, 5/15/92, (PB93-150282).

NCEER-92-0010 "Seismic Resistance of Slab-Column Connections in Existing Non-Ductile Flat-Plate Buildings," by A.J. Durrani and Y. Du, 5/18/92.

NCEER-92-0011 "The Hysteretic and Dynamic Behavior of Brick Masonry Walls Upgraded by Ferrocement Coatings Under Cyclic Loading and Strong Simulated Ground Motion," by H. Lee and S.P. Prawel, 5/11/92, to be published.

NCEER-92-0012 "Study of Wire Rope Systems for Seismic Protection of Equipment in Buildings," by G.F. Demetriades, M.C. Constantinou and A.M. Reinhorn, 5/20/92.

NCEER-92-0013 "Shape Memory Structural Dampers: Material Properties, Design and Seismic Testing," by P.R. Witting and F.A. Cozzarelli, 5/26/92.

NCEER-92-0014 "Longitudinal Permanent Ground Deformation Effects on Buried Continuous Pipelines," by M.J. O'Rourke, and C. Nordberg, 6/15/92.

NCEER-92-0015 "A Simulation Method for Stationary Gaussian Random Functions Based on the Sampling Theorem," by M. Grigoriu and S. Balopoulou, 6/11/92, (PB93-127496).

NCEER-92-0016 "Gravity-Load-Designed Reinforced Concrete Buildings: Seismic Evaluation of Existing Construction and Detailing Strategies for Improved Seismic Resistance," by G.W. Hoffmann, S.K. Kunnath, A.M. Reinhorn and J.B. Mander, 7/15/92, (PB94-142007, A08, MF-A02).

NCEER-92-0017 "Observations on Water System and Pipeline Performance in the Limón Area of Costa Rica Due to the April 22, 1991 Earthquake," by M. O'Rourke and D. Ballantyne, 6/30/92, (PB93-126811).

NCEER-92-0018 "Fourth Edition of Earthquake Education Materials for Grades K-12," Edited by K.E.K. Ross, 8/10/92.

NCEER-92-0019 "Proceedings from the Fourth Japan-U.S. Workshop on Earthquake Resistant Design of Lifeline Facilities and Countermeasures for Soil Liquefaction," Edited by M. Hamada and T.D. O'Rourke, 8/12/92, (PB93-163939).

NCEER-92-0020 "Active Bracing System: A Full Scale Implementation of Active Control," by A.M. Reinhorn, T.T. Soong, R.C. Lin, M.A. Riley, Y.P. Wang, S. Aizawa and M. Higashino, 8/14/92, (PB93-127512).

NCEER-92-0021 "Empirical Analysis of Horizontal Ground Displacement Generated by Liquefaction-Induced Lateral Spreads," by S.F. Bartlett and T.L. Youd, 8/17/92, (PB93-188241).

NCEER-92-0022 "IDARC Version 3.0: Inelastic Damage Analysis of Reinforced Concrete Structures," by S.K. Kunnath, A.M. Reinhorn and R.F. Lobo, 8/31/92, (PB93-227502, A07, MF-A02).

NCEER-92-0023 "A Semi-Empirical Analysis of Strong-Motion Peaks in Terms of Seismic Source, Propagation Path and Local Site Conditions, by M. Kamiyama, M.J. O'Rourke and R. Flores-Berrones, 9/9/92, (PB93-150266).

NCEER-92-0024 "Seismic Behavior of Reinforced Concrete Frame Structures with Nonductile Details, Part I: Summary of Experimental Findings of Full Scale Beam-Column Joint Tests," by A. Beres, R.N. White and P. Gergely, 9/30/92, (PB93-227783, A05, MF-A01).

NCEER-92-0025 "Experimental Results of Repaired and Retrofitted Beam-Column Joint Tests in Lightly Reinforced Concrete Frame Buildings," by A. Beres, S. El-Borgi, R.N. White and P. Gergely, 10/29/92, (PB93-227791, A05, MF-A01).

NCEER-92-0026 "A Generalization of Optimal Control Theory: Linear and Nonlinear Structures," by J.N. Yang, Z. Li and S. Vongchavalitkul, 11/2/92, (PB93-188621).

NCEER-92-0027 "Seismic Resistance of Reinforced Concrete Frame Structures Designed Only for Gravity Loads: Part I - Design and Properties of a One-Third Scale Model Structure," by J.M. Bracci, A.M. Reinhorn and J.B. Mander, 12/1/92, (PB94-104502, A08, MF-A02).

NCEER-92-0028 "Seismic Resistance of Reinforced Concrete Frame Structures Designed Only for Gravity Loads: Part II - Experimental Performance of Subassemblages," by L.E. Aycardi, J.B. Mander and A.M. Reinhorn, 12/1/92, (PB94-104510, A08, MF-A02).

NCEER-92-0029 "Seismic Resistance of Reinforced Concrete Frame Structures Designed Only for Gravity Loads: Part III - Experimental Performance and Analytical Study of a Structural Model," by J.M. Bracci, A.M. Reinhorn and J.B. Mander, 12/1/92, (PB93-227528, A09, MF-A01).

NCEER-92-0030 "Evaluation of Seismic Retrofit of Reinforced Concrete Frame Structures: Part I - Experimental Performance of Retrofitted Subassemblages," by D. Choudhuri, J.B. Mander and A.M. Reinhorn, 12/8/92, (PB93-198307, A07, MF-A02).

NCEER-92-0031 "Evaluation of Seismic Retrofit of Reinforced Concrete Frame Structures: Part II - Experimental Performance and Analytical Study of a Retrofitted Structural Model," by J.M. Bracci, A.M. Reinhorn and J.B. Mander, 12/8/92, (PB93-198315, A09, MF-A03).

NCEER-92-0032 "Experimental and Analytical Investigation of Seismic Response of Structures with Supplemental Fluid Viscous Dampers," by M.C. Constantinou and M.D. Symans, 12/21/92, (PB93-191435).

NCEER-92-0033 "Reconnaissance Report on the Cairo, Egypt Earthquake of October 12, 1992," by M. Khater, 12/23/92, (PB93-188621).

NCEER-92-0034 "Low-Level Dynamic Characteristics of Four Tall Flat-Plate Buildings in New York City," by H. Gavin, S. Yuan, J. Grossman, E. Pekelis and K. Jacob, 12/28/92, (PB93-188217).

NCEER-93-0001 "An Experimental Study on the Seismic Performance of Brick-Infilled Steel Frames With and Without Retrofit," by J.B. Mander, B. Nair, K. Wojtkowski and J. Ma, 1/29/93, (PB93-227510, A07, MF-A02).

NCEER-93-0002 "Social Accounting for Disaster Preparedness and Recovery Planning," by S. Cole, E. Pantoja and V. Razak, 2/22/93, (PB94-142114, A12, MF-A03).

NCEER-93-0003 "Assessment of 1991 NEHRP Provisions for Nonstructural Components and Recommended Revisions," by T.T. Soong, G. Chen, Z. Wu, R-H. Zhang and M. Grigoriu, 3/1/93, (PB93-188639).

NCEER-93-0004 "Evaluation of Static and Response Spectrum Analysis Procedures of SEAOC/UBC for Seismic Isolated Structures," by C.W. Winters and M.C. Constantinou, 3/23/93, (PB93-198299).

NCEER-93-0005 "Earthquakes in the Northeast - Are We Ignoring the Hazard? A Workshop on Earthquake Science and Safety for Educators," edited by K.E.K. Ross, 4/2/93, (PB94-103066, A09, MF-A02).

NCEER-93-0006 "Inelastic Response of Reinforced Concrete Structures with Viscoelastic Braces," by R.F. Lobo, J.M. Bracci, K.L. Shen, A.M. Reinhorn and T.T. Soong, 4/5/93, (PB93-227486, A05, MF-A02).

NCEER-93-0007 "Seismic Testing of Installation Methods for Computers and Data Processing Equipment," by K. Kosar, T.T. Soong, K.L. Shen, J.A. HoLung and Y.K. Lin, 4/12/93, (PB93-198299).

NCEER-93-0008 "Retrofit of Reinforced Concrete Frames Using Added Dampers," by A. Reinhorn, M. Constantinou and C. Li, *to be published*.

NCEER-93-0009 "Seismic Behavior and Design Guidelines for Steel Frame Structures with Added Viscoelastic Dampers," by K.C. Chang, M.L. Lai, T.T. Soong, D.S. Hao and Y.C. Yeh, 5/1/93, (PB94-141959, A07, MF-A02).

NCEER-93-0010 "Seismic Performance of Shear-Critical Reinforced Concrete Bridge Piers," by J.B. Mander, S.M. Waheed, M.T.A. Chaudhary and S.S. Chen, 5/12/93, (PB93-227494, A08, MF-A02).

NCEER-93-0011 "3D-BASIS-TABS: Computer Program for Nonlinear Dynamic Analysis of Three Dimensional Base Isolated Structures," by S. Nagarajaiah, C. Li, A.M. Reinhorn and M.C. Constantinou, 8/2/93, (PB94-141819, A09, MF-A02).

NCEER-93-0012 "Effects of Hydrocarbon Spills from an Oil Pipeline Break on Ground Water," by O.J. Helweg and H.H.M. Hwang, 8/3/93, (PB94-141942, A06, MF-A02).

NCEER-93-0013 "Simplified Procedures for Seismic Design of Nonstructural Components and Assessment of Current Code Provisions," by M.P. Singh, L.E. Suarez, E.E. Matheu and G.O. Maldonado, 8/4/93, (PB94-141827, A09, MF-A02).

NCEER-93-0014 "An Energy Approach to Seismic Analysis and Design of Secondary Systems," by G. Chen and T.T. Soong, 8/6/93, (PB94-142767, A11, MF-A03).

NCEER-93-0015 "Proceedings from School Sites: Becoming Prepared for Earthquakes - Commemorating the Third Anniversary of the Loma Prieta Earthquake," Edited by F.E. Winslow and K.E.K. Ross, 8/16/93.

NCEER-93-0016 "Reconnaissance Report of Damage to Historic Monuments in Cairo, Egypt Following the October 12, 1992 Dahshur Earthquake," by D. Sykora, D. Look, G. Croci, E. Karaesmen and E. Karaesmen, 8/19/93, (PB94-142221, A08, MF-A02).

NCEER-93-0017 "The Island of Guam Earthquake of August 8, 1993," by S.W. Swan and S.K. Harris, 9/30/93, (PB94-141843, A04, MF-A01).

NCEER-93-0018 "Engineering Aspects of the October 12, 1992 Egyptian Earthquake," by A.W. Elgamal, M. Amer, K. Adalier and A. Abul-Fadl, 10/7/93, (PB94-141983, A05, MF-A01).

NCEER-93-0019 "Development of an Earthquake Motion Simulator and its Application in Dynamic Centrifuge Testing," by I. Krstelj, Supervised by J.H. Prevost, 10/23/93, (PB94-181773, A-10, MF-A03).

NCEER-93-0020 "NCEER-Taisei Corporation Research Program on Sliding Seismic Isolation Systems for Bridges: Experimental and Analytical Study of a Friction Pendulum System (FPS)," by M.C. Constantinou, P. Tsopelas, Y-S. Kim and S. Okamoto, 11/1/93, (PB94-142775, A08, MF-A02).

NCEER-93-0021 "Finite Element Modeling of Elastomeric Seismic Isolation Bearings," by L.J. Billings, Supervised by R. Shepherd, 11/8/93, to be published.

NCEER-93-0022 "Seismic Vulnerability of Equipment in Critical Facilities: Life-Safety and Operational Consequences," by K. Porter, G.S. Johnson, M.M. Zadeh, C. Scawthorn and S. Eder, 11/24/93, (PB94-181765, A16, MF-A03).

NCEER-93-0023 "Hokkaido Nansei-oki, Japan Earthquake of July 12, 1993, by P.I. Yanev and C.R. Scawthorn, 12/23/93, (PB94-181500, A07, MF-A01).

NCEER-94-0001 "An Evaluation of Seismic Serviceability of Water Supply Networks with Application to the San Francisco Auxiliary Water Supply System," by I. Markov, Supervised by M. Grigoriu and T. O'Rourke, 1/21/94.

NCEER-94-0002 "NCEER-Taisei Corporation Research Program on Sliding Seismic Isolation Systems for Bridges: Experimental and Analytical Study of Systems Consisting of Sliding Bearings, Rubber Restoring Force Devices and Fluid Dampers," Volumes I and II, by P. Tsopelas, S. Okamoto, M.C. Constantinou, D. Ozaki and S. Fujii, 2/4/94, (PB94-181740, A09, MF-A02 and PB94-181757, A12, MF-A03).

NCEER-94-0003 "A Markov Model for Local and Global Damage Indices in Seismic Analysis," by S. Rahman and M. Grigoriu, 2/18/94.

NCEER-94-0004 "Proceedings from the NCEER Workshop on Seismic Response of Masonry Infills," edited by D.P. Abrams, 3/1/94, (PB94-180783, A07, MF-A02).

NCEER-94-0005 "The Northridge, California Earthquake of January 17, 1994: General Reconnaissance Report," edited by J.D. Goltz, 3/11/94, (PB193943, A10, MF-A03).

NCEER-94-0006 "Seismic Energy Based Fatigue Damage Analysis of Bridge Columns: Part I - Evaluation of Seismic Capacity," by G.A. Chang and J.B. Mander, 3/14/94, (PB94-219185, A11, MF-A03).

NCEER-94-0007 "Seismic Isolation of Multi-Story Frame Structures Using Spherical Sliding Isolation Systems," by T.M. Al-Hussaini, V.A. Zayas and M.C. Constantinou, 3/17/94, (PB193745, A09, MF-A02).

NCEER-94-0008 "The Northridge, California Earthquake of January 17, 1994: Performance of Highway Bridges," edited by I.G. Buckle, 3/24/94, (PB94-193851, A06, MF-A02).

NCEER-94-0009 "Proceedings of the Third U.S.-Japan Workshop on Earthquake Protective Systems for Bridges," edited by I.G. Buckle and I. Friedland, 3/31/94, (PB94-195815, A99, MF-MF).

NCEER-94-0010 "3D-BASIS-ME: Computer Program for Nonlinear Dynamic Analysis of Seismically Isolated Single and Multiple Structures and Liquid Storage Tanks," by P.C. Tsopelas, M.C. Constantinou and A.M. Reinhorn, 4/12/94.

NCEER-94-0011 "The Northridge, California Earthquake of January 17, 1994: Performance of Gas Transmission Pipelines," by T.D. O'Rourke and M.C. Palmer, 5/16/94.

NCEER-94-0012 "Feasibility Study of Replacement Procedures and Earthquake Performance Related to Gas Transmission Pipelines," by T.D. O'Rourke and M.C. Palmer, 5/25/94.

NCEER-94-0013 "Seismic Energy Based Fatigue Damage Analysis of Bridge Columns: Part II - Evaluation of Seismic Demand," by G.A. Chang and J.B. Mander, 6/1/94, to be published.

NCEER-94-0014 "NCEER-Taisei Corporation Research Program on Sliding Seismic Isolation Systems for Bridges: Experimental and Analytical Study of a System Consisting of Sliding Bearings and Fluid Restoring Force/Damping Devices," by P. Tsopelas and M.C. Constantinou, 6/13/94, (PB94-219144, A10, MF-A03).

NCEER-94-0015 "Generation of Hazard-Consistent Fragility Curves for Seismic Loss Estimation Studies," by H. Hwang and J-R. Huo, 6/14/94.

NCEER-94-0016 "Seismic Study of Building Frames with Added Energy-Absorbing Devices," by W.S. Pong, C.S. Tsai and G.C. Lee, 6/20/94, (PB94-219136, A10, A03).

NCEER-94-0017 "Sliding Mode Control for Seismic-Excited Linear and Nonlinear Civil Engineering Structures," by J. Yang, J. Wu, A. Agrawal and Z. Li, 6/21/94, (PB95-138483, A06, MF-A02).

NCEER-94-0018 "3D-BASIS-TABS Version 2.0: Computer Program for Nonlinear Dynamic Analysis of Three Dimensional Base Isolated Structures," by A.M. Reinhorn, S. Nagarajaiah, M.C. Constantinou, P. Tsopelas and R. Li, 6/22/94.

NCEER-94-0019 "Proceedings of the International Workshop on Civil Infrastructure Systems: Application of Intelligent Systems and Advanced Materials on Bridge Systems," Edited by G.C. Lee and K.C. Chang, 7/18/94.

NCEER-94-0020 "Study of Seismic Isolation Systems for Computer Floors," by V. Lambrou and M.C. Constantinou, 7/19/94, (PB95-138533, A10, MF-A03).

NCEER-94-0021 "Proceedings of the U.S.-Italian Workshop on Guidelines for Seismic Evaluation and Rehabilitation of Unreinforced Masonry Buildings," Edited by D.P. Abrams and G.M. Calvi, 7/20/94, (PB95-138749, A13, MF-A03).

NCEER-94-0022 "NCEER-Taisei Corporation Research Program on Sliding Seismic Isolation Systems for Bridges: Experimental and Analytical Study of a System Consisting of Lubricated PTFE Sliding Bearings and Mild Steel Dampers," by P. Tsopelas and M.C. Constantinou, 7/22/94.

NCEER-94-0023 "Development of Reliability-Based Design Criteria for Buildings Under Seismic Load," by Y.K. Wen, H. Hwang and M. Shinozuka, 8/1/94.

NCEER-94-0024 "Experimental Verification of Acceleration Feedback Control Strategies for an Active Tendon System," by S.J. Dyke, B.F. Spencer, Jr., P. Quast, M.K. Sain, D.C. Kaspari, Jr. and T.T. Soong, 8/29/94.

NCEER-94-0025 "Seismic Retrofitting Manual for Highway Bridges," Edited by I.G. Buckle and I.F. Friedland, to be published.

NCEER-94-0026 "Proceedings from the Fifth U.S.-Japan Workshop on Earthquake Resistant Design of Lifeline Facilities and Countermeasures Against Soil Liquefaction," Edited by T.D. O'Rourke and M. Hamada, 11/7/94.

NCEER-95-0001 "Experimental and Analytical Investigation of Seismic Retrofit of Structures with Supplemental Damping: Part 1 - Fluid Viscous Damping Devices," by A.M. Reinhorn, C. Li and M.C. Constantinou, 1/3/95, to be published.

NCEER-95-0002 "Experimental and Analytical Study of Low-Cycle Fatigue Behavior of Semi-Rigid Top-And-Seat Angle Connections," by G. Pekcan, J.B. Mander and S.S. Chen, 1/5/95.